AD-A050 155 TEXAS A AND M UNIV COLLEGE STATION DEPT OF METEOROLOGY F/G 17/9
REAL-TIME COMPUTER TECHNIQUES IN THE DETECTION AND ANALYSIS OF --ETC(U)
AUG 77 T E SIELAND AFOSR-77-3146

UNCLASSIFIED AFIT-CI-78-33 NL

1 OF 2
AD
A050 155

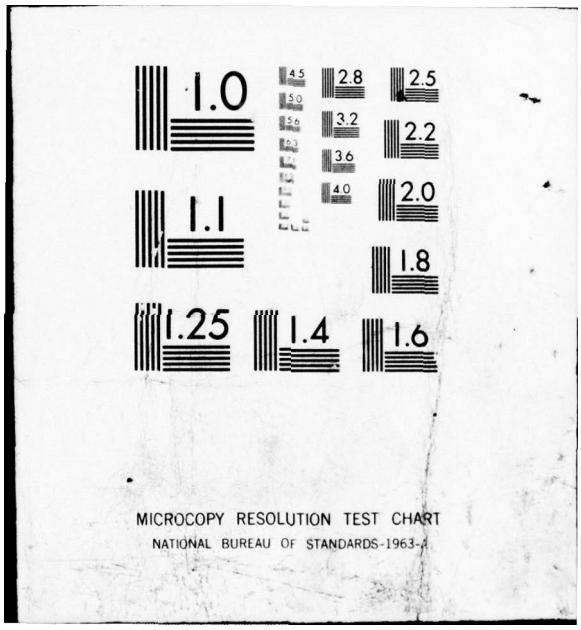
1.0
1.1
1.25
1.4
1.6
1.8
2.0
2.2
2.5
2.8
3.2
3.6
4.0
4.5
5.0
5.6
MICROCOPY RESOLUTION TEST CHART
NATIONAL BUREAU OF STANDARDS-1963-A

TEXAS A&M UNIVERSITY

DEPARTMENT OF METEOROLOGY

REAL-TIME COMPUTER TECHNIQUES IN THE DETECTION AND ANALYSIS OF SEVERE STORMS FROM DIGITAL RADAR DATA

BY
THOMAS E. SIELAND

AUGUST 1977

SECURITY CLASSIFICATION OF THIS PAGE (When Data Entered)

REPORT DOCUMENTATION PAGE

READ INSTRUCTIONS BEFORE COMPLETING FORM

1. REPORT NUMBER: AFOSR-TR-78-0123
2. GOVT ACCESSION NO.
3. RECIPIENT'S CATALOG NUMBER

4. TITLE (and Subtitle): REAL-TIME COMPUTER TECHNIQUES IN THE DETECTION AND ANALYSIS OF SEVERE STORMS FROM DIGITAL RADAR DATA.

5. TYPE OF REPORT & PERIOD COVERED: INTERIM Scientific Doctoral thesis.

6. PERFORMING ORG. REPORT NUMBER

7. AUTHOR(s): Thomas Edmund Sieland

8. CONTRACT OR GRANT NUMBER(s): AFOSR-77-3146

9. PERFORMING ORGANIZATION NAME AND ADDRESS
Department of Meteorology
Texas A&M University
College Station, TX 77843

10. PROGRAM ELEMENT, PROJECT, TASK AREA & WORK UNIT NUMBERS
2310 A1
61102F

11. CONTROLLING OFFICE NAME AND ADDRESS
AFOSR/NP
Bolling AFB, Bldg.#410
Wash DC 20332

12. REPORT DATE: Aug 77

13. NUMBER OF PAGES: 154 155 p.

14. MONITORING AGENCY NAME & ADDRESS (if different from Controlling Office)
AFIT, AFOSR
CI-78-33, TR-78-0123

15. SECURITY CLASS. (of this report): Unclassified

15a. DECLASSIFICATION/DOWNGRADING SCHEDULE

16. DISTRIBUTION STATEMENT (of this Report)

Approved for public release; distribution unlimited.

17. DISTRIBUTION STATEMENT (of the abstract entered in Block 20, if different from Report)

18. SUPPLEMENTARY NOTES

19. KEY WORDS (Continue on reverse side if necessary and identify by block number)

20. ABSTRACT (Continue on reverse side if necessary and identify by block number)

An improved computer method was developed by which multi-tilt digital radar data can be interpolated in three dimensions and reduced to a two-dimensional display of partially vertically-summed reflectivity (Z) maps (PVSZ) in near real time. The computer method was developed by using digital radar data collected with the 10-cm radar at the National Severe Storms Laboratory in Norman, Oklahoma. Various combinations of interpolation schemes were used to develop the new computer method, and the resultant products were compared to determine whether or not significant features of a severe storm evident in constant altitude

DD FORM 1 JAN 73 1473 EDITION OF 1 NOV 65 IS OBSOLETE

UNCLASSIFIED

SECURITY CLASSIFICATION OF THIS PAGE (When Data Entered)

400 161

reflectivity (Z) maps (CAZM) are retained by the new reduction technique. In addition, the number of PVSZ layers was varied to determine the minimum needed for adequate depiction of the tilt of the storm core. Finally, severe storm data from New England were processed by using the new data-reduction technique to find out whether or not any of the severe-storm signatures observed in analyses of Oklahoma storms were evident in the New England digital radar data. The new computer method developed during this investigation resulted in significant savings of computer processing time and memory as compared to a previously used method and yet retains all of the significant features of the severe storm complex revealed by the other, more cumbersome method. Three PVSZ layers appear to be sufficient to depict adequately the tilt of the storm core. A tornadic storm in Maine presented many severe storm signatures that have been observed in analyses of Okalhoma tornadoes.

AFIT-CI-78-33

REAL-TIME COMPUTER TECHNIQUES IN THE DETECTION AND ANALYSIS OF SEVERE STORMS FROM DIGITAL RADAR DATA

A Dissertation

by

THOMAS EDMUND SIELAND

Submitted to the Graduate College of
Texas A&M University
in partial fulfillment of the requirement for the degree of

DOCTOR OF PHILOSOPHY

August 1977

Major Subject: Meteorology

REAL-TIME COMPUTER TECHNIQUES IN THE DETECTION AND ANALYSIS OF SEVERE STORMS FROM DIGITAL RADAR DATA

A Dissertation

by

THOMAS EDMUND SIELAND

Approved as to style and content by:

Vance Mozer
(Chairman of Committee)

Kenneth C. Brundidge
(Head of Department)

Kenneth C. Brundidge
(Member)

Lloyd L Burns
(Member)

George L Huebner
(Member)

R Lee Hilleman
(Member)

August 1977

ABSTRACT

Real-Time Computer Techniques in the Detection and Analysis of Severe Storms from Digital Radar Data. (August 1977)

Thomas Edmund Sieland, B.S., Florida State University;
M.S., University of Michigan

Chairman of Advisory Committee: Dr. Vance Moyer

An improved computer method was developed by which multi-tilt digital radar data can be interpolated in three dimensions and reduced to a two-dimensional display of partially vertically-summed reflectivity (Z) maps (PVSZ) in near real time. The computer method was developed by using digital radar data collected with the 10-cm radar at the National Severe Storms Laboratory in Norman, Oklahoma. Various combinations of interpolation schemes were used to develop the new computer method, and the resultant products were compared to determine whether or not significant features of a severe storm evident in constant altitude reflectivity (Z) maps (CAZM) are retained by the new reduction technique. In addition, the number of PVSZ layers was varied to determine the minimum needed for adequate depiction of the tilt of the storm core. Finally, severe storm data from New England were processed by using the new data-reduction technique to find out whether or not any of the severe-storm signatures observed in analyses of Oklahoma storms were evident in the New England digital radar data.

The new computer method developed during this investigation resulted in significant savings of computer processing time and memory as compared to a previously used method and yet retains all of the

significant features of the severe storm complex revealed by the other, more cumbersome method. Three PVSZ layers appear to be sufficient to depict adequately the tilt of the storm core. A tornadic storm in Maine presented many severe-storm signatures that have been observed in analyses of Oklahoma tornadoes.

ACKNOWLEDGMENTS

The author's graduate program was sponsored and financed by the Air Force Institute of Technology, United States Air Force.

The author acknowledges the guidance and assistance of Dr. V. E. Moyer, Dr. K. C. Brundidge, Dr. G. L. Huebner, and Dr. G. N. Williams during the course of this investigation. Appreciation also is extended to Dr. D. L. Barrow and Dr. R. S. Wick for serving as members of my graduate committee.

Further acknowledgment is extended to S. G. Geotis and the staff at the Massachusetts Institute of Technology radar facility for furnishing the New England digital radar data and to Miss D. Richards for her assistance in unpacking the radar data tape. Appreciation is also extended to Mrs. P. Pearson of the Texas A&M Data Processing Center for her valuable assistance in solving several computing problems.

A portion of the funds for this investigation was provided by the Air Force Office of Scientific Research, United States Air Force, under grant No. AFOSR-77-3146 for computer rental and preparation of this paper.

Finally, appreciation is extended to my daughter, Melanie, and Mrs. Janie Leighman for their typing assistance.

DEDICATION

To my devoted wife, Doris, my children, Melanie, Lynn, and Debbie, and my parents, Clara and Ed Sieland, whose understanding and encouragement have made this dissertation possible.

TABLE OF CONTENTS

LIST OF TABLES

LIST OF FIGURES

LIST OF FIGURES (continued)

LIST OF FIGURES (continued)

LIST OF FIGURES (continued)

LIST OF FIGURES (continued)

CHAPTER I

INTRODUCTION

Severe local storms such as tornadoes, large hailstorms, and thunderstorms with high winds continue to wreak havoc throughout the eastern two-thirds of the United States. As recently as April 4, 1977, near Birmingham, Alabama, 19 persons were killed by a tornado. It is a well-known fact that our ability to identify tornadic storms with non-digitized storm radars is severely limited. In fact, our ability to identify tornadoes with digitized storm radars also is quite limited, because computerized data-reduction techniques have not yet been developed for use in processing the vast amount of real-time digital radar data required for displaying the storm complex in three dimensions. The value of such a computerized technique would be to identify areas where there is a high potential for tornadic activity. Once identified, these areas could be monitored so that forecasts and warnings could be issued with greater reliability.

The Need for this Investigation

In recent years, most of the research effort in connection with tornadoes has been conducted by using digital doppler radar data. Some of the results of these efforts have been very rewarding and show great promise for the future. In the meantime, however, the National Weather Service (NWS) has a plan to install digitizers on most of their storm radars in the United States to provide input to the new Automation of

---

The citations on the following pages follow the style of the Journal of Geophysical Research.

Field Operations and Services (AFOS) system. To date, the most widely accepted use of these data in real time is the computation of vertical integration of liquid water (VIL) developed by Greene [1971]. Vogel [1973], Canipe [1973], and Pittman [1976] all agree that while VIL may indeed be an indicator of the potential for severe storms to occur, the technique is not adequate to represent the important three-dimensional aspects of a severe storm complex. Canipe's partial vertical integration of liquid water (PVIL) and Pittman's partially vertically-summed reflectivity (Z) maps (PVSZ) are far superior to VIL in this respect. No one, however, has developed a computer program that conceivably could reduce the digital radar data in near real time and provide displays of PVSZ. A successful computer method to produce PVSZ maps in real time would be of great value to the National Weather Service (NWS) when their digital radar network becomes operational.

Objectives of this Investigation

The objective of this investigation has been to develop an improved computer method by which multi-tilt digital radar data can be interpolated in three dimensions and reduced to a two-dimensional display of partially vertically-summed reflectivity (Z) maps (PVSZ) in near real time. The technique was used to analyze severe-storm data.

Present Status of the Question

Tornadoes, hailstorms (hailstones > 3/4 in.), and thunderstorms with winds > 50 kt have been classified by NWS and the Air Weather Service (AWS) as severe storms. Radar meteorologists and operators in NWS and AWS have been working for years to perfect techniques by which

these severe storms can be detected so that warnings may be issued to civilian and military authorities and action taken to protect people and property.

Early efforts in this area were restricted to radar-scope pattern-recognition techniques. Some of the basic findings of this research were summarized by Whiton [1971] and include: hook-shaped echo, normally shaped like the figure "6"; fingers or scalloped echo edges protruding from the rear portion of the storm; an echo protrusion or pendant usually evident in the right rear portion of the storm; and the "V" notch. During later research, investigators studied the structure of severe storms in the vertical as well as the horizontal. Investigations revealed that such features as the height of echo tops in relation to the height of the tropopause [Pautz, 1963], echo-free vault or weak-echo region (WER) [Bigler, 1955], and high reflectivity spikes protruding from the tops of storms [Yates, 1963] were indicative of severe storms. All of these methods, however, rely upon the ability of the radar operator to recognize these phenomena adequately, and this ability varies with the operator's experience and exposure to severe storms. In addition, the radar operator often is required to assimilate mentally information pertaining to both the vertical and horizontal extent of the storm, an exceedingly difficult task. The recent introduction of electronic digitizing systems for weather radar has, to some extent, eased the burden on the radar operator. Now the problem becomes one of reducing the data in real time.

Digital Radar Data

Digitizing systems have been developed that quantize the power returned to a radar set over a given number of pulses and store the data in spherical coordinates of range (r), azimuth (α), and antenna elevation angle (ε). A typical data set for one sweep through a storm system may be composed of as many as 60 radials (200 range gates each) per elevation angle, and 10 antenna elevation angles. Add to this the fact that a storm is sampled continuously (5 to 10 min per scan) and the amount of data collected becomes unmanageable unless a computer is used. Therefore, computer methods are required to reduce the data for analysis and display.

One of the earliest efforts to display digital radar data was developed by Marshall [1957]. The digital data were processed and displayed in a constant-altitude plan-position-indicator (CAPPI) format. Greene [1971] developed a computerized technique to produce constant altitude reflectivity maps (CAZM) that transform the digital radar data from spherical coordinates (r, α, ε) to rectangular coordinates (x,y,h) by means of a quadratic interpolation scheme. These CAZMs were constructed at 5-kft intervals from 0-deg tilt to 50 kft and proved to be a valuable tool for analyzing severe-storm data. In addition, Greene originated the concept of integrating the liquid water content throughout the depth of a severe storm and labeled the technique "vertical integration of liquid water content" (VIL). The VIL technique was an attempt to represent the three-dimensional aspects of a severe storm in two dimensions (x,y). Greene realized moderate success with this technique; he noted that the magnitude of the VIL maxima of tornado-

producing storms would increase to very high values approximately 1 hr prior to the occurrence of a tornado and then would increase to even higher values at the time of a confirmed tornado. This pioneering effort led to additional research using VIL and variations of the technique.

Several investigators have studied the applicability of VIL to other aspects of radar meteorology. Morgan and Mueller [1972] studied the VIL and total water mass of a large hailstorm in Illinois by using photographically-derived digital data from a 3-cm radar. They discovered that hail-producing storms were characterized by very large values of VIL and rapid increases in the total water mass of the storm. Clark and Canipe [1972] investigated the applicability of VIL as an indicator of rainfall rate (R) for hydrological purposes. They concluded that VIL was a better indicator of R than simple Z-R relationships. Vogel [1973] used VIL and CAZM analyses to study several severe storms and concluded that: 1) CAZMs are the best method with which to analyze severe storms, 2) analyses of single-tilt data severely limit the detection of severe storms, and 3) VIL is a valuable indicator of the potential for severe storms to occur but masks some of the important three-dimensional aspects of severe storms such as the tilt of the maximum reflectivity core and the WER.

Canipe [1972] and Canipe and Das [1975], in an effort to overcome the deficiencies of VIL, developed the technique of partial vertical integration of liquid water content (PVIL). In this scheme, the liquid water content of a storm is integrated over three layers of the storm: 0-deg to 15 kft (the source region of the storm - no freezing);

15 kft to 35 kft (the active region - freezing); 35 kft to 50 kft (the ice region - above the -40-deg isotherm). Canipe found that a bounded weak echo region (BWER) was evident in the lower CAZM analyses of tornadic storms.[1] In addition, he concluded that PVIL was superior to VIL in that PVIL depicts not only the tilt of the storm system but also reveals a loss of mass in the upper levels of the storm as indicated in the upper-level PVIL map. These features were to be proven valuable as indicators of tornadic activity.

Elvander [1975] investigated severe-storm data from spring 1972 provided by NSSL. He studied the relationship between severe-storm events and both zero-tilt indicators and VIL. He considered storms with a zero-tilt reflectivity maximum of at least $10^{4.1}$ mm^6/m^3 (41 dBZ) and a VIL maximum of at least 10 (equivalent to 10 mm of liquid water per square meter of surface area). Correlation coefficients were computed between each indicator and severe-storm events. The correlation coefficient for zero-tilt indicators was 0.22 while the correlation coefficient for VIL was 0.45. Elvander attributes the increase of correlation to the fact that VIL is a three-dimensional measurement.

Pittman [1976] extended Canipe's work and studied additional data from tornadic storms. Instead of computing PVIL, however, Pittman simply summed the reflectivity at each grid point in the layer and converted this reflectivity to a dBZ value, and thus produced partially

---

[1] The BWER is an intense updraft within which the entrained water vapor is carried aloft so rapidly that it does not have time to condense. Therefore, the updraft has very few water droplets to backscatter radar energy and appears as a region of weak echo bounded by higher reflectivities. A more detailed discussion can be found on pp. 127-129.

vertically-summed reflectivity maps (PVSZ). He found that BWER's associated with tornadoes were evident in the lower-level PVSZ maps and the reflectivity contours exhibited a hook-shaped pattern around the BWER. This feature, together with the tilt of the storm becoming more vertical or inclined toward the BWER and a decrease of the upper-level reflectivity maximum, correlated well with the occurrence of tornadoes.

The Basis for the Investigation

A limiting factor of the PVIL and PVSZ techniques is the fact that the interpolation scheme used requires a vast amount (on the order of 512 Kbytes) of computer memory to retain the data arrays necessary in the subsequent integration or summation routines. In order to use either of the techniques operationally, a simpler, less cumbersome, method must be developed to reduce the data.

With the initiation of the Digitized Radar Experiment (D/RADEX) by NWS, the need for an operational technique to process digital radar data became evident. Since the NWS, and possibly the AWS, will have many of their radar systems digitized in the near future, a data-reduction scheme that can be used in real time is a necessity. Any system so devised must allow for easy analysis of the three-dimensional aspects of a storm, since research has shown that zero-tilt reflectivity patterns alone are poor indicators of severe storms. It is also imperative that any data-interpolation schemes preserve the significant characteristics of the individual CAZM analyses and the three-dimensional characteristics of the storm.

Most of the research to date has been conducted with storm data

provided by NSSL. Therefore, severe-storm data from locations other than Oklahoma should be investigated to determine whether or not any of the severe-storm signatures identified by Canipe and Pittman are applicable. At the same time, additional severe-storm signatures must be sought that may aid radar operators in the detection and prognostication of severe storms.

CHAPTER II

DATA REDUCTION TECHNIQUES

Severe Storm Data

Reports of severe storm occurrences were extracted from Storm Data, a monthly publication of the Environmental Data Service, National Oceanic and Atmospheric Administration. The publication contains such information as the location and time of occurrence of a severe-storm event, tornado path length and width, maximum hail size, maximum wind speed, and property damage.

Radar Data

The radar data used in this study were provided by NSSL and Massachusetts Institute of Technology (MIT), Cambridge, Massachusetts. The NSSL data were collected by using a modified WSR-57 radar system operated and maintained by NSSL. A complete description of the system is given by Wilk et al. [1967] and Wilk and Gray [1970]. The characteristics of the NSSL WSR-57 radar system are given in Table 1.

The data received from MIT were collected by using a WSR-73. The characteristics of the MIT WSR-73 radar are given in Table 2.

Basic Radar Theory

The form of the radar equation used for this investigation follows the derivation of Probert-Jones [1962], who assumed a more realistic beam-pattern in order to reduce the error in a derivation by Battan [1959].

TABLE 1. Characteristics of the NSSL WSR-57 Radar [after Wilk et al., 1967].

Peak transmitted power	450 kw
Antenna gain	7.079×10^3
Pulse length	1.20×10^3 m
Beam width	2.0 deg
Wavelength	10.4 cm
Pulse repetition frequency	164 sec^{-1}
Minimum detectable signal	-110 dbm

TABLE 2. Characteristics of the MIT WSR-73 Radar.

Peak transmitted power	250 kw
Antenna gain	7.94×10^3
Pulse length	3.0×10^2 m
Beam width	1.40 deg
Wavelength	5.5 cm
Pulse repetition frequency	250 sec^{-1}
Minimum detectable signal	-105 dbm

If we assume no significant attenuation of the microwave energy between the radar antenna and the target (a valid assumption for a radar with a wavelength $\sim$ 10 cm), and the spatial volume illuminated by the radar beam is completely filled by the target, the average backscattered power, $\overline{P_r}$ (watts), received from the target at range, r, is given by

$$\overline{P_r} = \frac{C|k|^2}{r^2} Z_e \qquad (1)$$

where C and $|k|^2$ are the radar constant (unique for each individual radar) and the dialectric constant used in scattering theory and Z_e is the equivalent radar reflectivity factor. The equation for C is

$$C = \frac{\pi^3 P_t G^2 h \theta \phi}{512 \lambda^2 \ell n\ 2} \qquad (2)$$

where P_t is the power output during a radar pulse (mw), G the antenna gain (dimensionless), h the pulse length of the transmitted pulse (cm), θ the horizontal beam width (radians), ϕ the vertical beam width (radians), and λ the wavelength of the transmitted microwave energy (cm). The factor 2 ℓn 2 is the so-called Probert-Jones correction factor which results from the fact that the beam power density is approximately Gaussian in nature and therefore the transmitting and receiving gains are not equal. The value of C for the NSSL WSR-57 radar is 1.332 x 10^{-10} w $km^2 m^3 mm^{-6}$. Likewise, the value of $|k|^2$ is chosen as 0.9 [Battan, 1973].

The digitized values of the power returned must be converted to reflectivity before further data-reduction techniques can be used. The standard practice is to measure the power returned in terms of decibels with respect to a reference power level, normally 1 mw. Power levels thus are expressed as dbm above (+) or below (-) 1 mw. The equation is

$$P(\text{dbm}) = 10 \log_{10} \frac{P(\text{watts})}{10^{-3} \text{ watts}} \qquad (3)$$

For example, if the power received was 10^{-12} watts, this would equate

to -90 dbm.[2]

To arrive at values of Z_e, we solve Eq (1) for Z_e and have

$$Z_e = \frac{r^2}{C|k|^2} \overline{P_r} \tag{4}$$

The logarithm of Eq (4) is

$$\log Z_e = 2 \log r + \log \overline{P_r} - \log C|k|^2 \tag{5}$$

Using the value of C for the NSSL radar and $|k|^2$ given earlier, we have

$$\log C|k|^2 = -9.9 \tag{6}$$

Equation (6) substituted into Eq (5) gives us

$$\log Z_e = 2 \log r + \log \overline{P_r} + 9.9 \tag{7}$$

The digital value of $\overline{P_r}$ is converted to its equivalent value in dbm (always negative) by using the calibration coefficients supplied by NSSL.[3] The power received in watts is related to the power received in dbm by

$$\log \overline{P_r} \text{ (watts)} = 0.1 \overline{P_r} \text{ (dbm)} - 3 \tag{8}$$

---

[2]A more complete discussion of radar reflectivity factor, Z, equivalent radar reflectivity factor, Z_e, and dbm is found in Battan [1973].

[3]Actually, the digital system obtains $\overline{\log P_r}$ instead of $\log \overline{P_r}$. Wilk and Kessler [1970] developed an equation which corrects (7) and the correction generally is less than 1 db.

We then substitute Eq (8) into Eq (7) to give us

$$\log Z_e = 0.1 \overline{P_r} + 2 \log r + 6.9 \tag{9}$$

Finally, the value of Z_e is given by

$$Z_e = 10^{(0.1 \overline{P_r} + 2 \log r + 6.9)} \tag{10}$$

where Z_e has the units $mm^6 m^{-3}$ by convention.

Assumptions inherent in the derivation of Eq (10) are:

1. The transmitted microwave energy is not attenuated significantly between the radar antenna and the target. This has been shown to be valid for 10-cm radars [Greene, 1964].

2. The spatial volume illuminated by the beam is filled by the target. On the periphery of a storm there will be occasions when this assumption will not be met. This error will result in a loss in the resolution of fine-scale detail [Greene, 1971], but will not significantly alter the main features present in the digital data.

3. The Rayleigh approximation is used that adequately describes the scattering properties of spherical liquid-water drops having diameters $\sim 0.04\lambda$, where λ is the radar wavelength in centimeters. In the case of some severe storms, large water drops are non-spherical and hail stones may be present. In these cases, however, the enhanced reflectivity may be beneficial in identifying severe storms.

For the purpose of this investigation it is assumed further that:

1. Each digital datum value represents a point in the center of the radar volume.

2. The equivalent reflectivity factors, Z_e, obtained from the

digital data are representative of a continuous scalar field.

The Earth Curvature Correction

Microwave energy propagating in free space will follow a straight-line path. In the atmosphere, however, microwave energy transmitted from a radar antenna will follow a curved path due to refraction. The amount of curvature depends on the vertical gradient of the index of refraction (n). Under normal atmospheric conditions, when the temperature and humidity generally decrease with height, the radar beam will be bent slightly toward the surface of the earth. Appleton [1946] studied the curvature of a radio wave traveling through an atmosphere in which the index of refraction varies with height. He considered the case in which the transmitter is located at a height h_o above Earth's surface and sends out a beam at an angle ε with the horizontal plane as shown in Figure 1.

If the change of the index of refraction with height, $\frac{dn}{dh}$, is small, then ray theory may be applied and the exact differential equation for a ray in a spherically stratified atmosphere is

$$\frac{d^2h}{ds^2} = \left(\frac{2}{R+h} + \frac{1}{n}\frac{dn}{dh}\right)\left(\frac{dh}{ds}\right)^2 + \left(\frac{R+h}{R}\right)^2\left(\frac{1}{R+h} + \frac{1}{n}\frac{dn}{dh}\right) \qquad (11)$$

where h is the vertical height of the radar beam axis above Earth's surface at a distance s, R is the radius of Earth, and n is the index of refraction. Under most conditions, ε is very small and thus $\left(\frac{dh}{ds}\right)^2 = \tan^2 \varepsilon << 1$. In addition, $n \cong 1$ and $h << R$. Thus for all practical purposes, Eq (11) can be reduced to

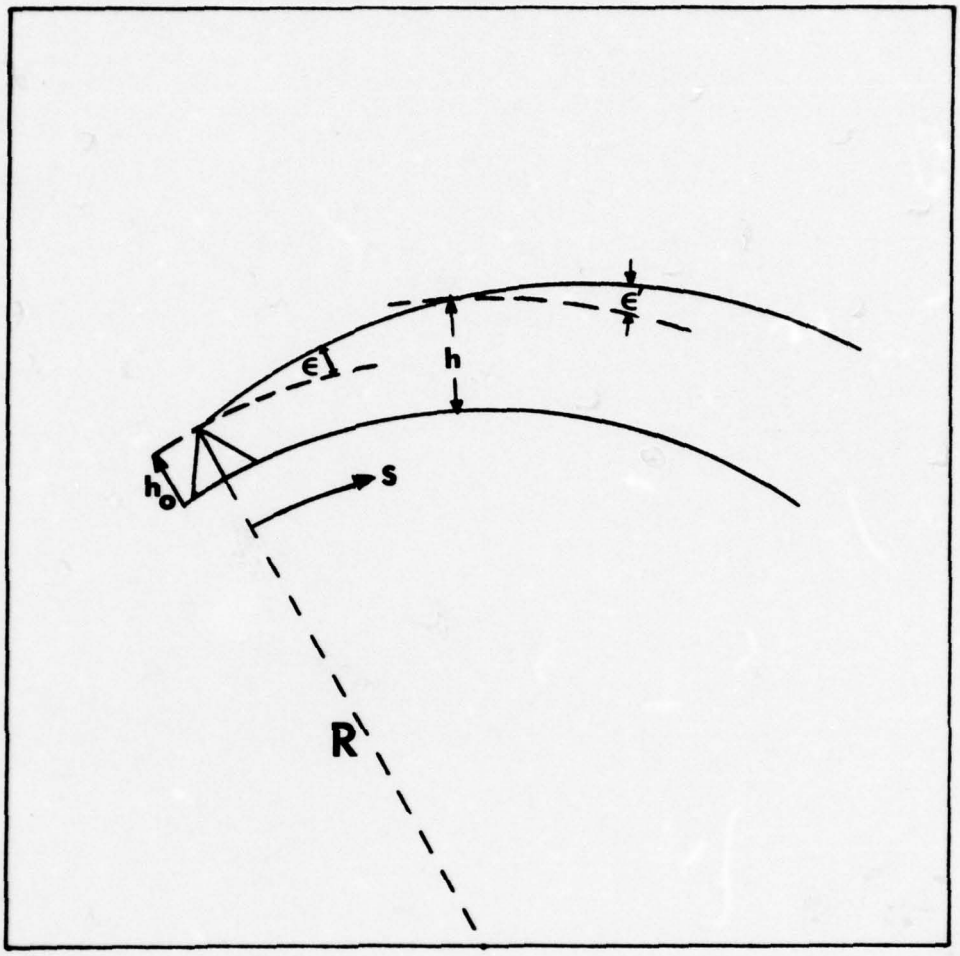

Fig. 1. Schematic of a ray path.

$$\frac{d^2h}{ds^2} = \frac{1}{R} + \frac{dn}{dh} \tag{12}$$

For the purpose of this investigation, it is necessary to consider the radar beam axis as a straight line. To accomplish this, we assume a fictitious Earth having a radius R' given by [Battan, 1959]

$$R' = \frac{R}{1 + R\frac{dn}{dh}} \tag{13}$$

It has been shown that $\frac{dn}{dh}$ is small and nearly linear with a value of $-4 \times 10^{-8} m^{-1}$. Therefore, for this investigation we will use $R' = \frac{4}{3} R$ and the radar beam may be considered a straight line as shown in Figure 2.

Previous Data Processing Techniques

The amount of digital data available from any quadrant of 100 deg of azimuth (50 radials, one every 2 deg) and 200 km is 10^4 data bits. If this value is multiplied by 12 tilt angles, the result is 12×10^4 data bits from which the three-dimensional structure of a storm system must be reproduced. It can be seen readily that no radar operator would be able to assimilate this amount of data and construct mentally the detailed three-dimensional structure of a storm system. Therefore, computerized data reduction techniques are required to assist the radar operator.

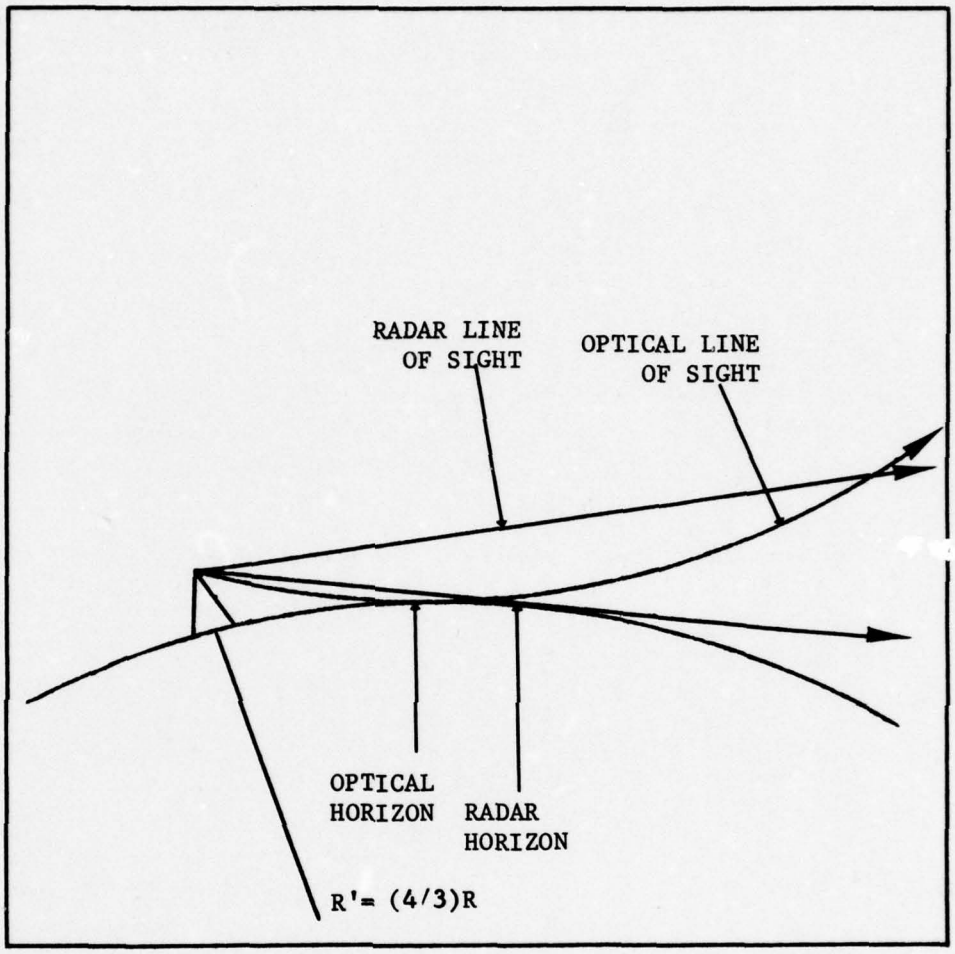

Fig. 2. Radar and optical lines of sight over an earth having an effective radius, R' = (4/3)R. [After Battan, 1959].

Constant Altitude Reflectivity Maps

Canipe [1973] and Pittman [1976] used a technique developed by Greene [1971] and modified by Vogel [1973] with which the reflectivity data are linearly interpolated from a spherical coordinate system of range (r), azimuth (α), and antenna elevation angle (ε) and mapped into a cylindrical coordinate system of (s,α,h), where s is the distance along a flat Earth's surface and h is the height above ground in increments of 5 kft from the surface to 50 kft. For s, Canipe used a grid interval (Δs) of 1 n mi and Pittman used a grid interval (Δs) of 2 km. To produce a CAZM, we first interpolate in the vertical plane of α in two steps (see Figure 3). The first step is to interpolate the value of the equivalent reflectivity factor (Z_e) at constant-altitude points in terms of spherical coordinates (r',α,ε'), where

$$\varepsilon' = \tan^{-1}\left(\frac{h}{r} - \frac{r}{2R'}\right) \tag{14}$$

and

$$r' = r/\cos\varepsilon' \tag{15}$$

with $R' = \frac{4}{3}R$. Equation (14) includes corrections for Earth's curvature and refraction of the radar beam under standard atmospheric conditions. The value of Z_e at points A and B are interpolated linearly and are given by

$$A = Z_e(r+1, \varepsilon_i) + \left[Z_e(r+1, \varepsilon_{i+1}) - Z_e(r+1, \varepsilon_i)\right]\frac{\delta\varepsilon}{\Delta\varepsilon} \tag{16}$$

$$B = Z_e(r, \varepsilon_i) + \left[Z_e(r, \varepsilon_{i+1}) - Z_e(r, \varepsilon_{i+1})\right]\frac{\delta\varepsilon}{\Delta\varepsilon} \tag{17}$$

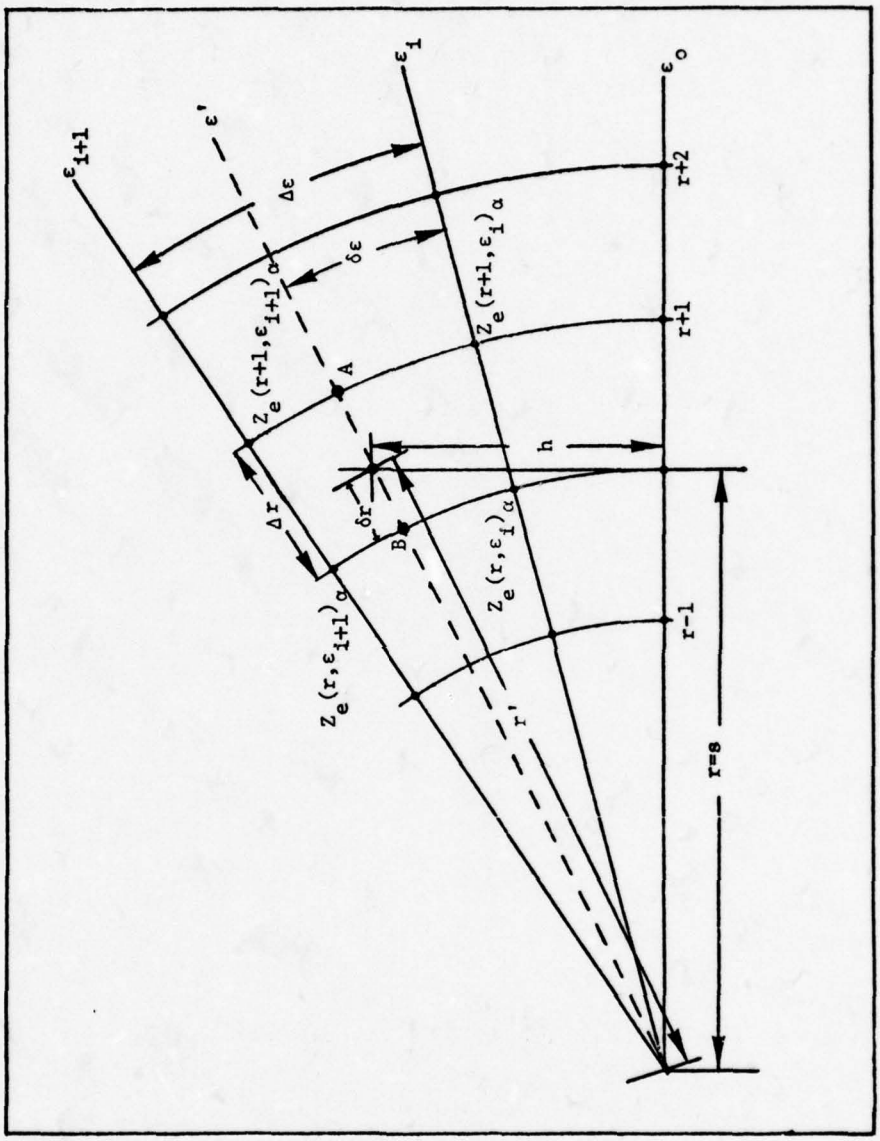

Fig. 3. The interpolation of $Z_e(s,h)_\alpha$ in the vertical plane of α.

Next, the value of the reflectivity factor at $Z_e(s,h)_\alpha$ is determined by linear interpolation from the values of A and B, viz.,

$$Z_e(s,\alpha,h) = B + [A - B] \frac{\delta r}{\Delta r} \tag{18}$$

The result is a plan view of the interpolated reflectivity factors at a constant height, h, where the data points are aligned vertically with the range gate locations at the 0-deg level. Thus, if we have a range interval of 2 km (Δr) at the surface we will have the data array at height, h, with the same 2-km interval (Δs).

Quadratic Interpolation Technique

The next step in producing a CAZM is to map the reflectivity values from cylindrical coordinates into a rectangular coordinate system (x,y,h) where x and y are the rectangular coordinates on a flat Earth and h is held constant. The technique is termed a quadratic interpolation scheme but is basically a finite-difference form of the Taylor series expansion in two dimensions truncated after the second-order terms. Greene [1971] presents a complete discussion of the technique in detail. In short, however, the scheme entails selection of the nearest six $(s,\alpha)_h$ grid points from the nine possible grid points closest to the $(x,y)_h$ point in question. For example, in Figure 4, the i^{th} point is the closest to the desired point $(x,y)_h$. Therefore, the points (S_i,α_i), (S_{i+1},α_i), (S_{i-1},α_i) are always selected along with (S_i,α_{i+1}) and (S_i,α_{i-1}). The sixth point is determined by the sign of $\delta\alpha$ and δs. The sixth point in any case will always be such that the point $(x,y)_h$ is encompassed by the nearest four points. The completed

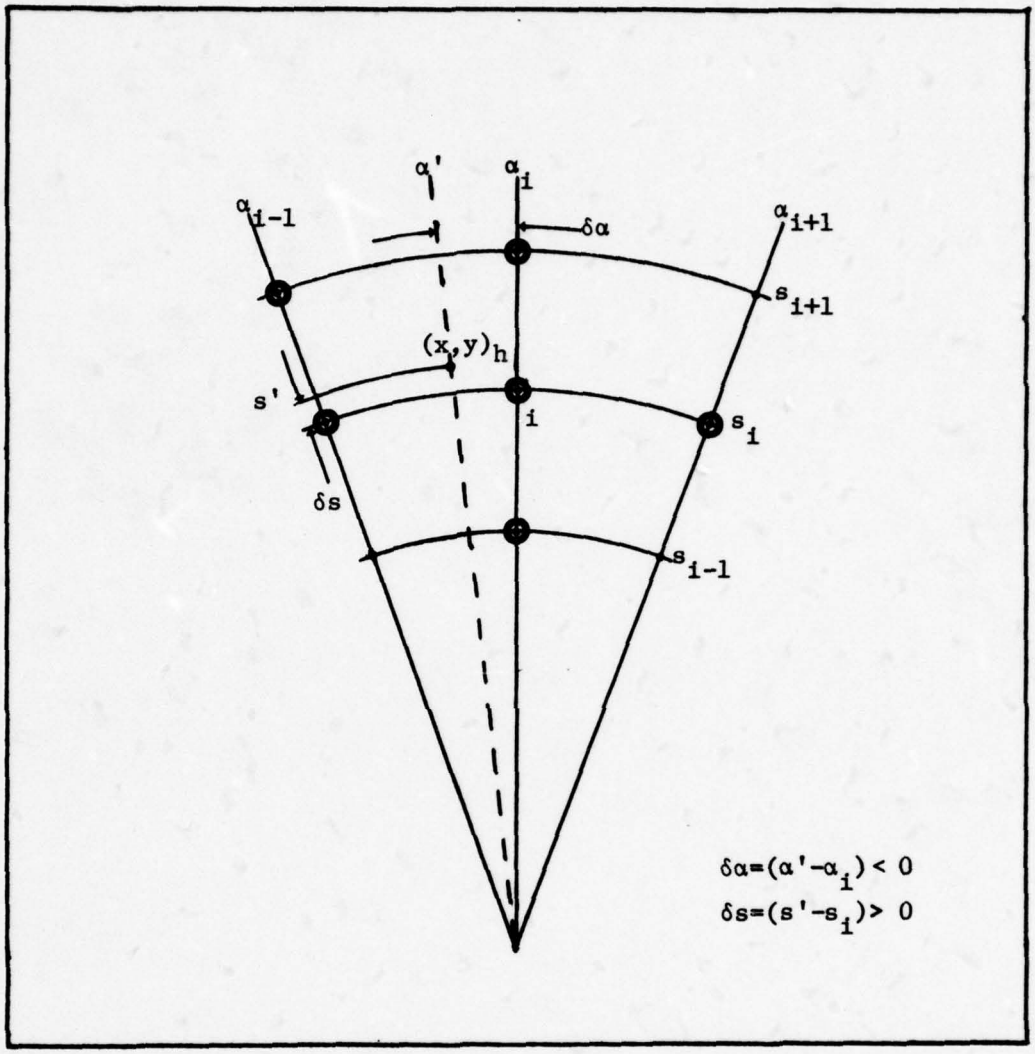

Fig. 4. Selection of the six grid points used in the interpolation of $Z_e(x,y)$ in the horizontal plane of h.

CAZM covers an area of 100 km^2 and if reduced to page size would be nearly illegible. Therefore, examples of a portion of the resultant CAZM's for 1800 CST, 23 May 1974, are shown in Figures 5 through 14.[4] The 50-kft CAZM has been excluded because all reflectivities were less than 10 dBZ and therefore a blank map was produced. The isopleths of reflectivity are expressed in units of dBZ where

$$Z_e \text{ (dBZ)} = 10 \log_{10} Z_e \text{ (mm}^6\text{m}^{-3}\text{)} \tag{19}$$

Vertical Integration of Liquid Water (VIL)

Greene [1971] developed a technique by which the reflectivity factors are converted to liquid water content (M) and then are integrated vertically throughout the depth of a storm system. This technique results in a two-dimensional display of the storm system. Vogel [1973] presents a detailed discussion of the technique. All VIL displays in this investigation are produced by using this technique. Greene [1971] also studied the time rate of change of the VIL maxima to isolate severe-storm signatures. He found that tornado-producing meso-systems are characterized by high values of VIL for approximately 1 hr prior to the reported tornado, and then a rapid increase in VIL to greater values appeared to accompany the development of a confirmed tornado. Greene termed this phenomenon "explosive development."

---

[4] All maps displayed were produced by using a library subroutine named CONREC and plotted on the CALCOMP plotter at the Texas A&M Data Processing Center. Any peculiarities in the contour lines are a result of the computer processing techniques employed by CONREC.

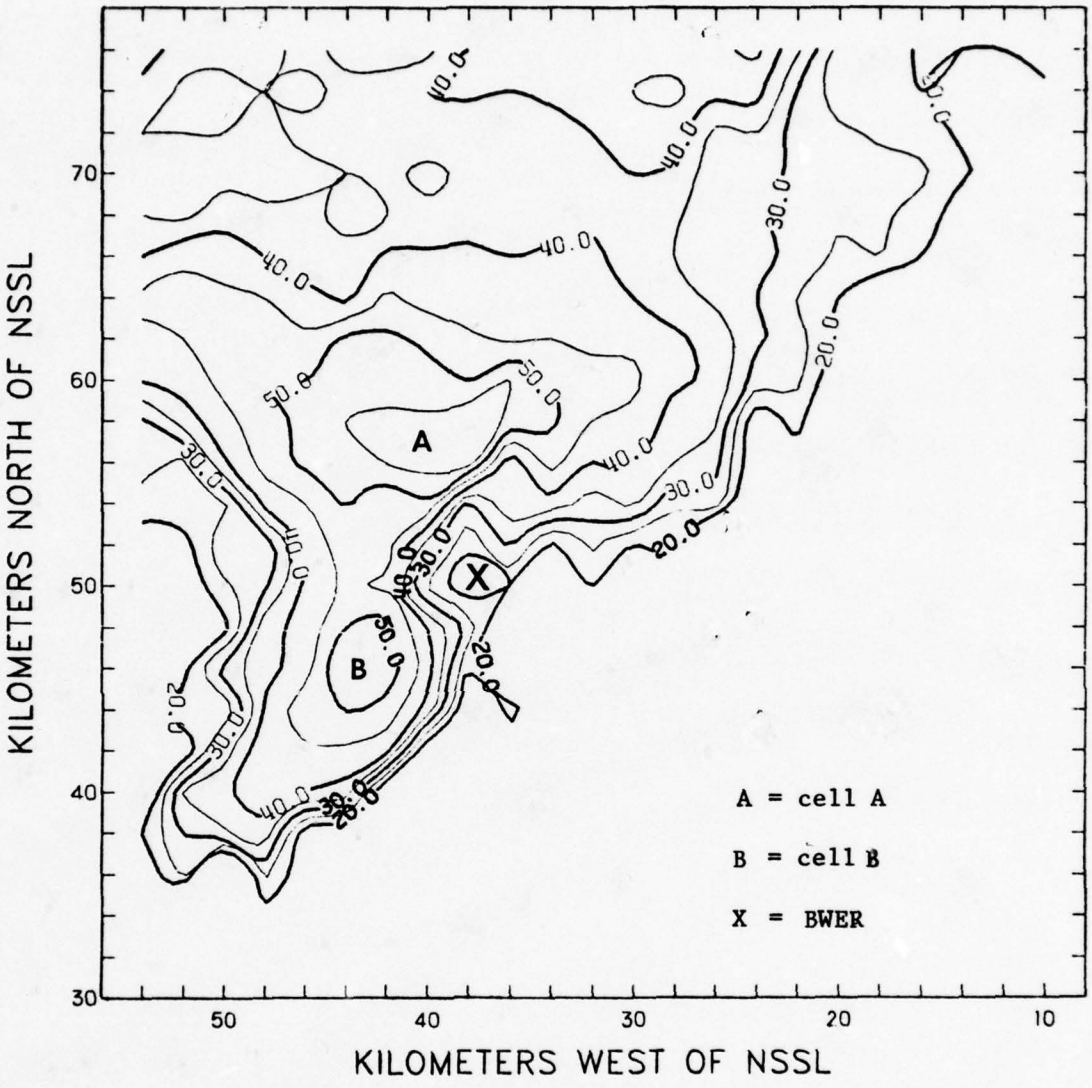

Fig 5. Reflectivity map for 0-deg tilt, 1800 CST, 23 May 1974. Isopleths of reflectivity in dBZ.

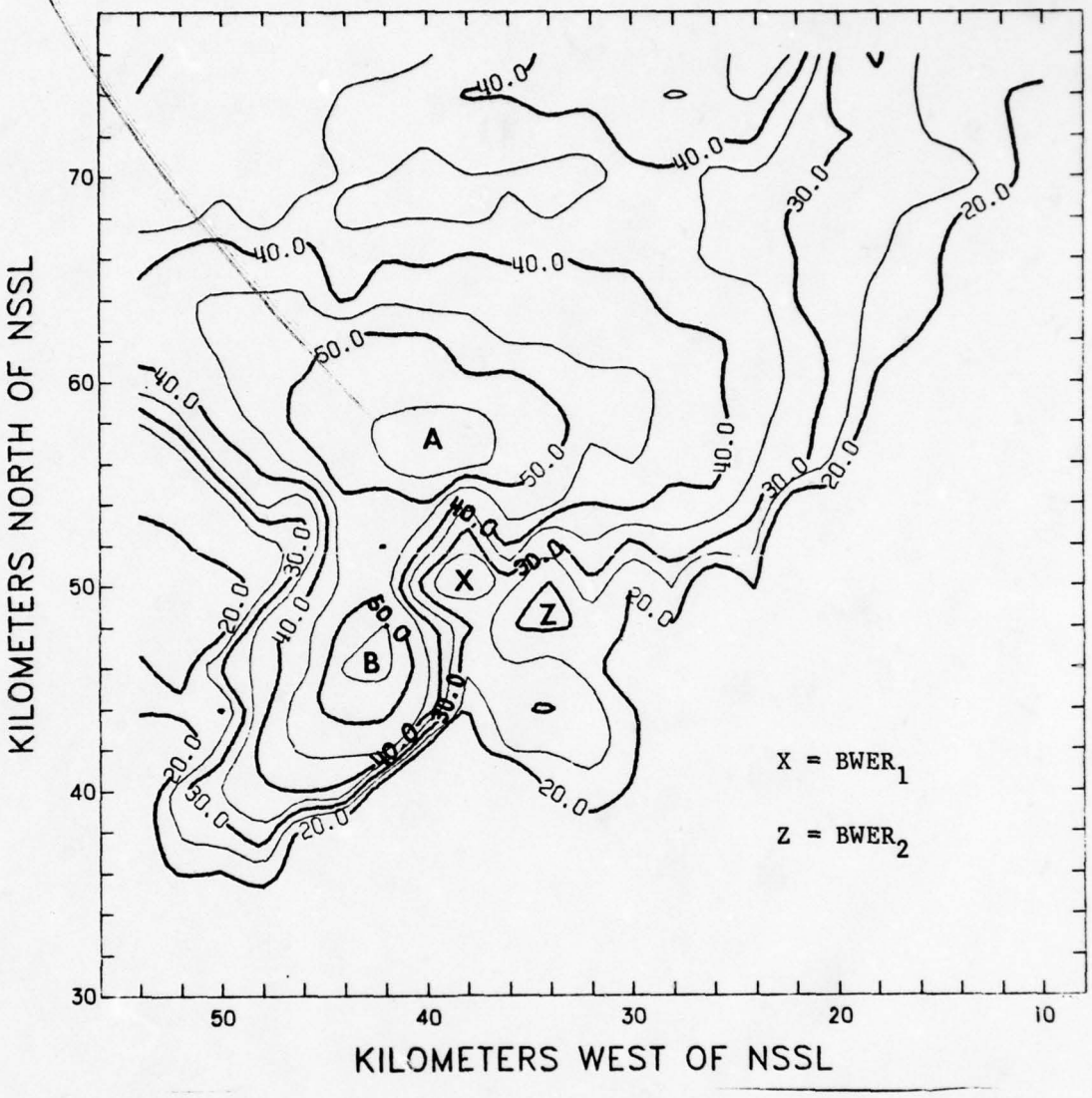

Fig. 6. The 5-kft CAZM, 1800 CST, 23 May 1974. Isopleths of reflectivity in dBZ.

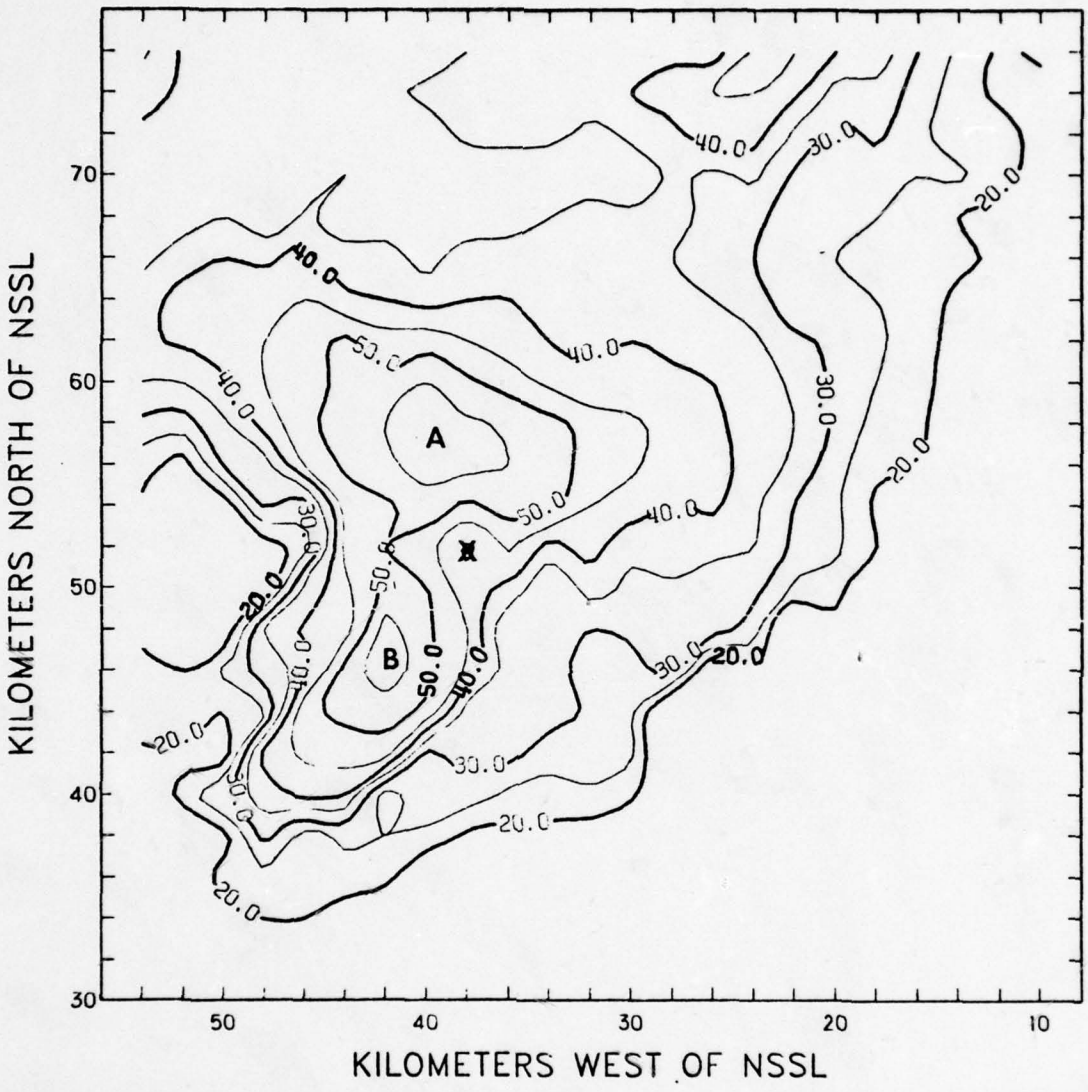

Fig. 7. The 10-kft CAZM, 1800 CST, 23 May 1974. Isopleths of reflectivity in dBZ.

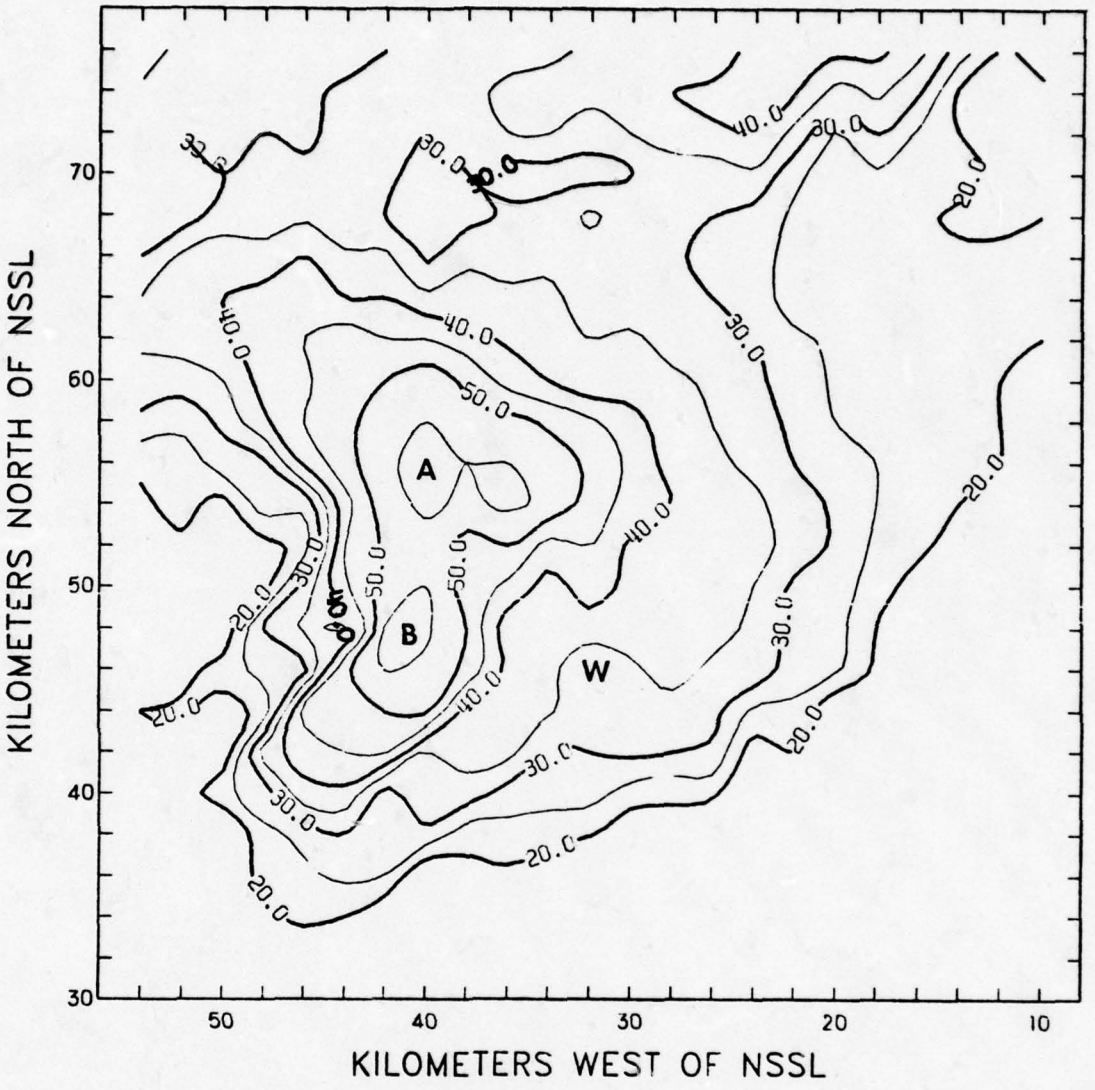

Fig. 8. The 15-kft CAZM, 1800 CST, 23 May 1974. Isopleths of reflectivity in dBZ.

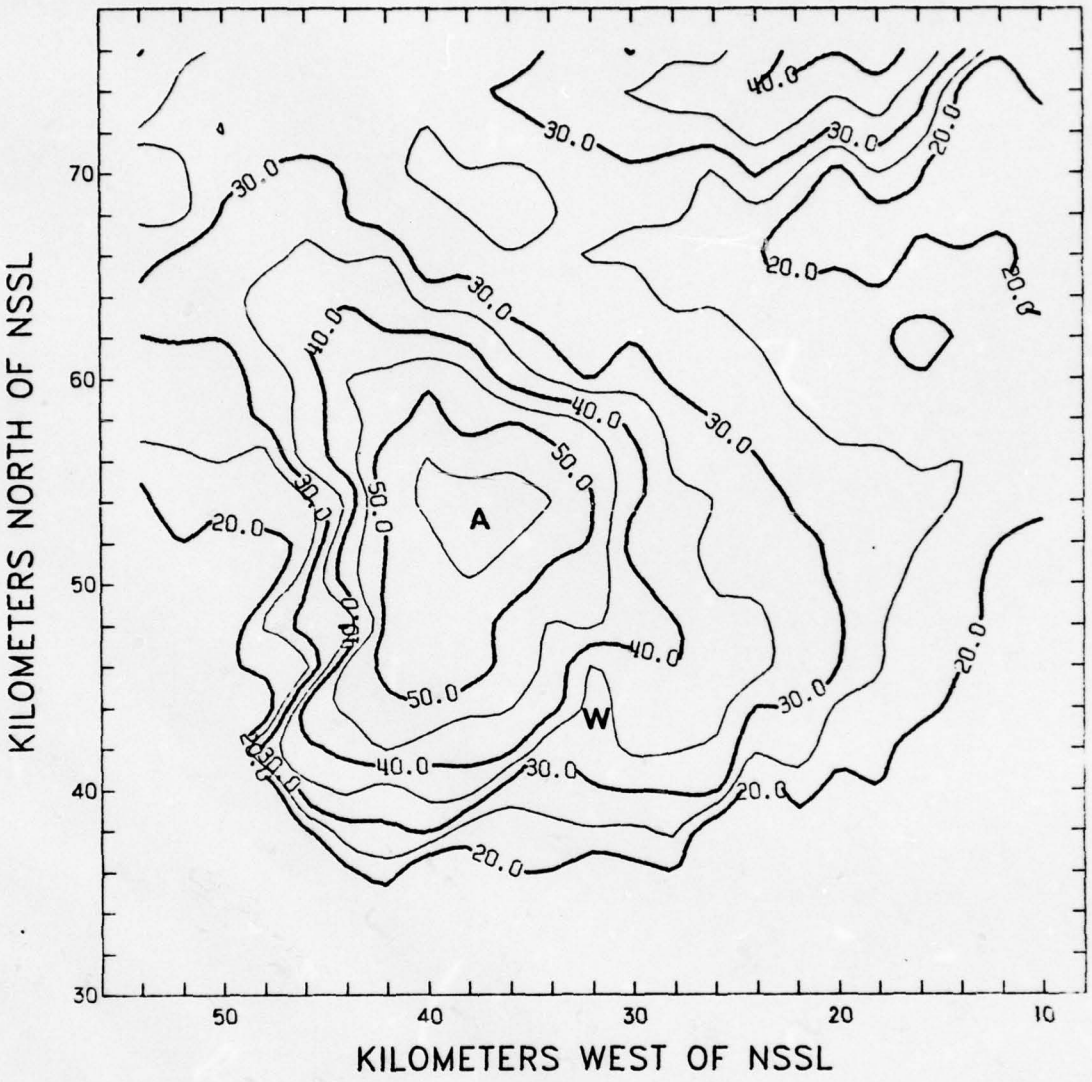

Fig. 9. The 20-kft CAZM, 1800 CST, 23 May 1974. Isopleths of reflectivity in dBZ.

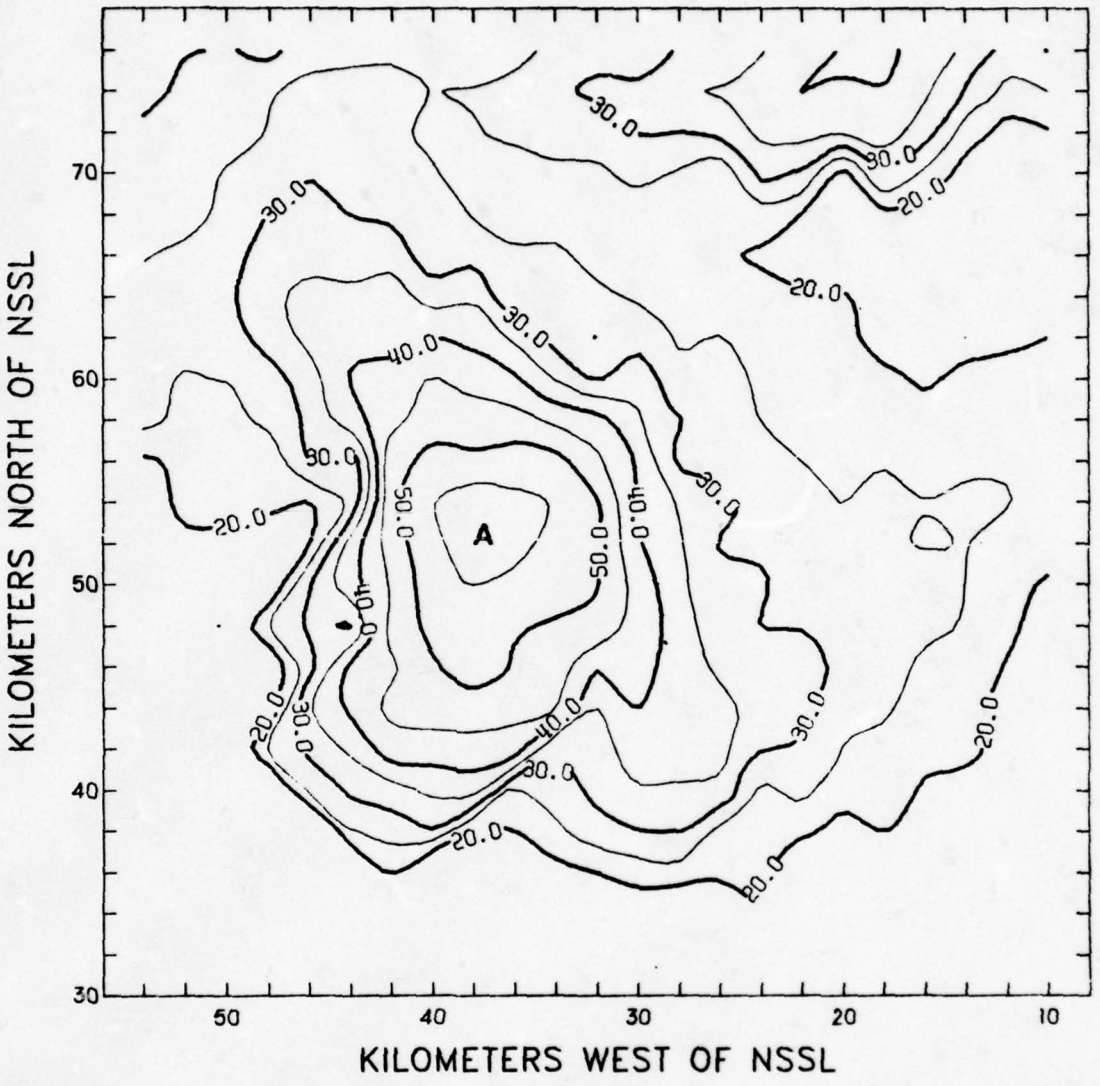

Fig. 10. The 25-kft CAZM, 1800 CST, 23 May 1974. Isopleths of reflectivity in dBZ.

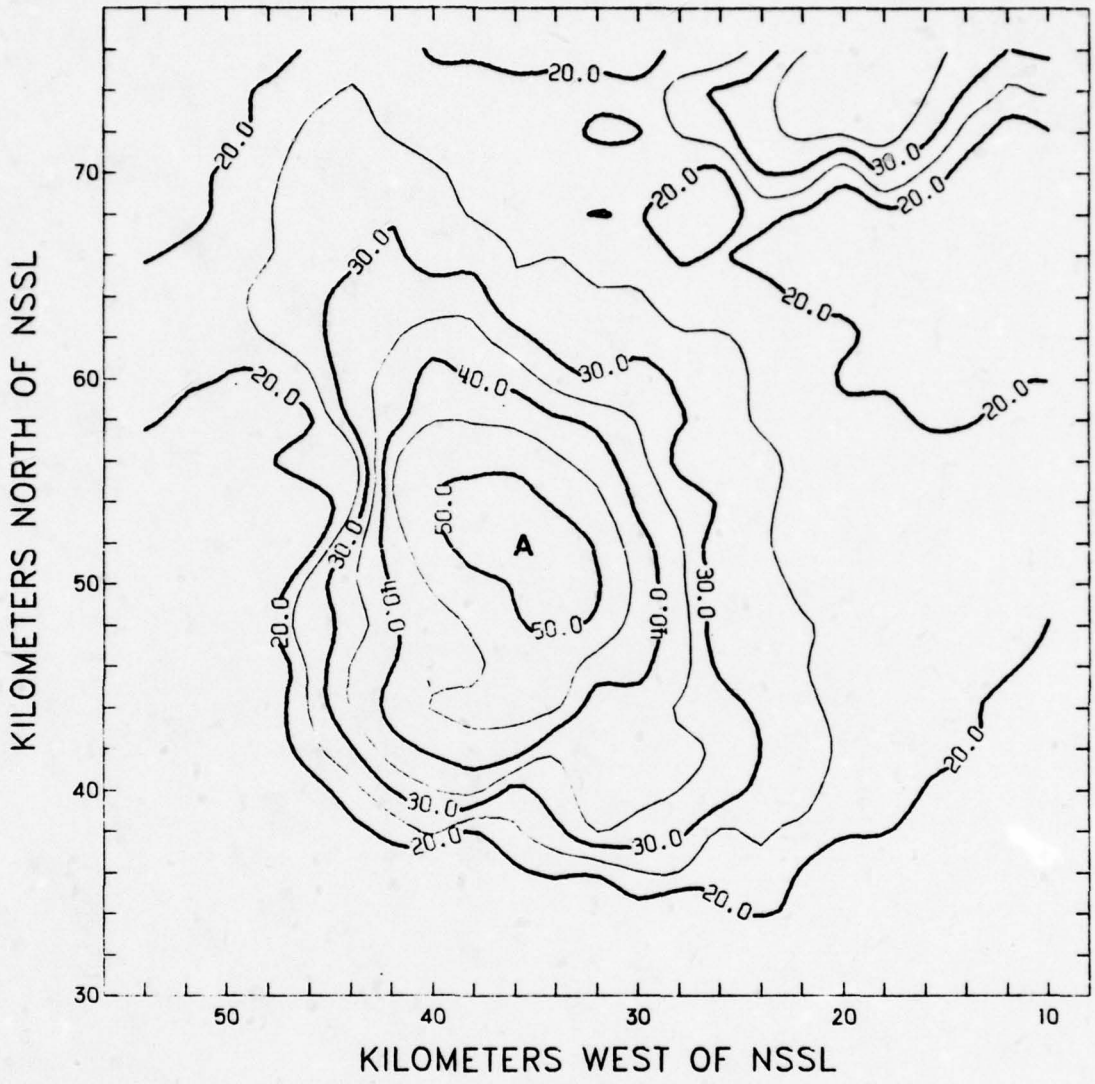

Fig. 11. The 30-kft CAZM, 1800 CST, 23 May 1974. Isopleths of reflectivity in dBZ.

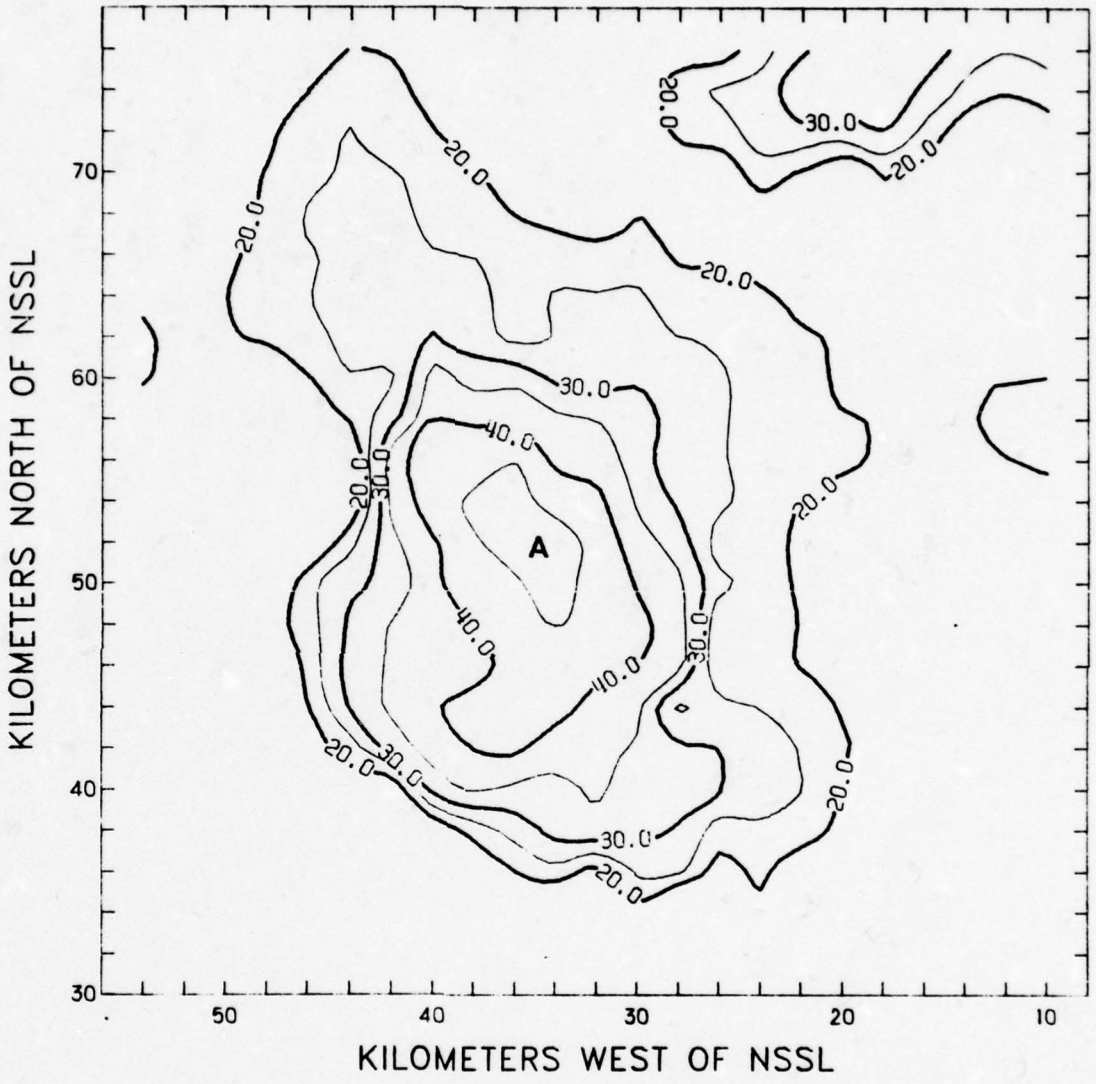

Fig. 12. The 35-kft CAZM, 1800 CST, 23 May 1974. Isopleths of reflectivity in dBZ.

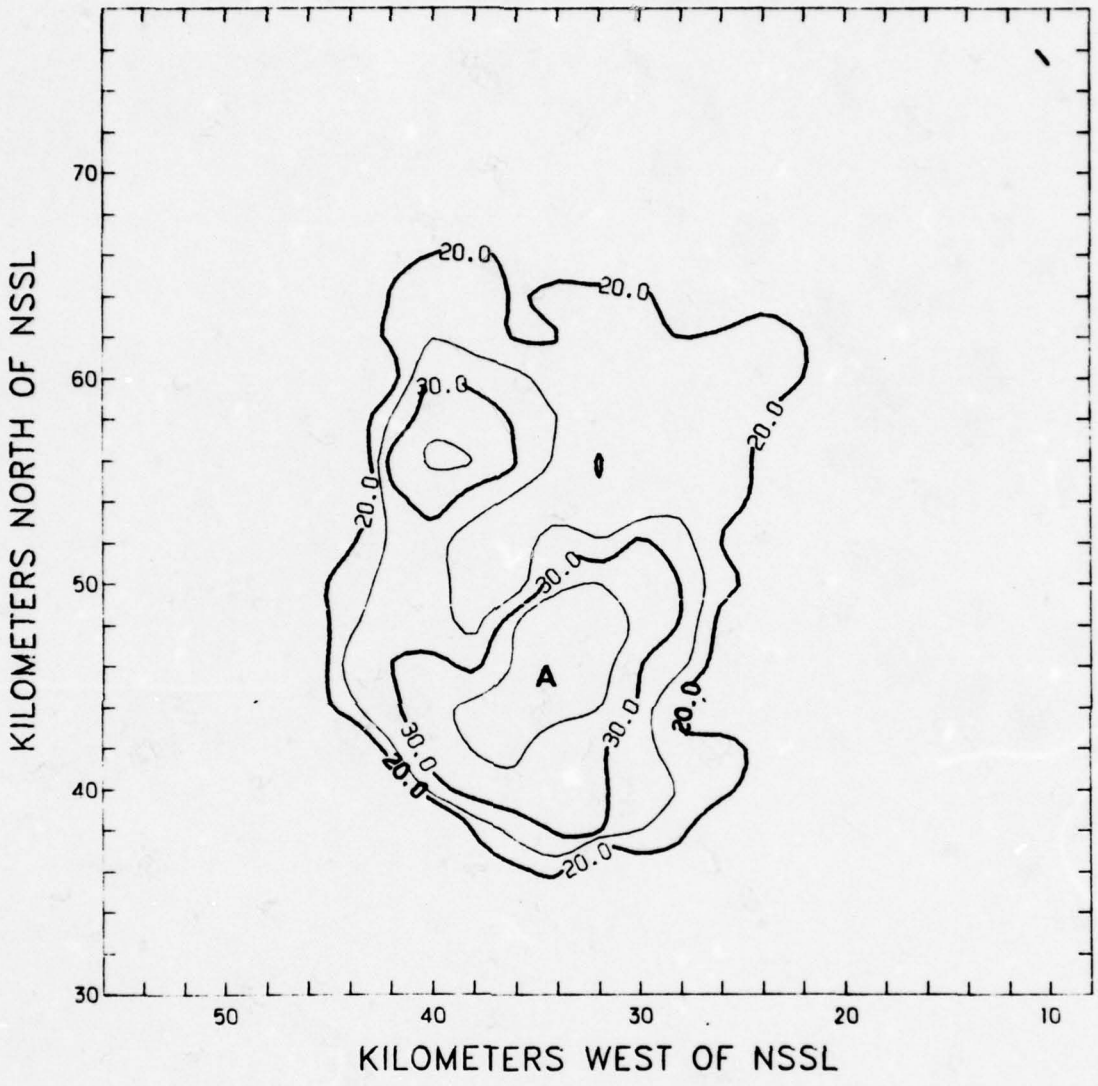

Fig. 13. The 40-kft CAZM, 1800 CST, 23 May 1974. Isopleths of reflectivity in dBZ.

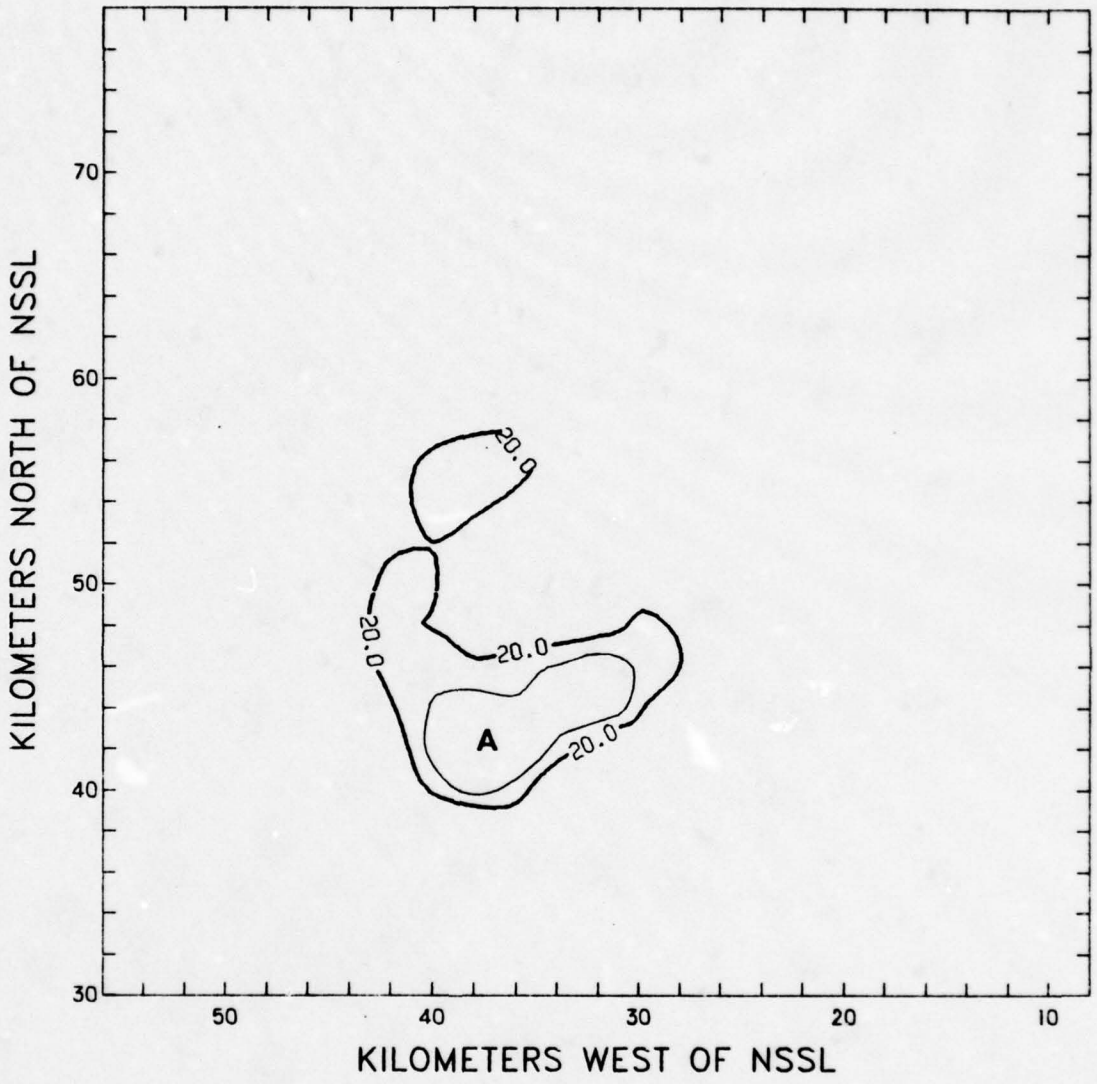

Fig. 14. The 45-kft CAZM, 1800 CST, 23 May 1974. Isopleths of reflectivity in dBZ.

Vogel [1973] continued Greene's work and discovered that "explosive development" in VIL appeared to be a necessary, but not sufficient, condition for the development of a tornado. It was inferred, however, that "explosive development" may be an indicator of the potential for a severe storm to develop, in itself of great value to a radar meteorologist.

Canipe [1973] discovered that VIL displays tend to mask the important small-scale features evident in the CAZM analyses of a severe-storm complex. Such features as a satellite cell, the bounded weak echo region (BWER), and the tilt of the storm core with height were masked. He concluded that while the VIL technique may have the advantage of being an expeditious and simple method of analysis for a real-time operation, it tends to smooth the data too much for a detailed examination of the structure and development of the severe storm. Therefore, Canipe developed a technique called the partial vertical integration of liquid water (PVIL). This technique entails integrating the liquid water content of a storm system in layers from 0 deg to 15 kft (the source region of the storm - no freezing), 15 kft to 35 kft (the active region - freezing), 35 kft to 50 kft (the ice region - above the -40-deg isotherm). By monitoring the changes taking place at each level, one can observe where development is occurring, and by plotting the centers of each layer, one can observe the dominant tilt of the storm system. This technique proved to be superior to VIL in that it retained some of the important features of the CAZM analyses and provided additional severe-storm signatures.

Partially Vertically-Summed Reflectivity Maps (PVSZ)

Pittman [1976] in cooperation with this author extended Canipe's [1973] work. Instead of converting the reflectivity factors to liquid water, Pittman simply summed the reflectivity factors in a vertical column above a given (x,y) point at the surface for the lower layer (0-deg to 15 kft), the middle layer (15 kft to 35 kft), and the upper layer (35 kft to 50 kft) of a storm complex. These PVSZ maps appear to retain the significant features of the CAZMs from which they are derived. Although the PVSZ technique requires less time than Canipe's PVIL scheme, the technique still uses too much computer memory and takes too much time ever to be useful in real-time operations.

Pittman's program requires 512 Kbytes of computer memory to process every other (even) range gate of information and takes approximately 18-20 sec to complete. In order to process every range gate of data it would require on the order of 1000 Kbytes or 1 Mbyte of computer memory and a significant increase in the time to complete the program. To be useful as a real-time operational technique, an alternate, less time-consuming method is required to process the data and at the same time insure that the significant features evident in the CAZM analyses of a severe storm are retained. This need led to the development of the data-reduction technique used in this investigation.

A New Data-Processing Technique

Digital radar data are collected and stored on magnetic tape in a spherical array of (r,α,ε). The primary requirement of any data-processing technique to be used in an operational environment is to min-

imize the amount of computer memory and time required to produce results. The time required to collect a typical three-dimensional data set for a storm system is approximately 3-4 min depending on the number of tilt angles needed. Since we must maintain continuity in time, we need to record a data set approximately every 10 min. If we use 3-4 min to collect the data set, we have 6-7 min left for processing the data set. The key to the new data processing technique used in this investigation is to interpolate along each radial of information by using the Lagrangian linear or cubic interpolation scheme.

For the new technique, the 0-deg tilt level is the base level for all summations and the vertical columns through which the reflectivity factors are to be summed are centered on the range gates at the 0-deg level. In Figure 15, each dot at the intersection of a column and radial is an interpolation point. The procedure to produce a PVSZ map requires several steps. Thus for each azimuthal radial at a given elevation angle:

1. Proceed sequentially in range along a given radial (α_i) until the first non-zero reflectivity factor is found.

2. If the reflectivity factors at the given range, r_i, and at r_{i+1} are equal, no interpolation is required.

3. If, however, the reflectivity factors are unequal, then calculate the radial distance, r', to the point on the data radial that intersects the vertical column extending above the applicable range gate, r_i, at the surface (see Figure 16). Here h is derived from Eq (14) and is given by

$$h = r \tan \varepsilon_i + \frac{r^2}{2R'} \qquad (20)$$

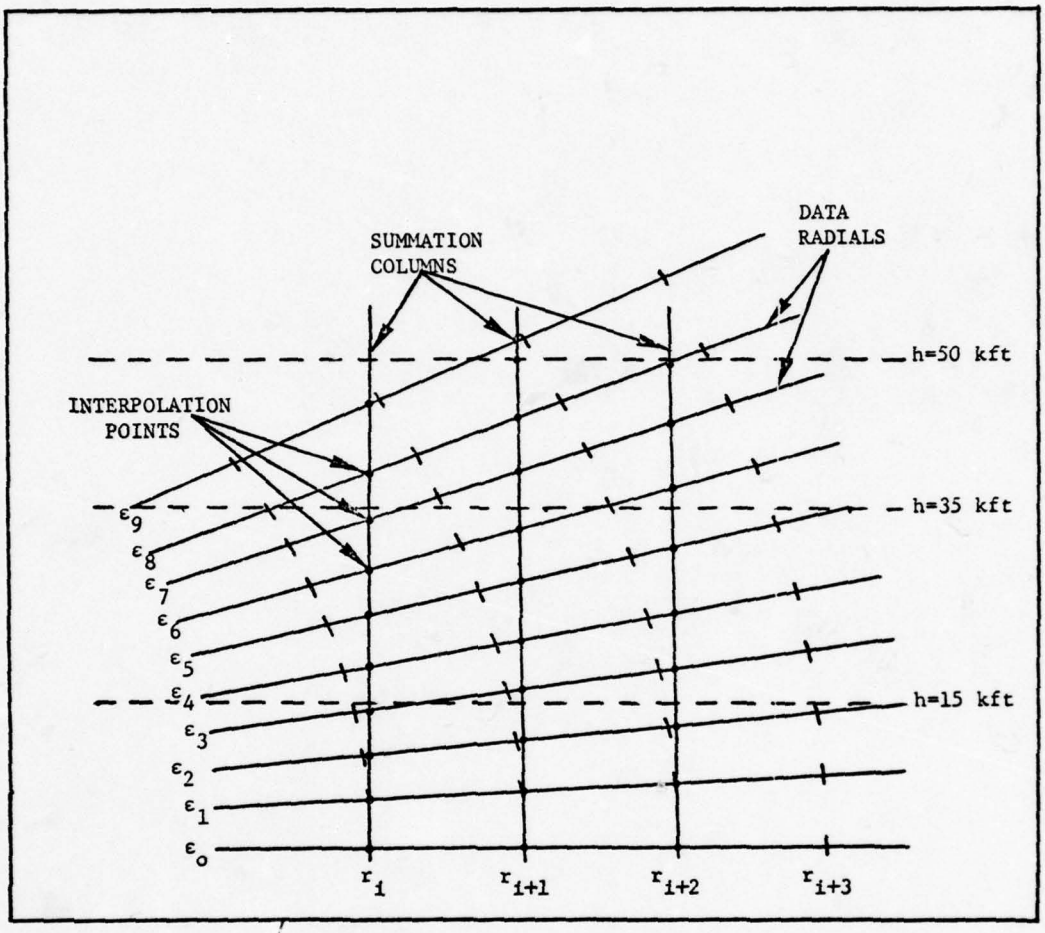

Fig. 15. Interpolation points in the plane of α used in constructing PVSZ layers.

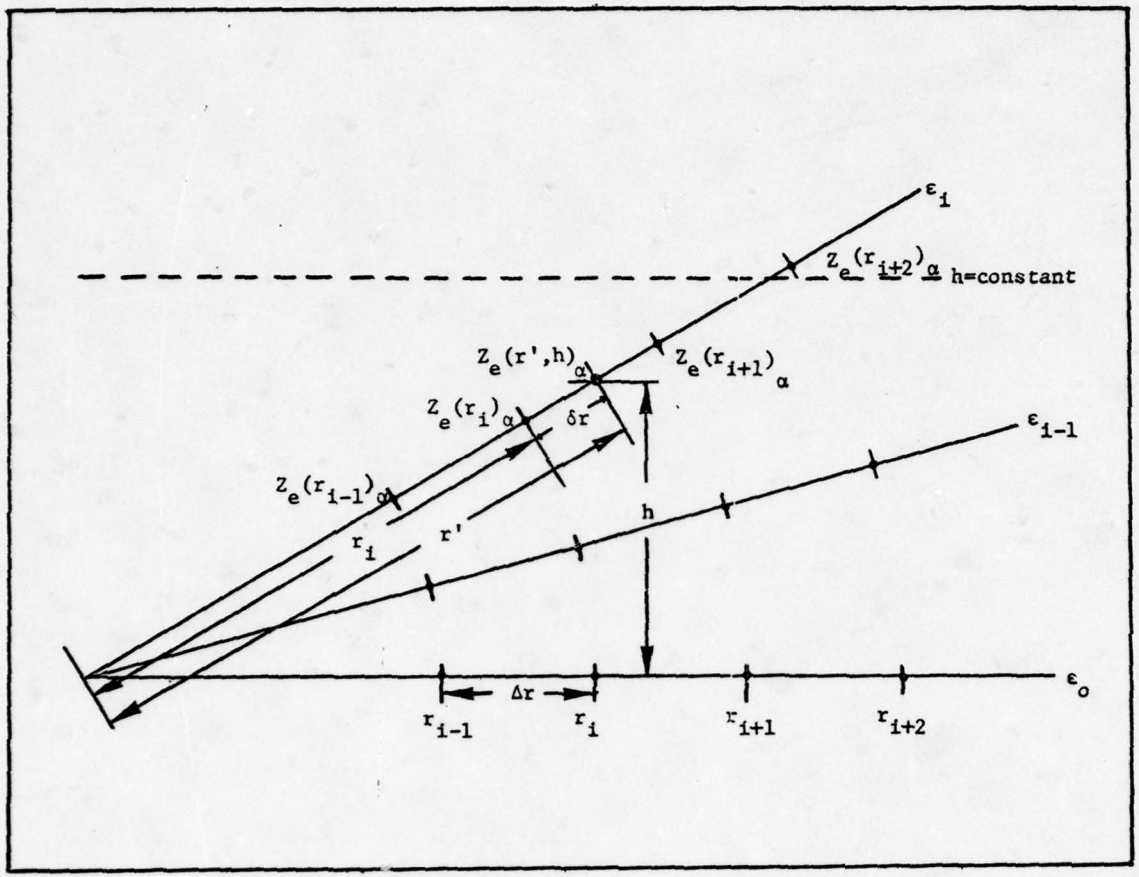

Fig. 16. The interpolation of $Z_e(r',h)_\alpha$ along a radial (ε_i) in the plane of α.

and

$$r' = \sqrt{r^2 + h^2} \tag{21}$$

4. Compute the distance from r_i to r'

$$\delta r = r' - r_i \tag{22}$$

If $\delta r < 1$, the four data points used in the Lagrangian cubic interpolation formula are r_{i-1}, r_i, r_{i+1} and r_{i+2}. If $\delta r \geq 1$, i is increased by 1 and δr decreased by 1; if $\delta r \geq 2$, i is increased by 2 and δr is decreased by 2; etc.

5. Interpolate the value of the reflectivity factor at the point (r',h) by using the Lagrangian cubic form of the interpolating polynomial given by

$$Z_e(r') = \sum_{k=0}^{3} Ze(r_{i-1+k})\, L_k(r') \tag{23}$$

where

$$L_k(r') = \prod_{\substack{j=0 \\ j\neq k}}^{3} \frac{r' - r_{i-1+j}}{r_{i-1+k} - r_{i-1+j}} \tag{24}$$

An alternate form of the Lagrangian interpolating polynomial used in this investigation is given by

$$\begin{aligned} Z_e(r') = {} & a_0 (r'-r_i)(r'-r_{i+1})(r'-r_{i+2}) \\ & + a_1 (r'-r_{i-1})(r'-r_{i+1})(r'-r_{i+2}) \\ & + a_2 (r'-r_{i-1})(r'-r_i)(r'-r_{i+2}) \\ & + a_3 (r'-r_{i-1})(r'-r_i)(r'-r_{i+1}) \end{aligned} \tag{25}$$

where

$$a_0 = \frac{Z_e(r_{i-1})}{(r_{i-1}-r_i)(r_{i-1}-r_{i+1})(r_{i-1}-r_{i+2})}$$

$$a_1 = \frac{Z_e(r_i)}{(r_i-r_{i-1})(r_i-r_{i+1})(r_i-r_{i+2})}$$

$$a_2 = \frac{Z_e(r_{i+1})}{(r_{i+1}-r_{i-1})(r_{i+1}-r_i)(r_{i+1}-r_{i+2})}$$

$$a_3 = \frac{Z_e(r_{i+2})}{(r_{i+2}-r_{i-1})(r_{i+2}-r_i)(r_{i+2}-r_{i+1})} \qquad (26)$$

We always use a constant base interval, Δr, so that the programming steps are greatly simplified. The off-diagonal elements of the matrix used to calculate the value of $Z_e(r')$ are constant and thus only the diagonal elements of the matrix need be computed. If a linear interpolation is required, only the two points immediately adjacent to r' are used.

6. Once the value of $Z_e(r',h)$ is known, the value of h is tested to determine whether $Z_e(r',h)$ is to be added into the lower PVSZ layer (0-deg to 15 kft), the middle PVSZ layer (15 kft to 35 kft), or the upper PVSZ layer (35 kft to 50 kft).

7. Note in Figure 15 that the number of interpolation points at r_i included in the lower layer will be four, the middle layer four, and the upper layer two; at r_{i+1}, the interpolation points included in the lower layer will be three, the middle layer four, and the upper layer two; etc. Therefore, we cannot simply sum the interpolated reflectivity factors in a layer at each range or we will produce erroneous

gradients of reflectivity due to the fact that in the lower layer at r_i there are four reflectivity factors summed and at r_{i+1} there are three reflectivity factors summed. Thus the value of each Z_e (r',h) is divided by the number of tilt angles of data that are actually available in the applicable layer for that range. The number of tilt angles included in the lower, middle, and upper layers at each range are calculated at the beginning of the program and maintained in arrays IDIV1 for the lower layer, IDIV2 for the middle layer, and IDIV3 for the upper layer. The resultant value of the reflectivity factor divided by IDIV1, IDIV2, or IDIV3 then is added to the previous values for that column and layer. For example, if we have ten elevation angles (0,1,2, 4,6,8,10,12,14, and 16 deg) in our data set and we are processing the 217^{o} radial at an elevation angle, ε = 4 deg, and r = 50 km,

h_4 = 11.95 kft

r'_4 = 50.122 km

δr = 0.122 km

IDIV1 = 4

IDIV2 = 3

IDIV3 = 3

Since h < 15 kft the interpolated reflectivity factor $Z_e\ (r'_4,h_4)_{\varepsilon=4\ deg}$ will be included in the lower layer and we then have for the column at range r

$$PVSZ1\ (r,\alpha) = \left(\frac{Z_e(r,h_0)_{\varepsilon=0\ deg}}{4} + \frac{Z_e(r'_1,h_1)_{\varepsilon=1\ deg}}{4} + \frac{Z_e(r'_2,h_2)_{\varepsilon=2\ deg}}{4}\right) + \frac{Z_e(r'_3,h_3)_{\varepsilon=4\ deg}}{4} \qquad (26)$$

These steps are repeated until all of the data have been processed for one sequence of tilt angles. Thus, we have three PVSZ arrays in (r,α) coordinates representing the three layers of the storm complex. The value of the summed reflectivity factors at any given point in a PVSZ array represents the average reflectivity in the layer at that point. Therefore, the elements of the three PVSZ arrays are multiplied by the appropriate number of CAZM levels in each layer in order to provide a weighted average reflectivity. That is, PVSZ1 (r,α) is multiplied by 4 because there are 4 CAZM levels (0-deg, 5 kft, 10 kft, and 15 kft) in the lower level; PVSZ2 (r,α) is multiplied by 4; PVSZ3 (r,α) is multiplied by 3. The final PVSZ arrays then are transformed from (r,α) coordinates to (x,y) coordinates by using an altered version of the quadratic scheme used by Pittman [1976] and modified to interpolate data at 1-km instead of 2-km intervals. In addition, the PVSZ arrays were transformed to (x,y) coordinates by using a simple linear scheme. Examples of the results obtained by using various combinations of Lagrangian cubic (LAG) and linear (LIN) interpolation along radials and quadratic (QUAD) and linear (LIN) schemes in the x,y plane along with a comparison of these PVSZ maps with PVSZ maps generated by using Pittman's [1976] technique are presented in the next chapter.

CHAPTER III

PRESENTATION AND DISCUSSION OF RESULTS

Although CAZM analyses provide the most detail for studying the three-dimensional structure of a severe-storm complex, the program to produce CAZMs is far too complex and time consuming for real-time applications. Therefore, a simpler, less cumbersome, method must be developed to reduce the digital radar data in near real time. It is imperative, however, that any data-reduction technique developed for use in such an operation preserve the significant characteristics evident in the CAZM analyses and the important three-dimensional characteristics of the storm complex.

The severe-storm data recorded by NSSL on 23 May 1974 and 8 June 1974 were used to test the applicability of the various interpolation schemes used in this investigation. The digitized radar data were processed by means of Lagrangian cubic (LAG) and linear (LIN) interpolation schemes along each radial of information and then by means of linear and quadratic (QUAD) interpolation schemes in the horizontal plane. PVSZ maps were generated for each technique and time period. The resultant PVSZ maps are labelled according to the interpolation scheme used. For example, a PVSZ map which was constructed by using a Lagrangian cubic interpolation scheme along the radial and the quadratic interpolation scheme in the horizontal plane would be labelled (LAG-QUAD). The PVSZ maps generated by using various combinations of interpolation schemes were compared to determine whether or not the PVSZ maps show any major differences in appearance of the storm. Next,

the PVSZ maps were compared to CAZM and PVSZ maps generated by Pittman [1976] for the same time period. In addition, the number of PVSZ layers was varied to determine whether or not the vertical structure of a storm is better represented by three or four layers. Finally, the severe-storm data from MIT were processed and analyzed. The results of these comparisons follow.

Comparison of Various Interpolation Schemes

The first storm system analyzed was the Yukon storm which is explained in detail by Pittman [1976]. The CAZM analyses for 1800 CST, 23 May 1974, are shown in Figures 5 through 14. The lower-, middle-, and upper-layer PVSZ maps generated by using the Lagrangian cubic and quadratic interpolation schemes (LAG-QUAD) are shown in Figures 17 through 19. The lower-, middle-, and upper-layer PVSZ maps generated by using the linear and quadratic interpolation schemes (LIN-QUAD) are shown in Figures 20 through 22. It can be seen from these analyses that the basic appearance of the storm complex remains unchanged. The main advantage of using the Lagrangian cubic interpolation scheme along each radial is that any quadratic or cubic tendencies in the data will be retained, whereas the reflectivities generated by using the linear interpolation scheme will not reflect these tendencies and will result in a slightly smoother appearance of the reflectivity contours. Of primary importance, however, is the fact that the significant characteristics of the CAZMs (see Figures 5 through 8) in the lower layer (surface to 15 kft) are all retained in the lower layer PVSZ map. The main or parent cell (cell A), the satellite cell (cell B), and the

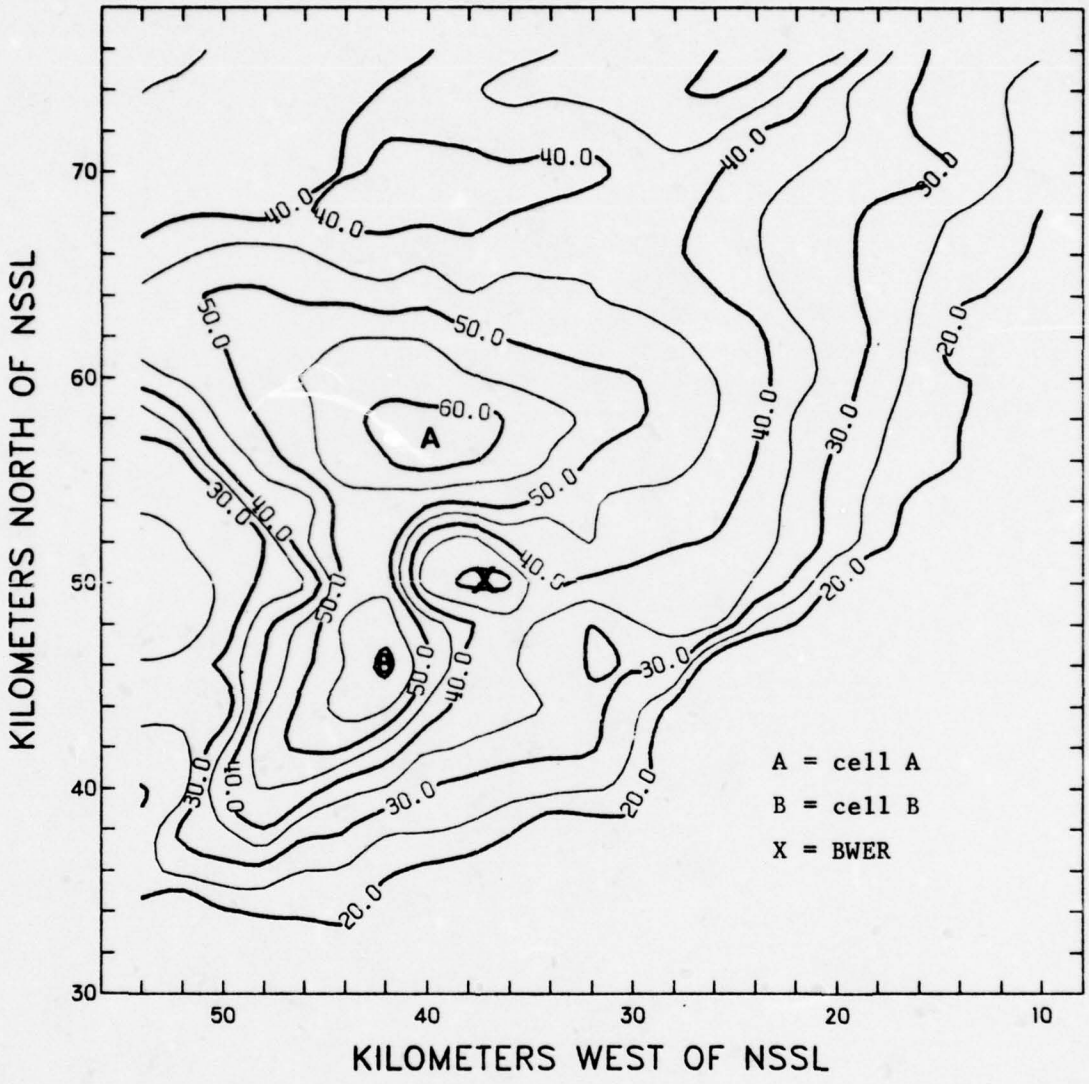

Fig. 17. Lower-layer PVSZ map (LAG-QUAD) for 1800 CST, 23 May 1974. Isopleths of reflectivity in dBZ.

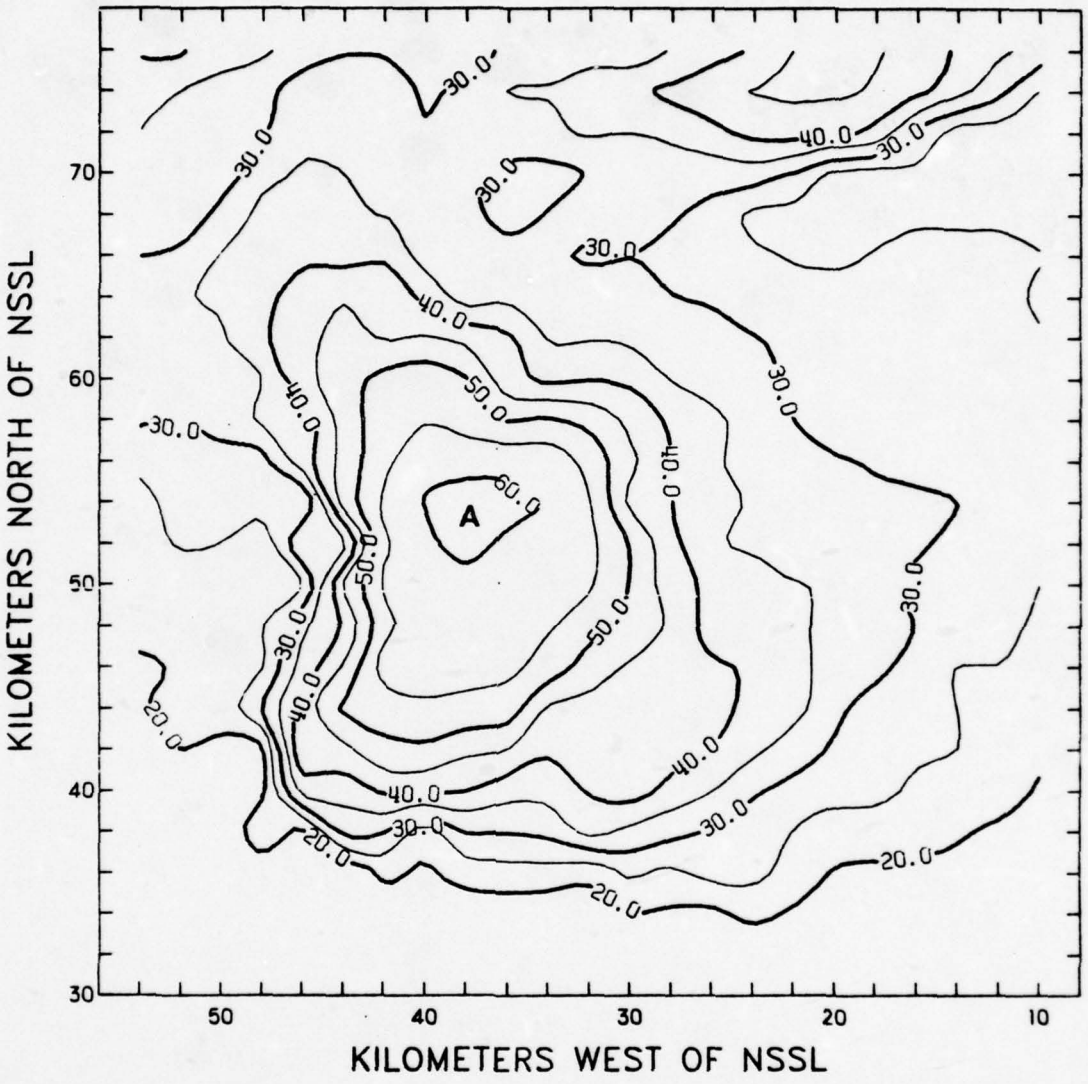

Fig. 18. Middle-layer PVSZ map (LAG-QUAD) for 1800 CST, 23 May 1974. Isopleths of reflectivity in dBZ.

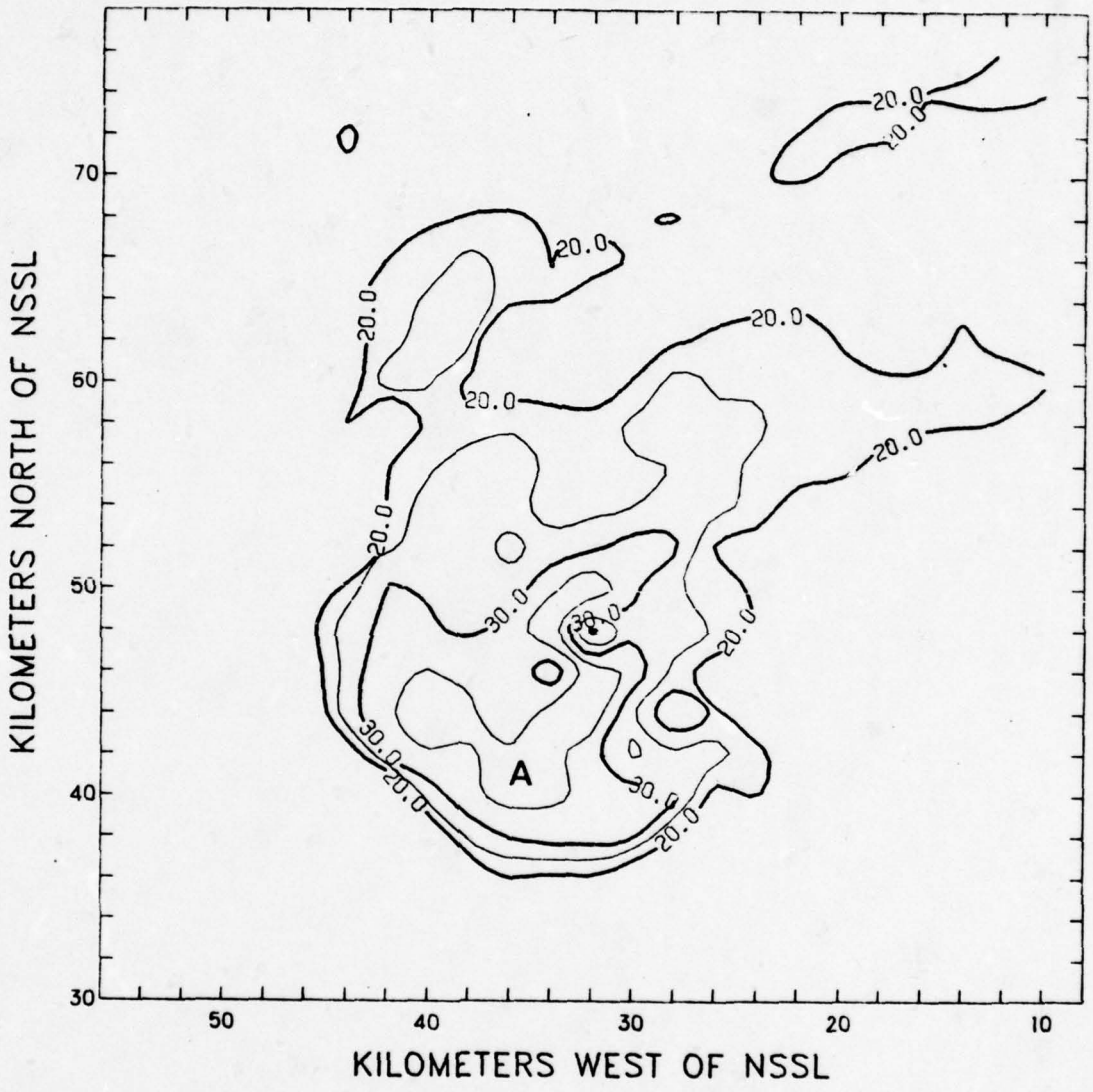

Fig. 19. Upper-layer PVSZ map (LAG-QUAD) for 1800 CST, 23 May 1974. Isopleths of reflectivity in dBZ.

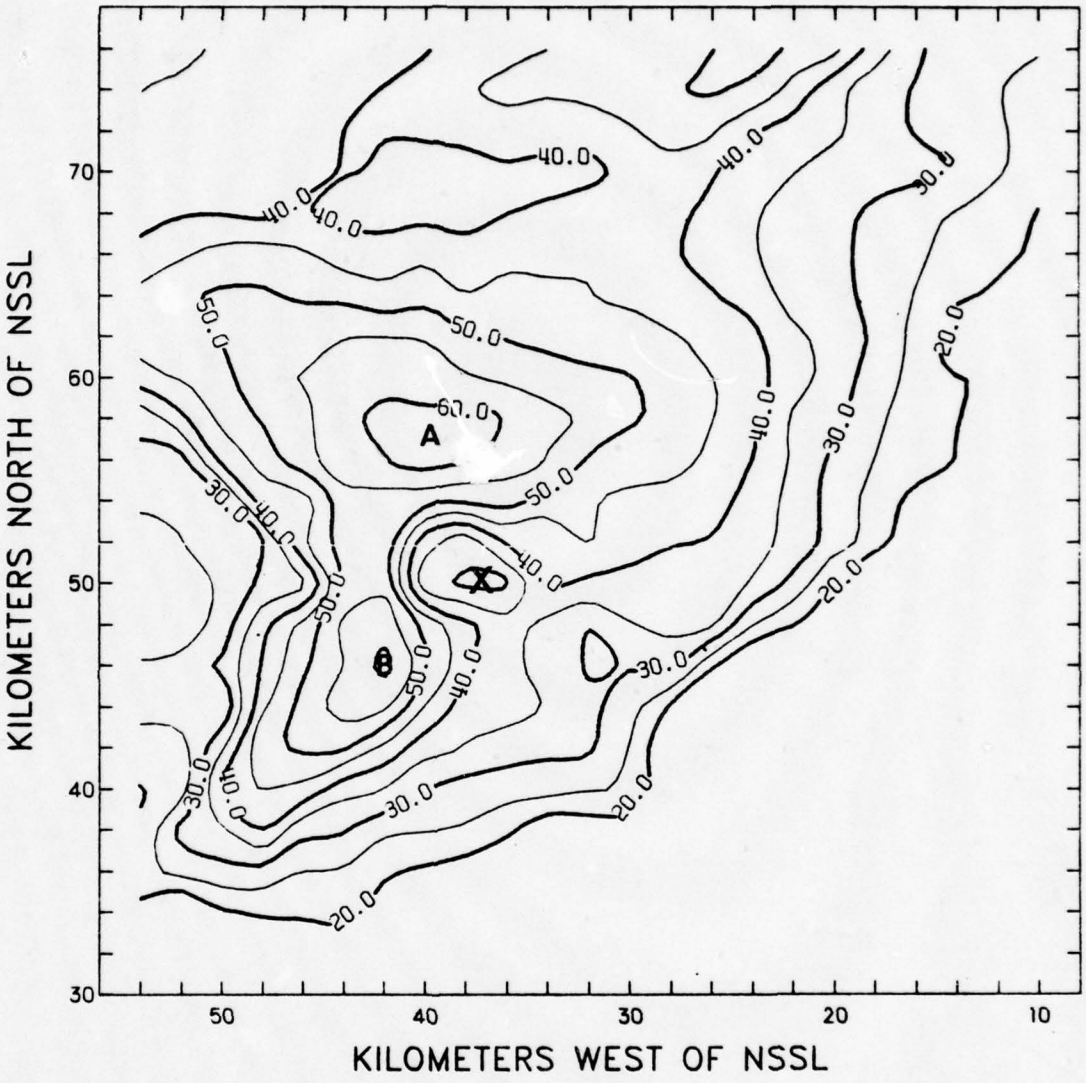

Fig. 20. Lower-layer PVSZ map (LIN-QUAD) for 1800 CST, 23 May 1974. Isopleths of reflectivity in dBZ.

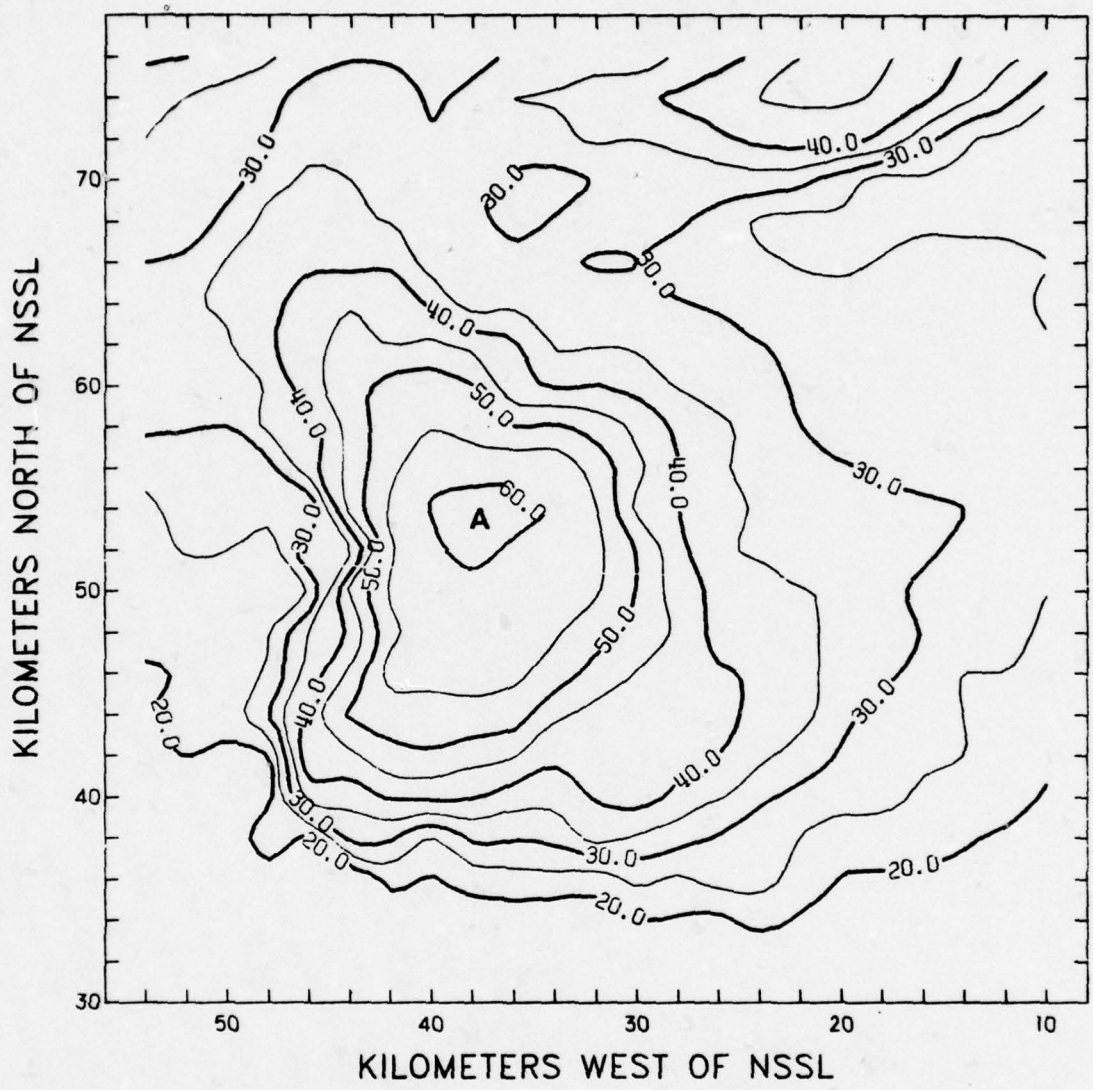

Fig. 21. Middle-layer PVSZ map (LIN-QUAD) for 1800 CST, 23 May 1974. Isopleths of reflectivity in dBZ.

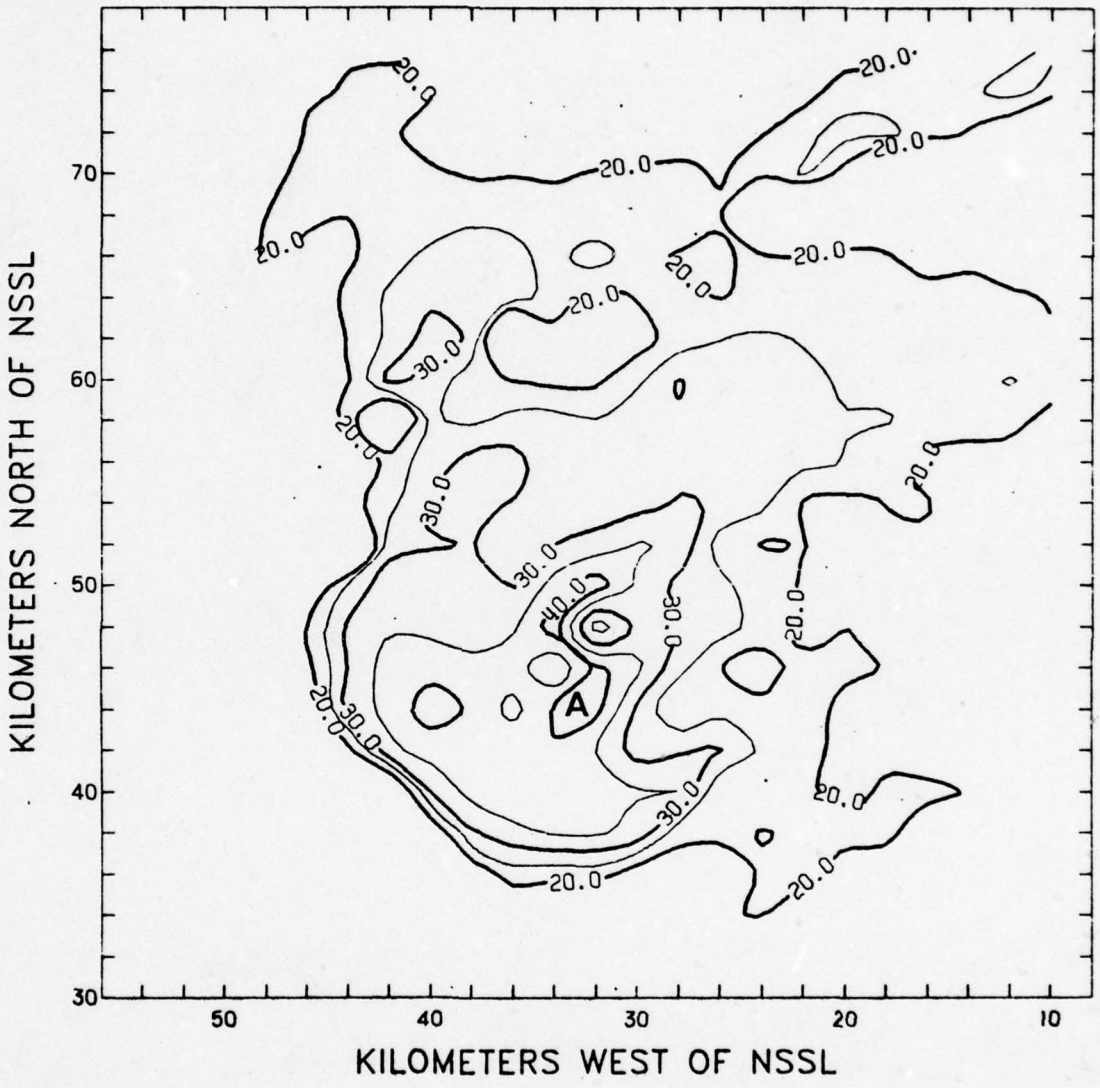

Fig. 22. Upper-layer PVSZ map (LIN-QUAD) for 1800 CST, 23 May 1974. Isopleths of reflectivity in dBZ.

bounded weak echo region (BWER) (cell X) are all preserved. In addition, note the strong gradient of reflectivity between the BWER and cell B. As indicated by Pittman [1976], this may be one of the criteria for identifying a severe storm with tornadic tendencies. The gradient of reflectivity in the LAG-QUAD case and the LIN-QUAD case are on the order of 6.8 dBZ/km.

The PVSZ maps that resulted from using the Lagrangian cubic and linear interpolation schemes (LAG-LIN) together with the PVSZ maps that resulted from using the linear and linear interpolation schemes (LIN-LIN) are shown in Figures 23 through 28. It is obvious that by using the linear interpolation scheme in the x,y plane, the reflectivity contour patterns are much smoother and the gradient of reflectivity between the BWER and cell B is weaker (on the order of 5.7 dBZ/km). In addition, any non-linear tendencies in the data will not be reflected in maps generated by using the linear interpolation scheme. Notice, however, that even the LIN-LIN combination of interpolation schemes retains the significant features of the CAZM analyses.

The middle- and upper-layer PVSZ maps show much the same results. The Lagrangian cubic and quadratic combination of interpolation schemes (LAG-QUAD) exhibits the most detail, while the linear interpolation scheme in the x,y plane causes the small scale wriggles in the reflectivity contour patterns to be smoothed out. Furthermore, the gradients of reflectivity become much weaker by use of the linear interpolation scheme. However, as was the case for the lower-layer PVSZ maps, the significant features of the CAZMs are retained in all four combinations of interpolation schemes. It is interesting to note that

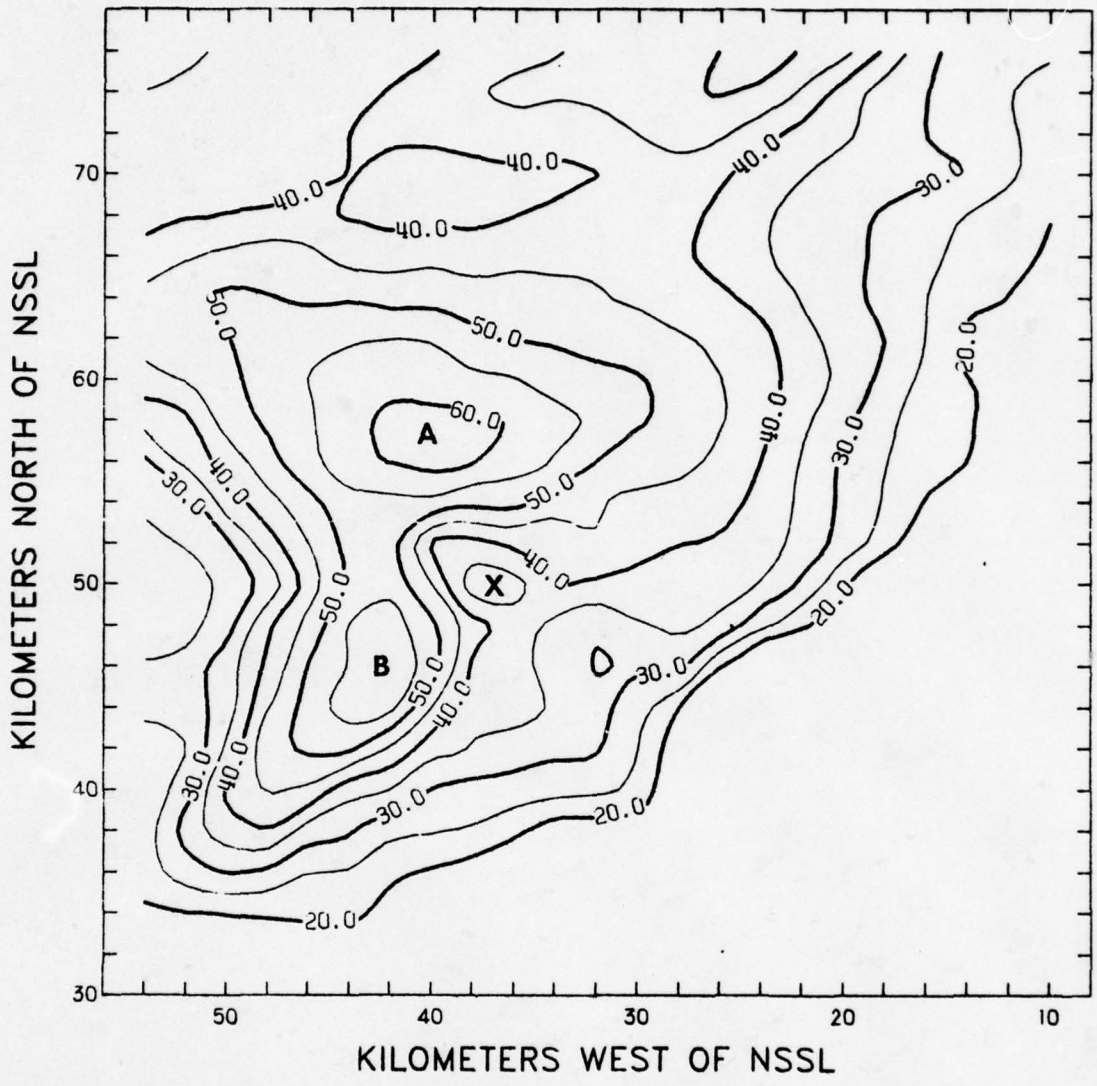

Fig. 23. Lower-layer PVSZ map (LAG-LIN) for 1800 CST, 23 May 1974. Isopleths of reflectivity in dBZ.

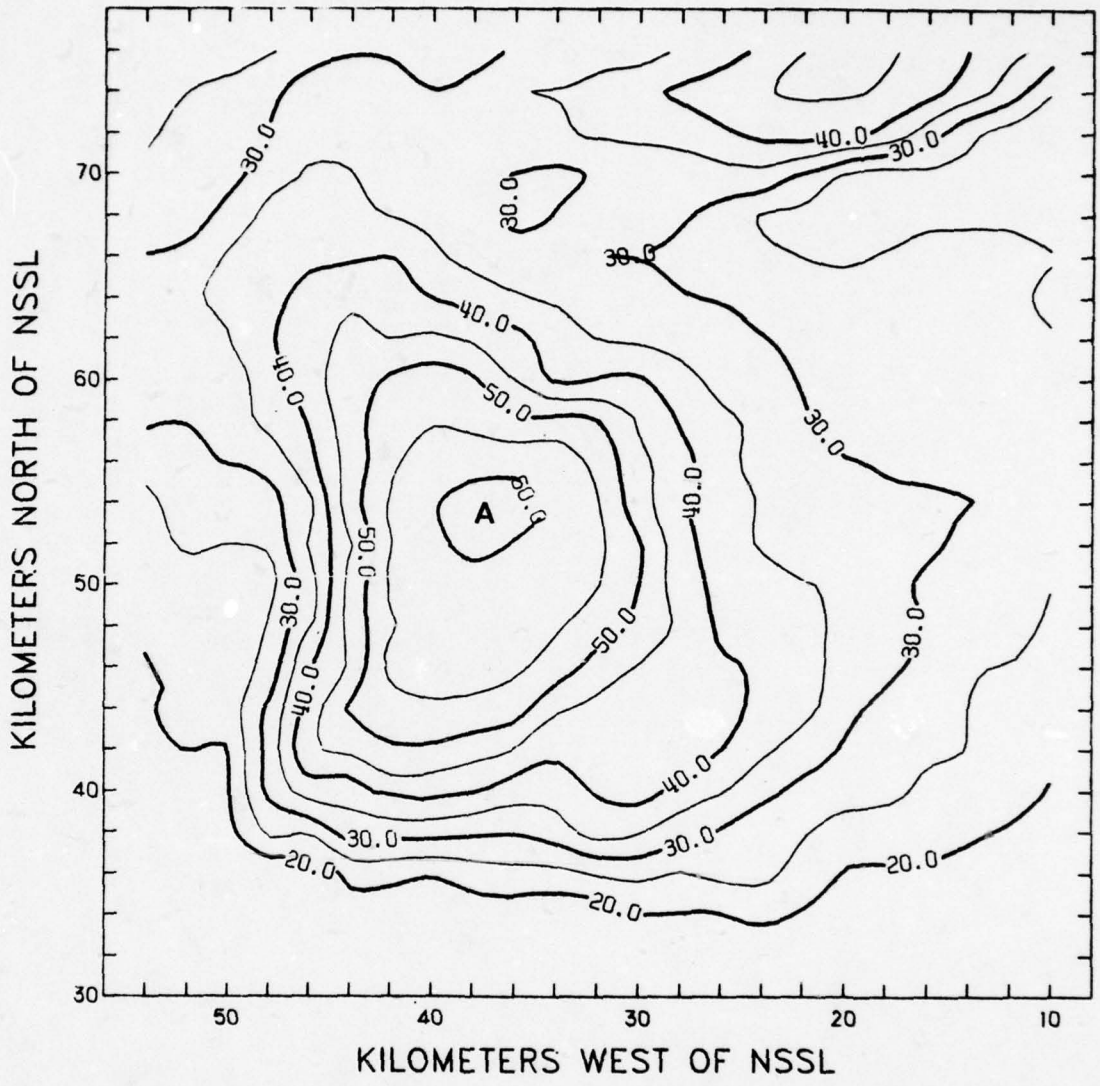

Fig. 24. Middle-layer PVSZ map (LAG-LIN) for 1800 CST, 23 May 1974. Isopleths of reflectivity in dBZ.

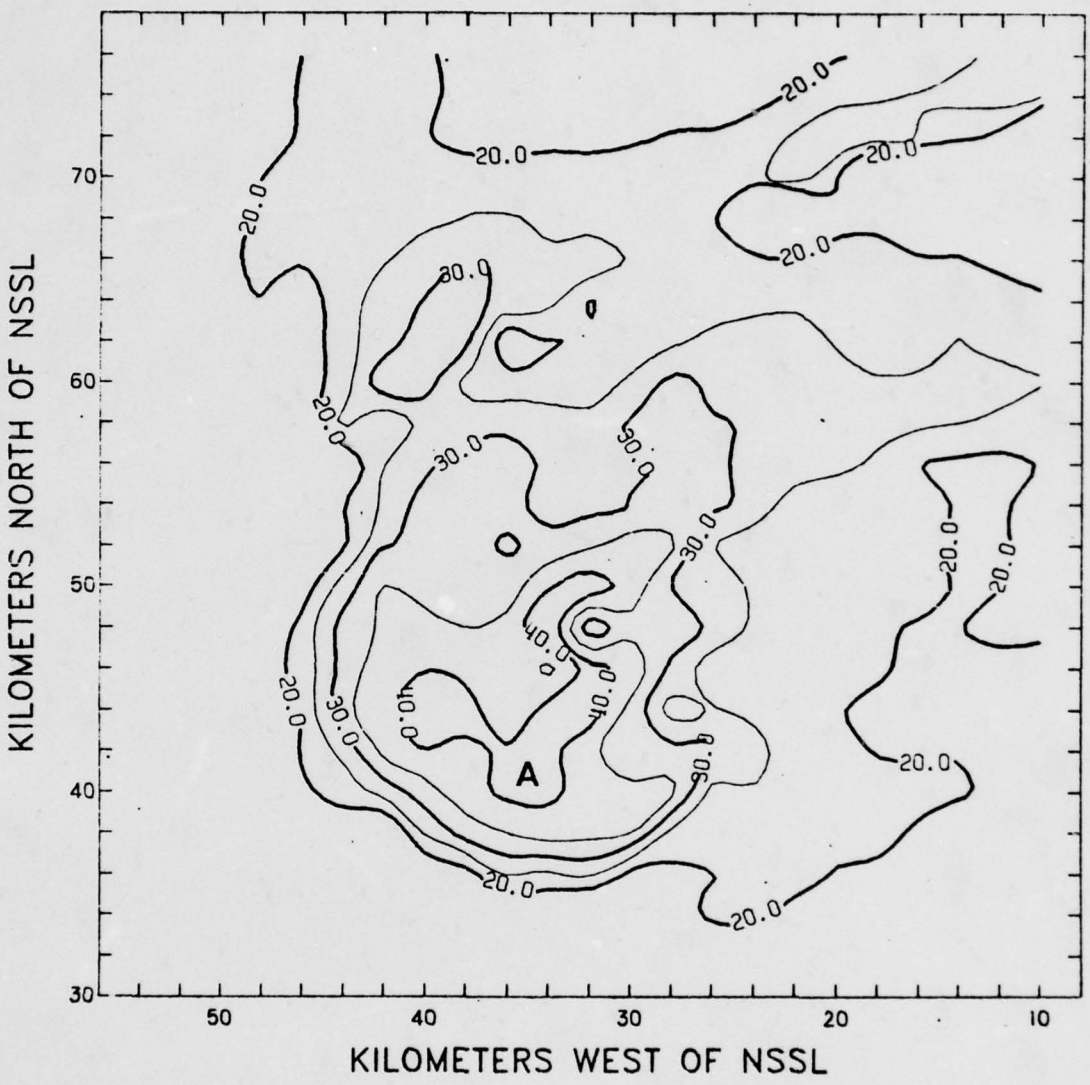

Fig. 25. Upper-layer PVSZ map (LAG-LIN) for 1800 CST, 23 May 1974. Isopleths of reflectivity in dBZ.

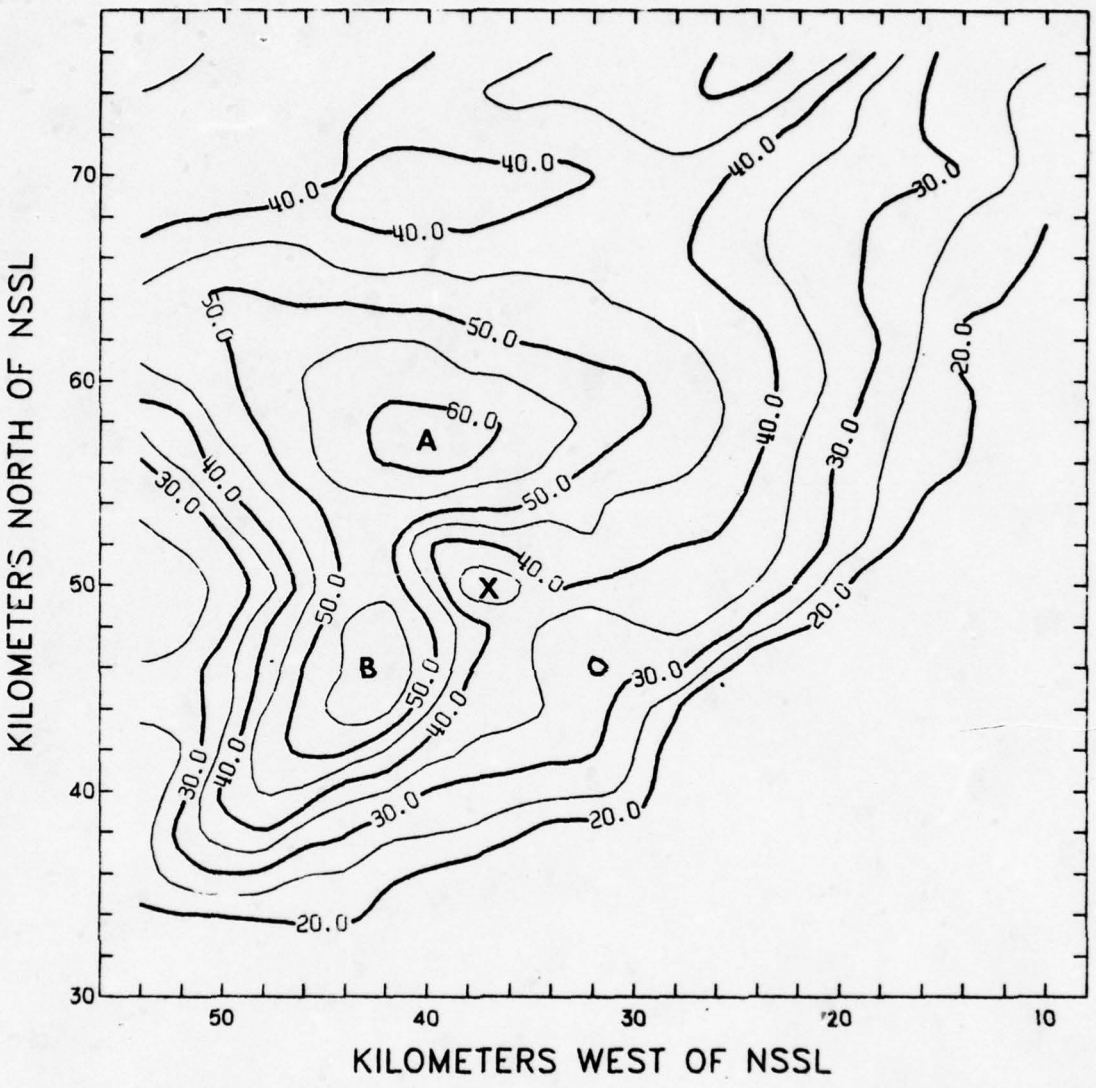

Fig. 26. Lower-layer PVSZ map (LIN-LIN) for 1800 CST, 23 May 1974. Isopleths of reflectivity in dBZ.

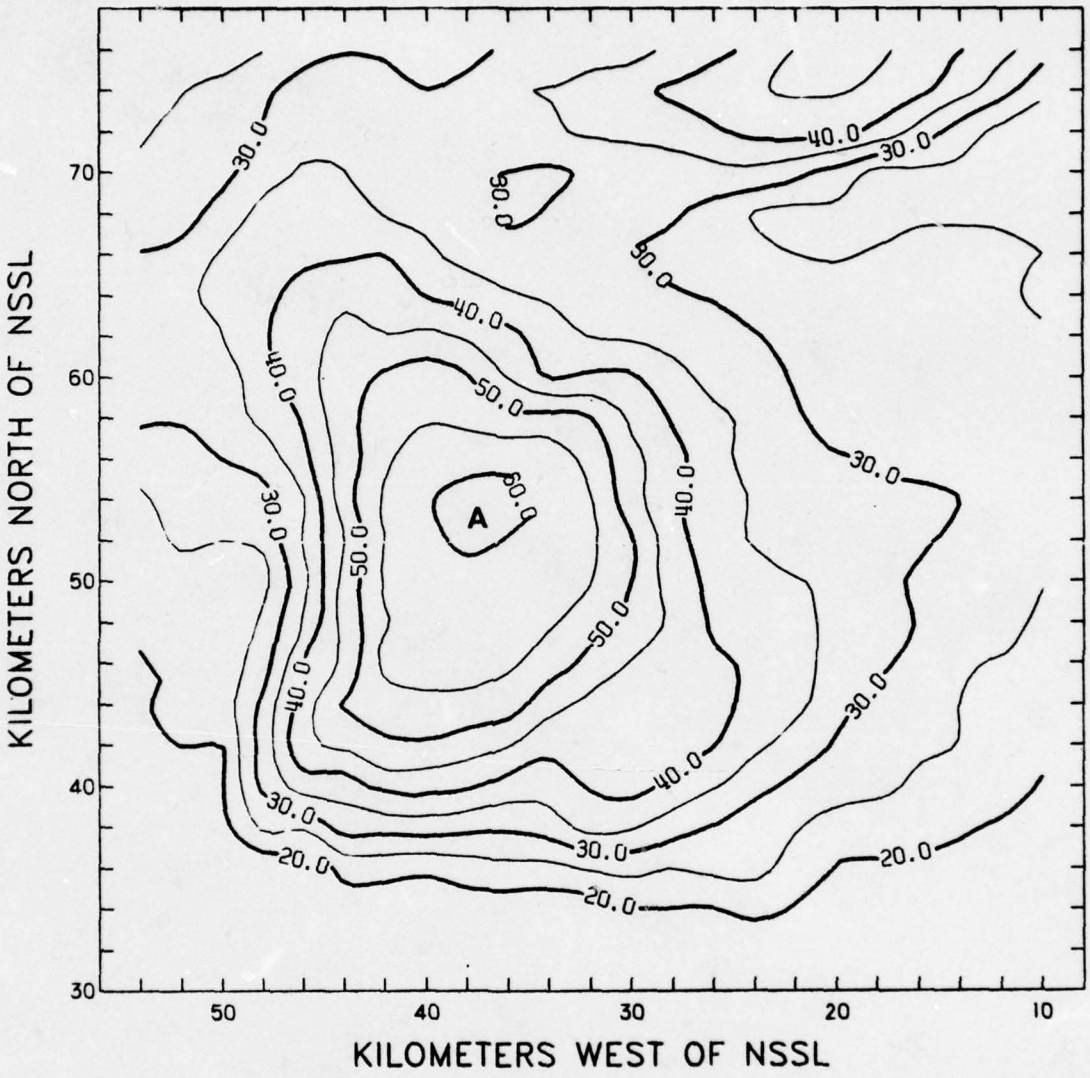

Fig. 27. Middle-layer PVSZ map (LIN-LIN) for 1800 CST, 23 May 1974. Isopleths of reflectivity in dBZ.

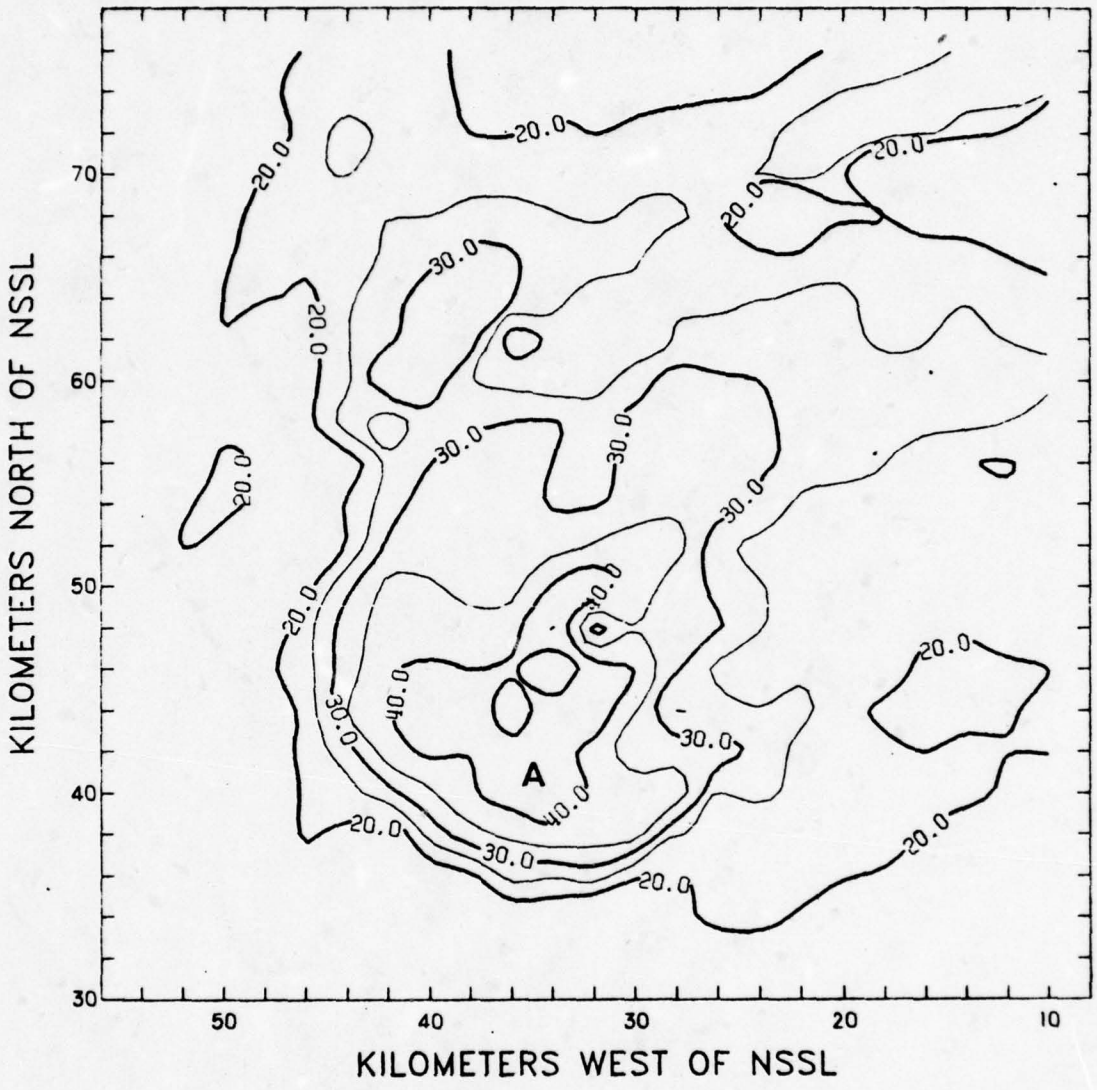

Fig. 28. Upper-layer PVSZ map (LIN-LIN) for 1800 CST, 23 May 1974. Isopleths of reflectivity in dBZ.

the amount of computer (execution) time to complete the LAG-QUAD program on the Amdahl 470 V/6 was ∿ 9.3 sec while the LIN-LIN program requires ∿ 9.0 sec to complete. Of course, the time required to execute the program is dependent upon the size of the analysis area (100 km^2 in our case) and the percentage of this area covered by detectable radar echoes.

Comparisons with Pittman's PVSZ Maps

As stated earlier, Pittman [1976] produced PVSZ maps for the same time period. Therefore, it was logical to compare the PVSZ maps generated by using the new interpolation schemes with Pittman's PVSZ maps. The PVSZ maps obtained from Pittman's program were processed by using the same CONREC contour subroutine which produced all of the CAZMs and PVSZ maps previously shown.

The first sets of maps compared were for 1800 CST, 23 May 1974. The lower-, middle-, and upper-layer PVSZ maps generated by using the Lagrangian cubic and quadratic interpolation schemes (see Figures 17 through 19) were compared with Pittman's PVSZ maps shown in Figures 29 through 31. For comparison, the CAZMs for this time period were used (see Figures 5 through 14).

When the lower-layer PVSZ map (LAG-QUAD) is compared with Pittman's lower-layer PVSZ map, there are significant differences. The first and most important difference is the fact that the LAG-QUAD PVSZ map shows a BWER and Pittman's PVSZ map shows only a weak echo region (WER). Note, however, that the CAZM analyses for the lower layer (see Figures 5 through 8) indicate that a BWER does in fact exist in the

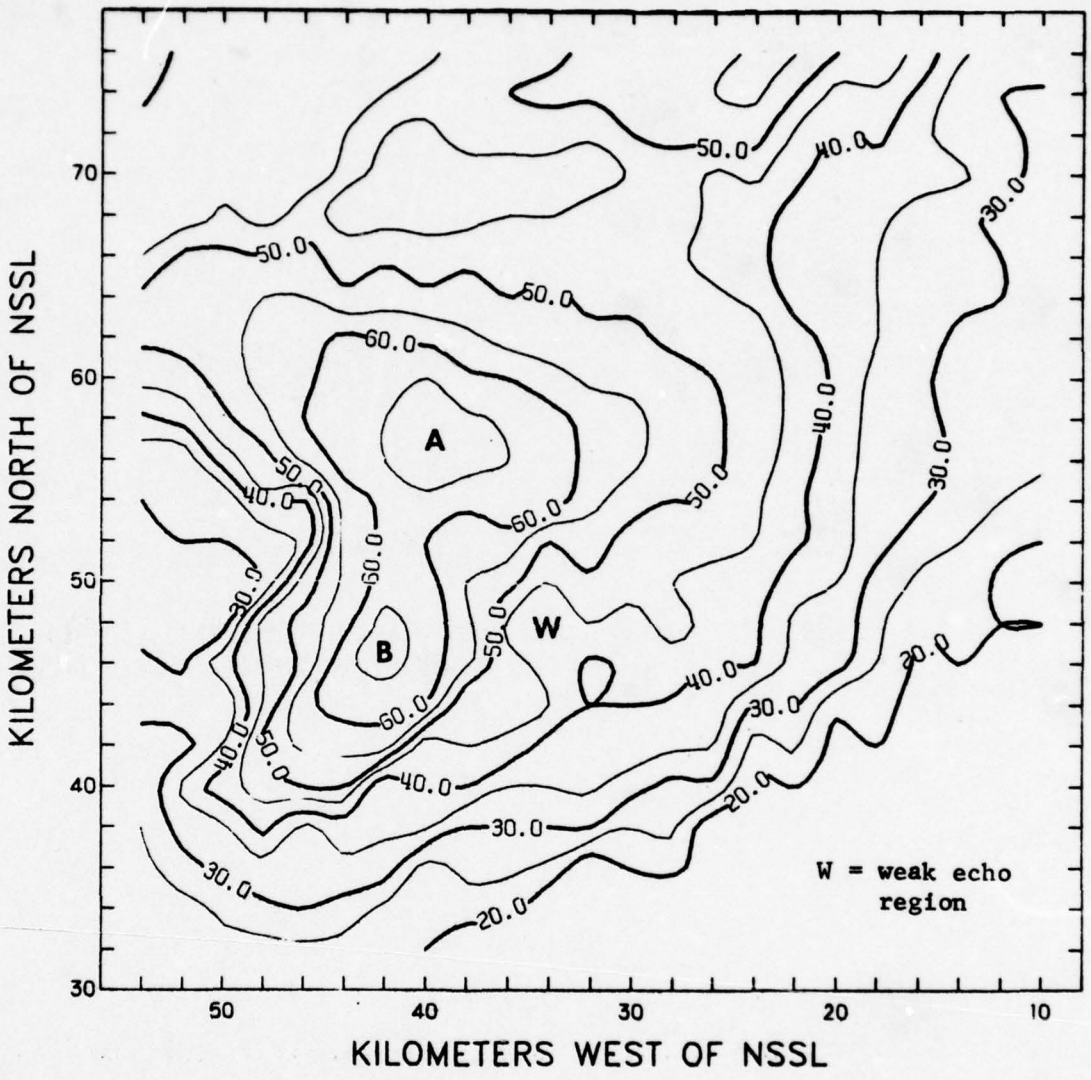

Fig. 29. Pittman's lower-layer PVSZ map for 1800 CST, 23 May 1974. Isopleths of reflectivity in dBZ.

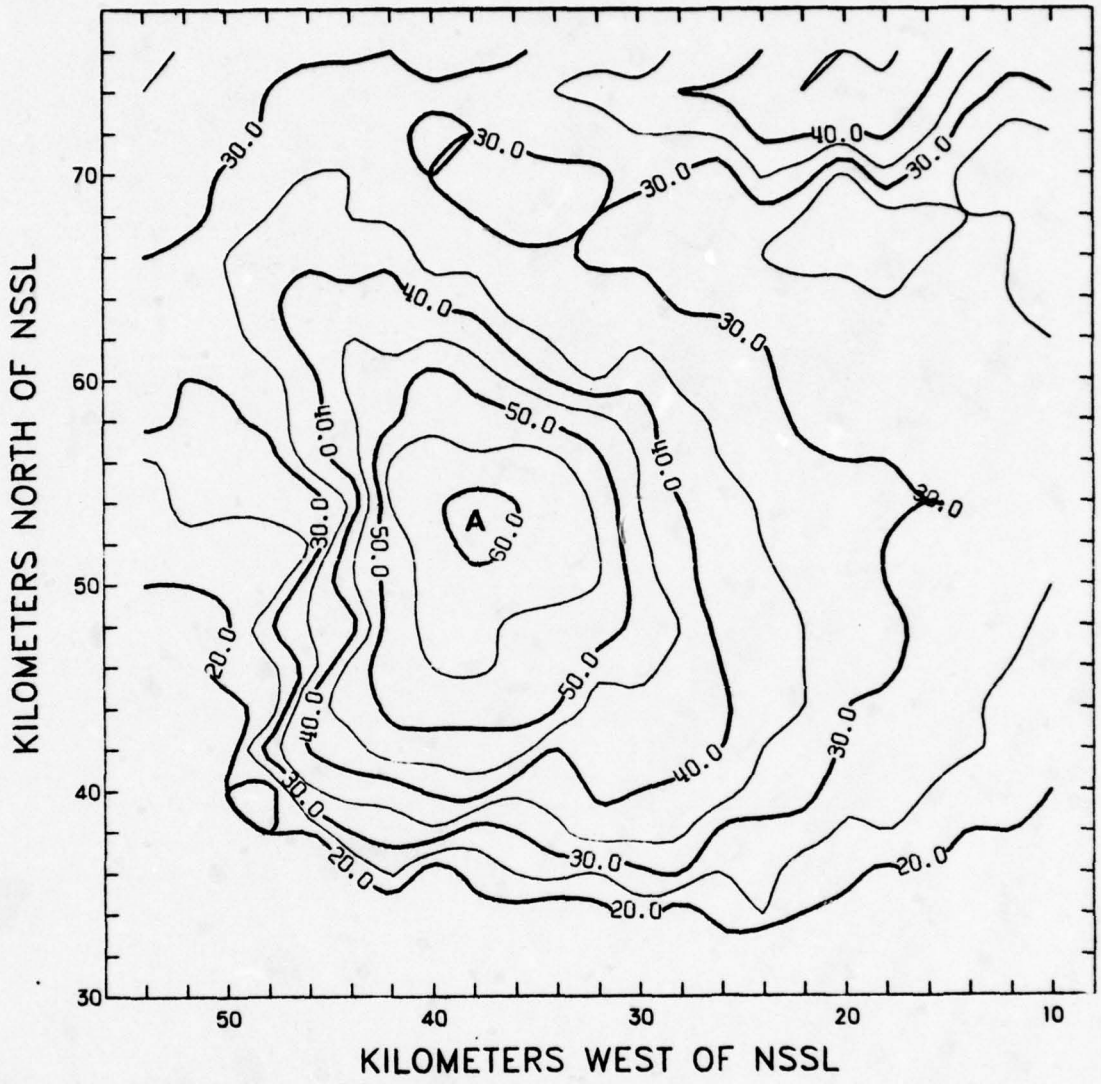

Fig. 30. Pittman's middle-layer PVSZ map for 1800 CST, 23 May 1974. Isopleths of reflectivity in dBZ.

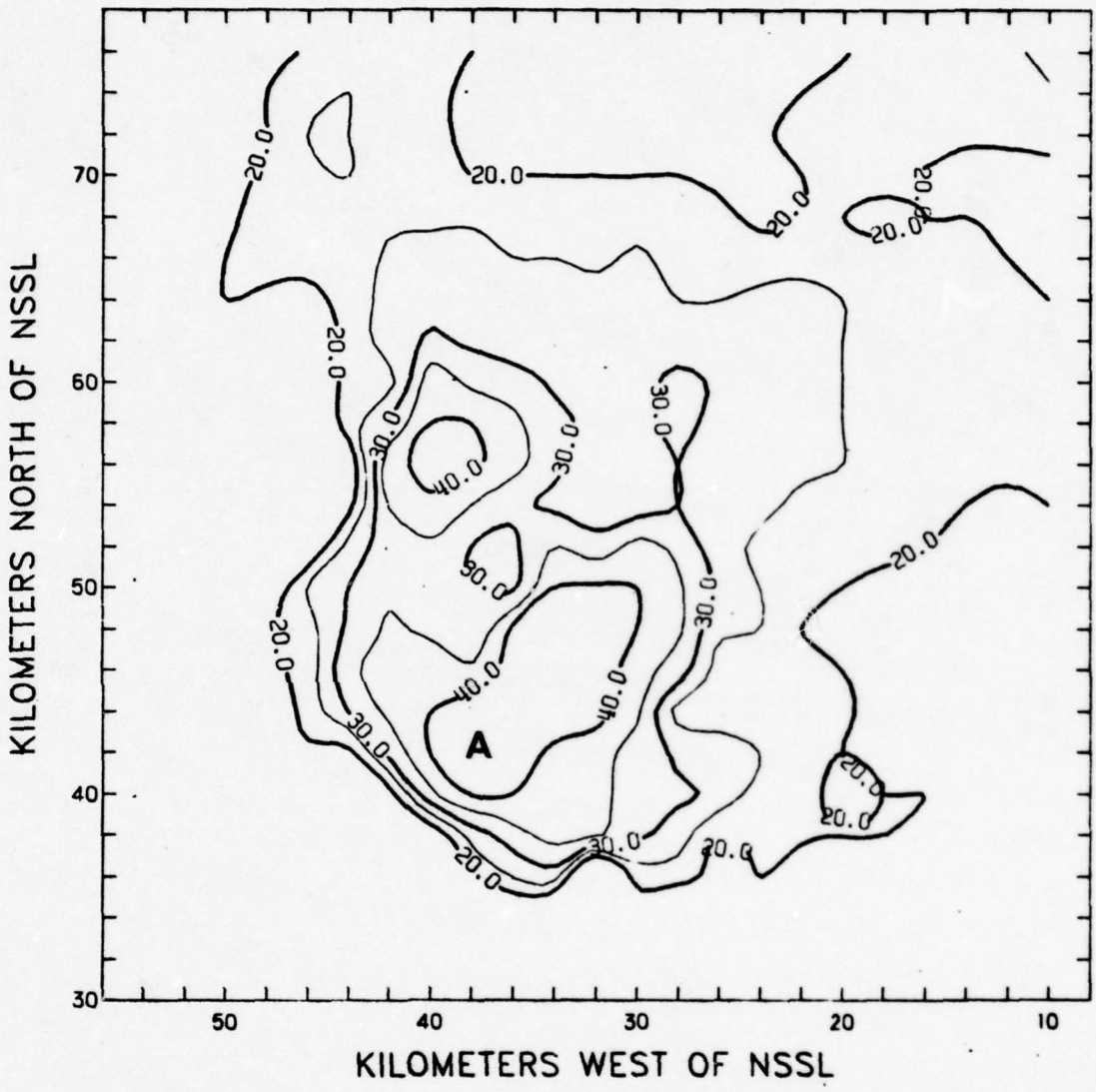

Fig. 31. Pittman's upper-layer PVSZ map for 1800 CST, 23 May 1974. Isopleths of reflectivity in dBZ.

lower layer from the surface through 10 kft. The primary reason that the BWER is not evident in Pittman's PVSZ map is because the lower-layer PVSZ map is created by summing the 5-kft, 10-kft, and 15-kft CAZMs.

Recall that the reflectivity factor at the 15-kft level is interpolated by using digitized radar data along radials for tilt angles above and below the 15-kft level (see Figure 3). Thus, if the actual distribution of reflectivities in the storm is such that digitized reflectivities for the upper tilt-angle radial are large compared to the digitized reflectivities for the lower tilt-angle radial, then the value of the reflectivity at 15 kft may be larger than actually exists. This is especially true if there is a non-linear distribution of reflectivities between the two radials. The purpose of this discussion is not to negate the validity of CAZMs, but only to point out the problems encountered when using the point values of the CAZMs in a summation or integration routine. With this in mind then, observe that the reflectivity factor, Z,[5] at the point on the 15-kft CAZM directly above the BWER (see Figure 8, 37 km west and 50 km north of NSSL) is on the order of 10^5 mm^6 m^{-3} (50 dBZ). Therefore, when the reflectivity factors at 5 kft ($10^{2.5}$ mm^6 m^{-3}) and 10 kft (10^4 mm^6 m^{-3}) are summed with the reflectivity factor at 15 kft, the resultant PVSZ value is approximately $10^{5.1}$ mm^6 m^{-3}. The final result is that the BWER in the lower levels is masked by a large value of reflectivity at the upper level (15 kft). In fact, Pittman's lower-layer PVSZ map is very sim-

---

[5]For convenience, the subscript e has been dropped from the symbol for equivalent radar reflectivity factor, Z_e. All Zs in this study are Z_es.

ilar in appearance to the 15-kft CAZM. In contrast, the LAG-QUAD technique sums only the actual reflectivity factors for each tilt-angle radial in the lower layer. It should be noted, however, that this technique also will mask a BWER if the reflectivity factor at an upper, tilt-angle data point is large.

Another difference between the lower-layer PVSZ map (LAG-QUAD) and Pittman's PVSZ map is the magnitude of the reflectivity contours. Pittman's PVSZ maps give larger values of reflectivity, whereas the magnitude of the reflectivity contours on the LAG-QUAD PVSZ maps more closely represent the actual magnitude of the reflectivity contours in the lower-level CAZMs. This is due primarily to the fact that the LAG-QUAD PVSZ maps are constructed by using the average reflectivity factors for the layer, and all of the digital-radar data are included in the interpolation schemes. In addition, the 0-deg tilt data are explicitly included in the LAG-QUAD technique while the 0-deg tilt data are used in Pittman's technique only to interpolate the reflectivities for the 5-kft CAZM, and then only at distances beyond 87 km from the radar. For ranges < 87 km, the lower tilt angle used for interpolation of the 5-kft CAZM is 1 deg or 2 deg, depending on the distance from the radar.

A comparison of the middle-layer PVSZ maps for each technique reveals relatively minor differences in the appearance and the magnitude of the contour patterns. The center of maximum reflectivity (cell A) for each PVSZ map is located in the same position relative to the radar. The upper-layer PVSZ maps show some minor differences. Note that the (LAG-QUAD) PVSZ map, however, is still a better representa-

tion of the CAZMs in the upper layer of the storm.

Since Pittman's lower-layer PVSZ map did not reflect the BWER, the PVSZ maps for 1810 CST, 23 May 1974, were compared. The PVSZ maps generated by using the Lagrangian cubic and quadratic interpolation schemes are shown in Figures 32 through 34 and Pittman's PVSZ maps are shown in Figures 35 through 37. Once again, there are major differences reflected in the lower-layer PVSZ maps. Pittman's lower-layer PVSZ map (see Figure 35) shows a BWER 38 km north and 29 km west of NSSL. The lower-layer LAG-QUAD PVSZ map (see Figure 32) shows the BWER 35 km north and 26 km west of NSSL. A comparison of the PVSZ maps with the 0-deg reflectivity map (see Figure 38) generated by Pittman's program seems to support the position of the BWER reflected by Pittman's lower-layer PVSZ map. An inspection of the raw radar data, however, indicates that the BWER is located near 35 km north and 26 km west of NSSL as indicated by the LAG-QUAD PVSZ map. Therefore, a review of both techniques was conducted to determine the reason that the BWER does not appear in the same position on both PVSZ maps.

In order to reduce the computer time and memory required to produce PVSZ maps, Pittman [1976] decreased the amount of data to be processed. He accomplished this by processing the reflectivity data from every even-valued range gate instead of from every range gate. Thus, Pittman uses a 2-km (1.079 n mi) grid interval which is comparable to the 1-n mi grid interval used by Canipe [1973]. The important fact to consider, however, is that Pittman excludes data from his interpolation scheme, whereas Canipe and this author do not. The significance of this fact will be demonstrated later.

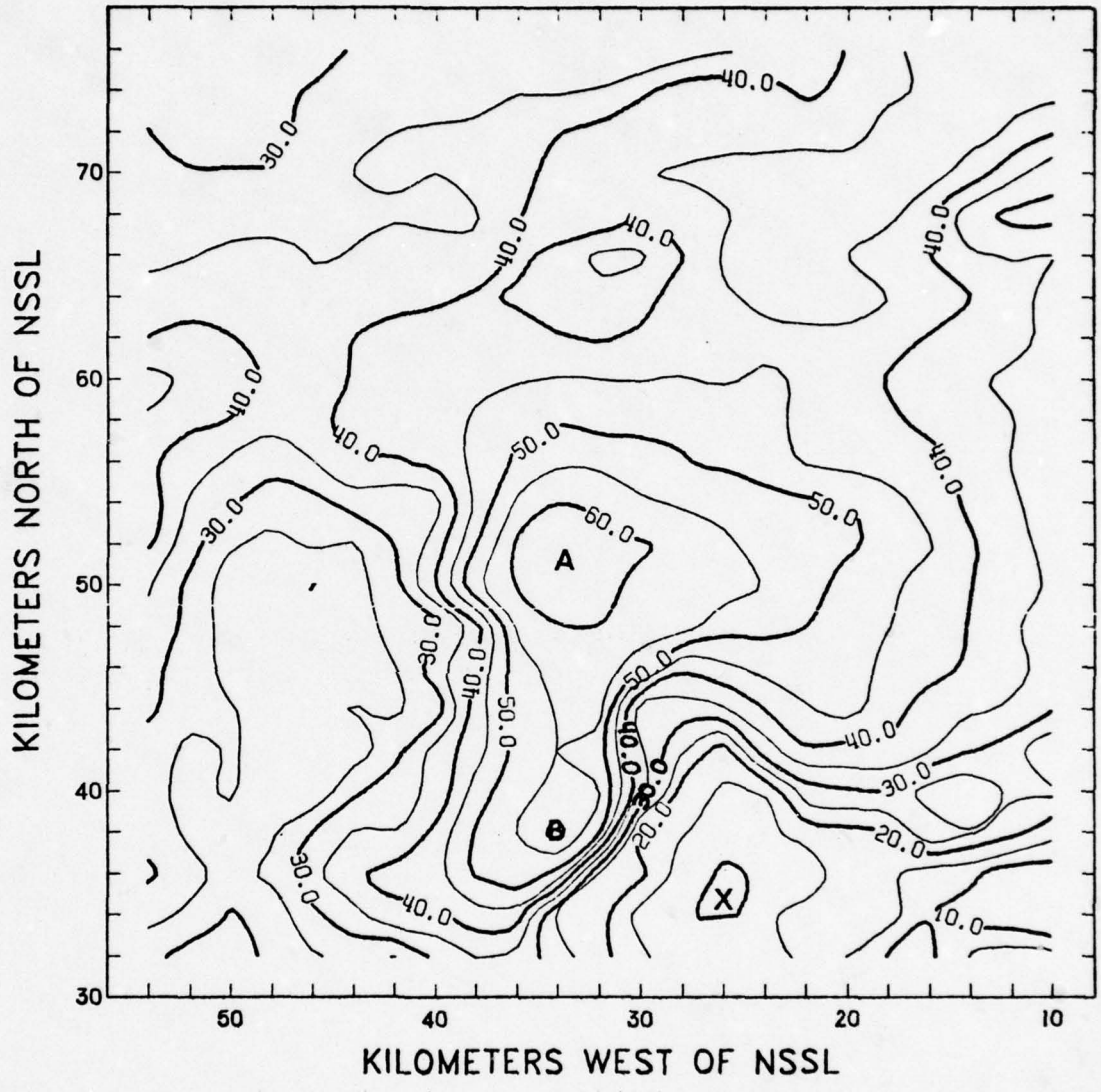

Fig. 32. Lower-layer PVSZ map (LAG-QUAD) for 1810 CST, 23 May 1974. Isopleths of reflectivity in dBZ.

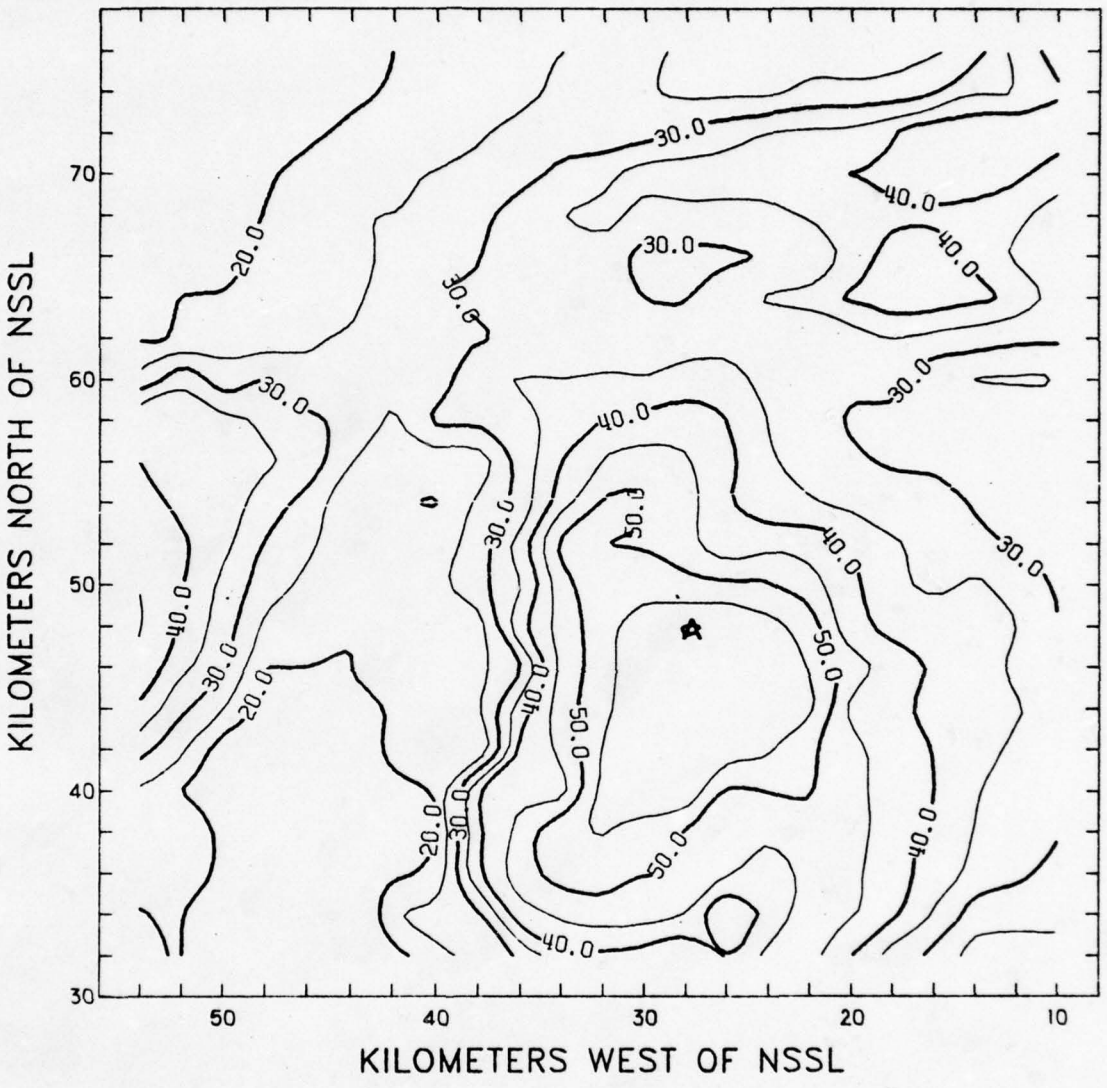

Fig. 33. Middle-layer PVSZ map (LAG-QUAD) for 1810 CST, 23 May 1974. Isopleths of reflectivity in dBZ.

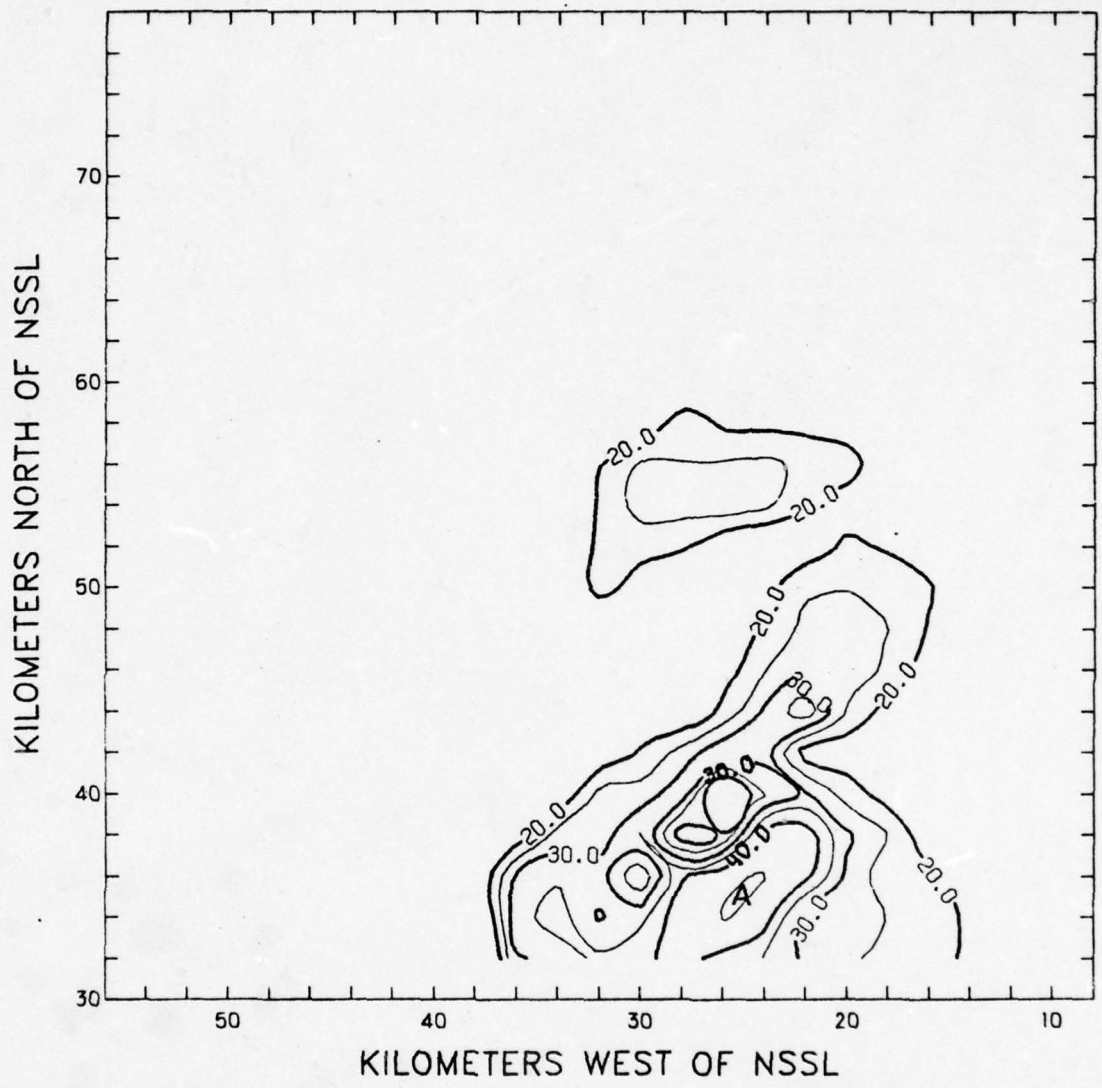

Fig. 34. Upper-layer PVSZ map (LAG-QUAD) for 1810 CST, 23 May 1974. Isopleths of reflectivity in dBZ.

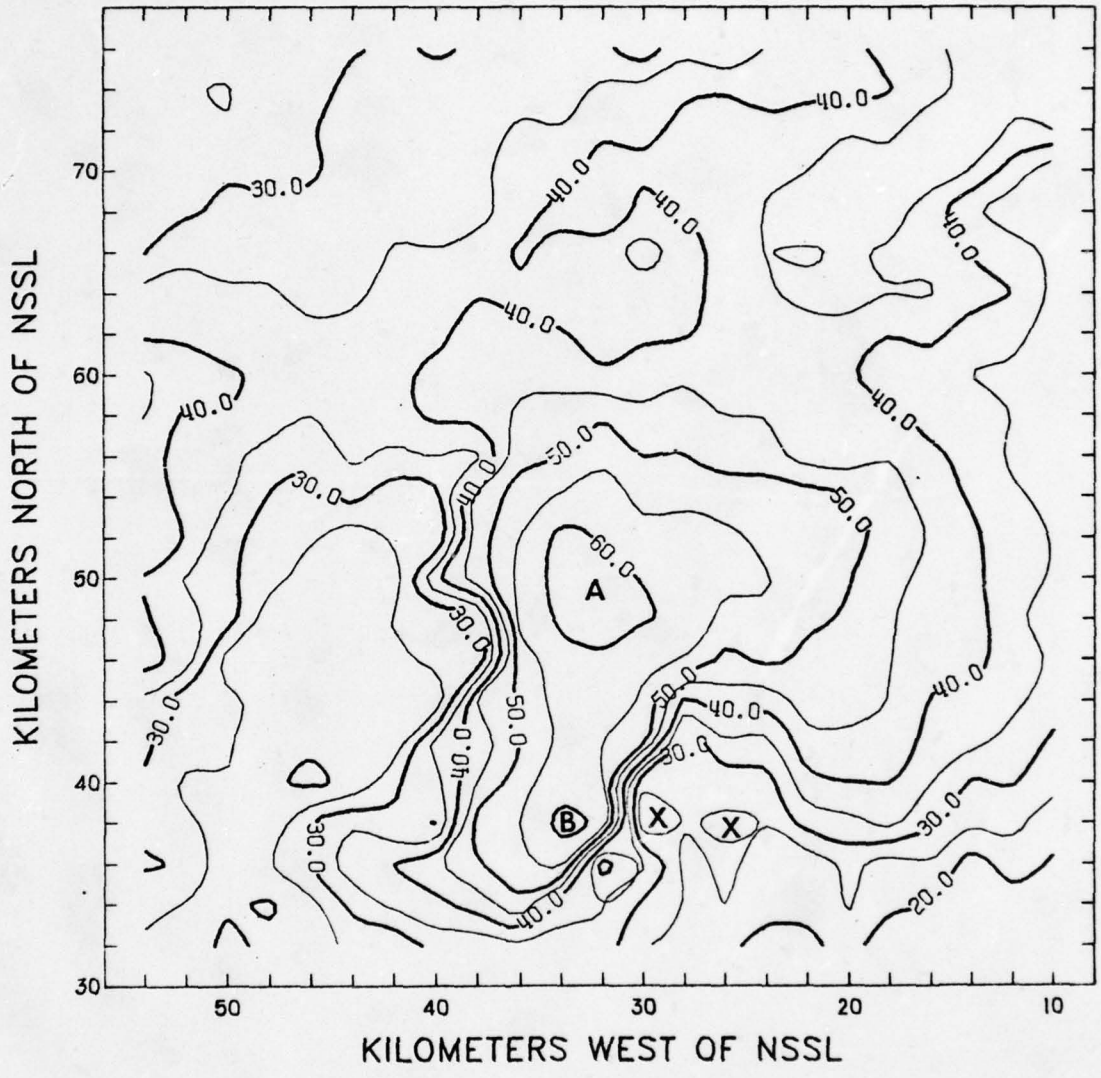

Fig. 35. Pittman's lower-layer PVSZ map for 1810 CST, 23 May 1974. Isopleths of reflectivity in dBZ.

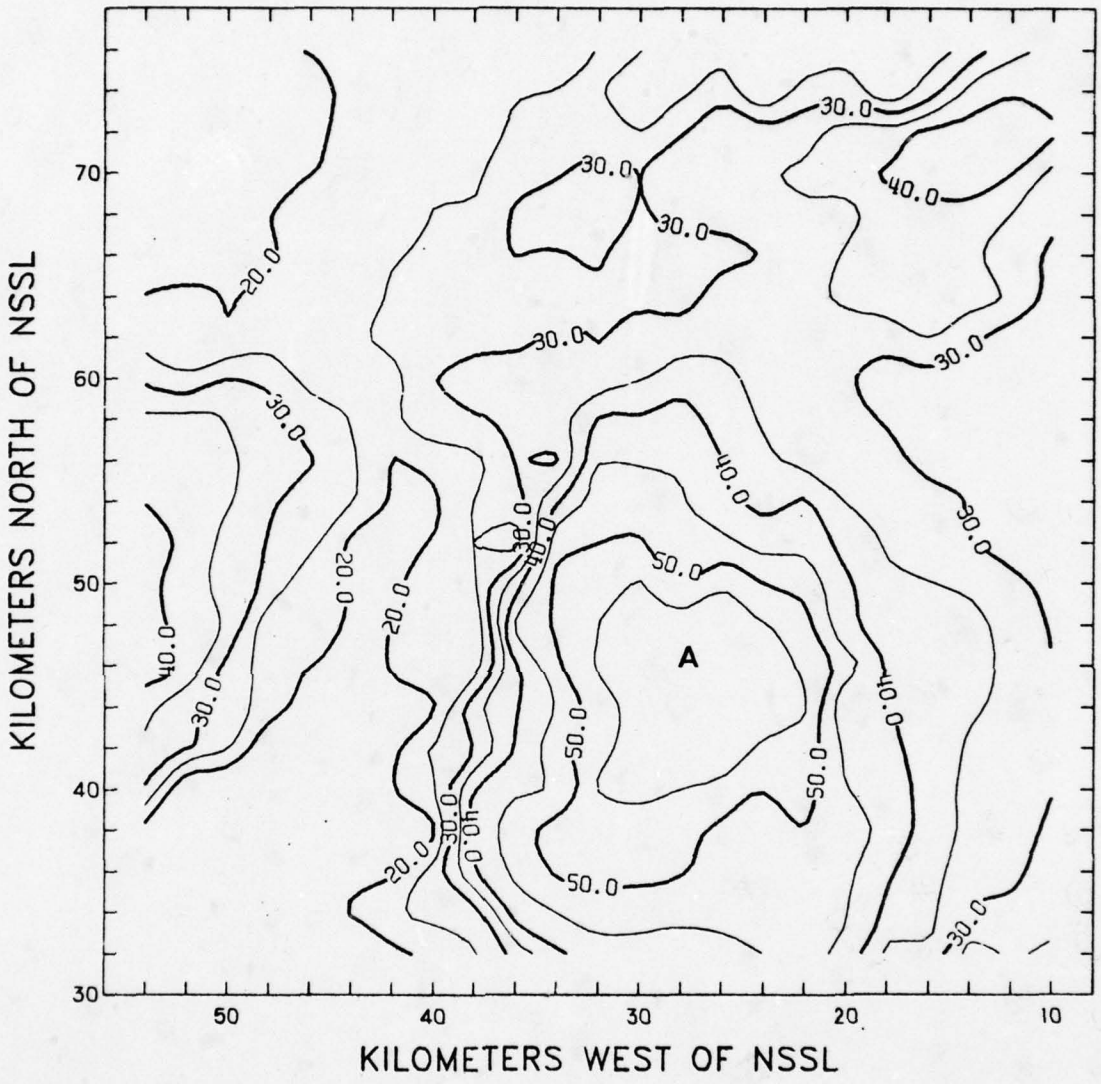

Fig. 36. Pittman's middle-layer PVSZ map for 1810 CST, 23 May 1974. Isopleths of reflectivity in dBZ.

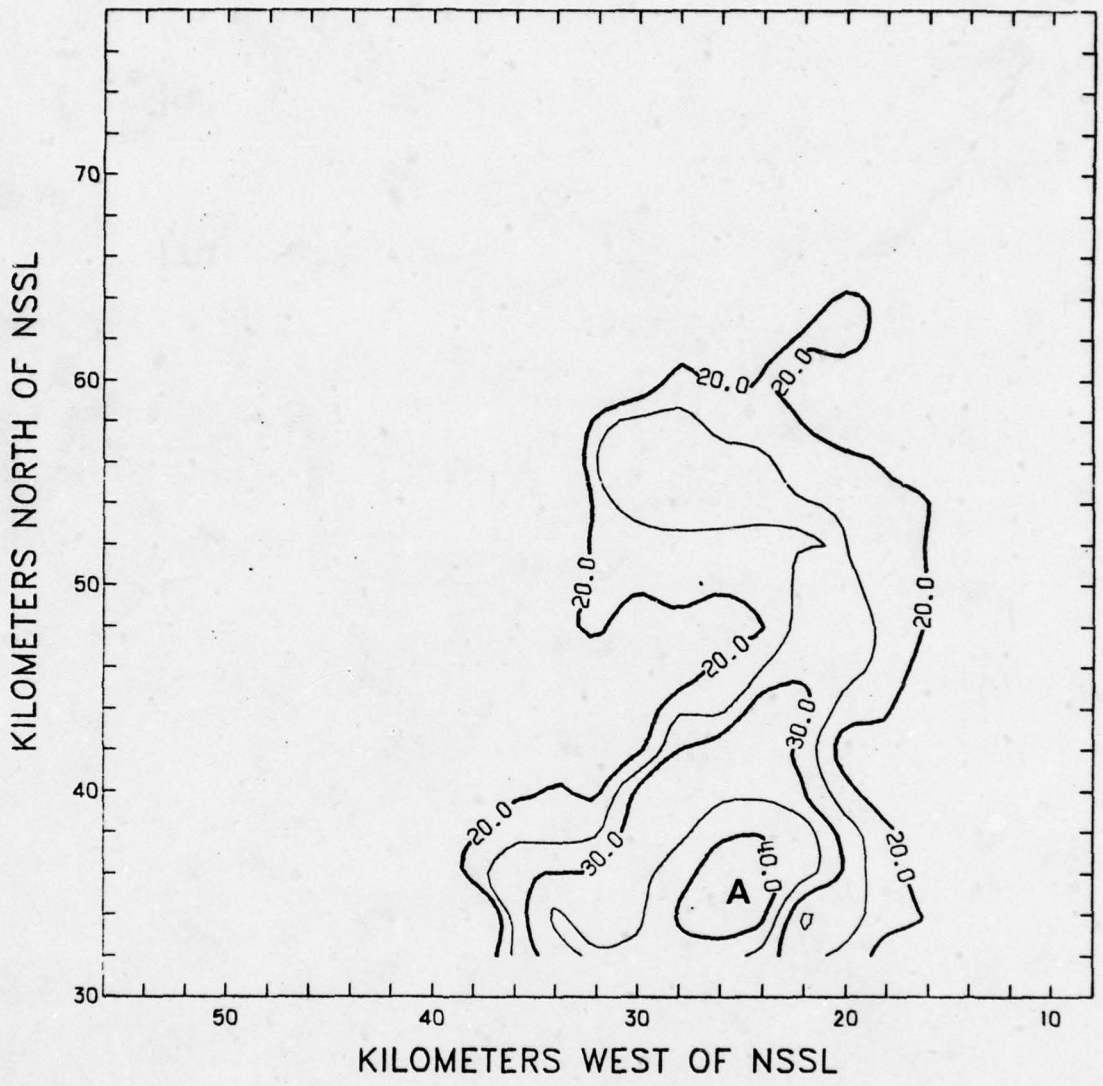

Fig. 37. Pittman's upper-layer PVSZ map for 1810 CST, 23 May 1974. Isopleths of reflectivity in dBZ.

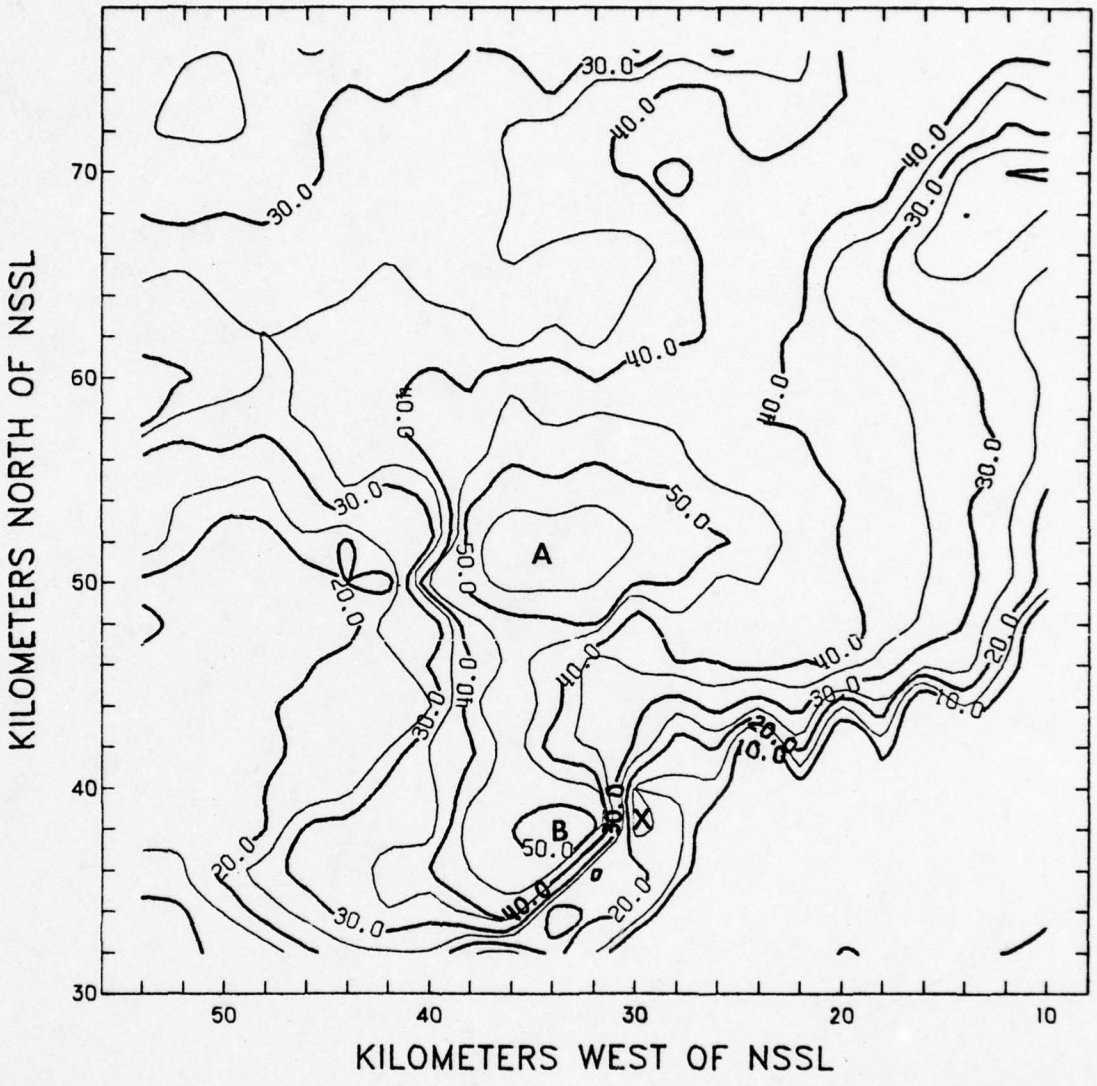

Fig. 38. Pittman's 0-deg reflectivity map for 1810 CST, 23 May 1974. Isopleths of reflectivity in dBZ.

The quadratic interpolation scheme developed by Greene [1971] and used by Canipe [1972, 1973], Vogel [1973], Phillips [1975], Pittman [1976], and this author is used to convert data from the r,α to the x,y coordinate system. As discussed in Chapter II, this technique interpolates the value of the reflectivity factor at a point (x,y) by selecting the six data points (r,α) closest to the x,y point (see Figure 4). Since Pittman did not use the digital-radar data at the odd-numbered range gates, the six data points he used were not the closest six data points. Therefore, Pittman's program was modified to produce a 0-deg reflectivity map by using the quadratic interpolation scheme which includes all of the digital-radar data in the interpolation schemes. This 0-deg reflectivity map is shown in Figure 39. When all of the data are included, the BWER is located near 33 km north and 25 km west of NSSL, as also is indicated by the LAG-QUAD PVSZ map. A more complete investigation of the quadratic interpolation scheme reveals a startling result.

As part of this investigation, the value of the reflectivity at the point (x = 30 km west of NSSL, y = 38 km north of NSSL) was calculated by hand in order to determine the reason that the value at that point varies if the grid interval is changed from 1 km to 2 km. The actual data array used to interpolate the value of reflectivity, Z(x,y), at this point is shown in Figure 40. If we interpolate the value of Z(x,y) by using the reflectivity factors (converted from digital radar data) at only the even-numbered range gates, we get

$$Z(x,y) = -5,388 \text{ mm}^6 \text{ m}^{-3}$$

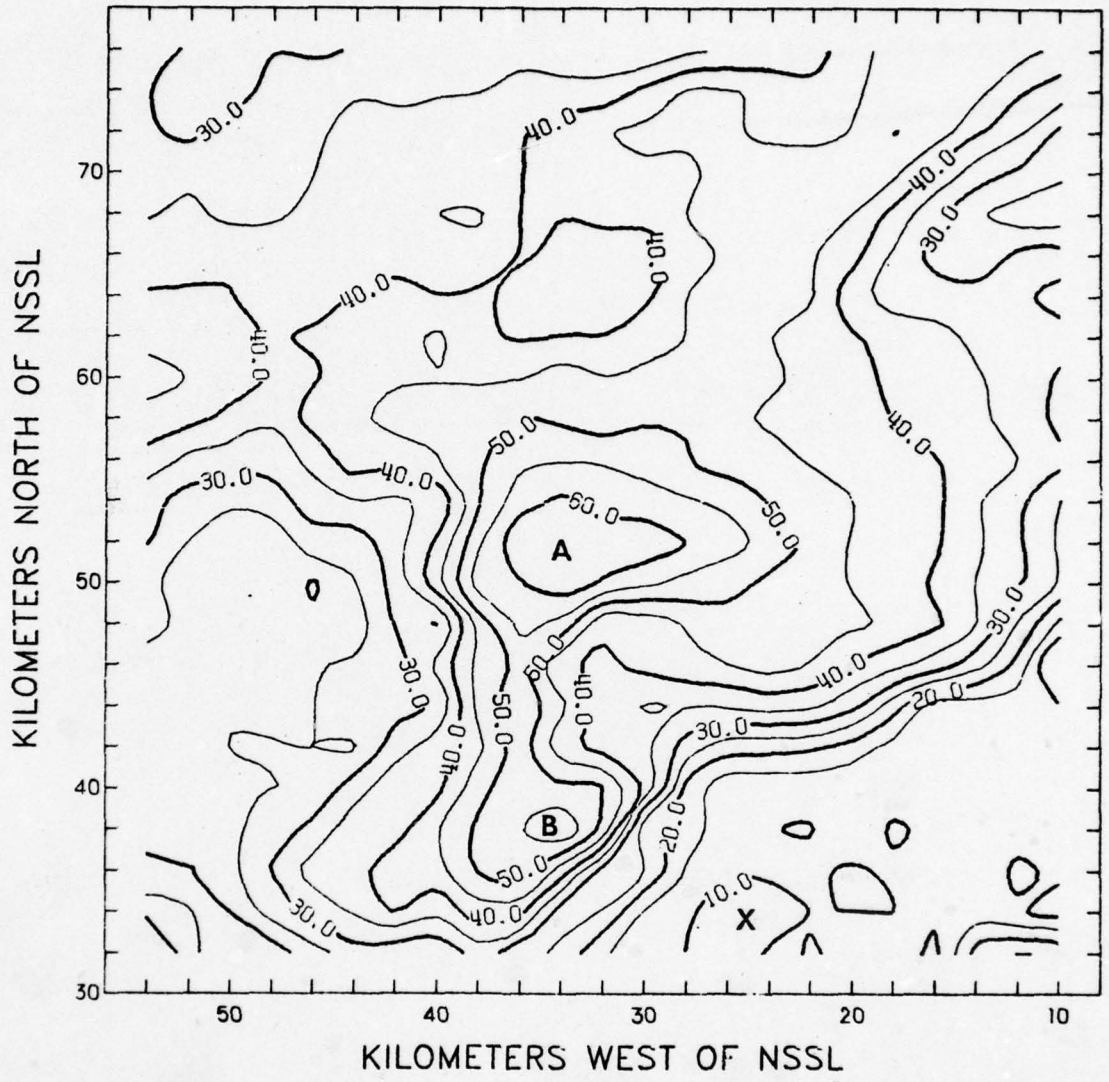

Fig. 39. A modified 0-deg reflectivity map for 1810 CST, 23 May 1974. Isopleths of reflectivity in dBZ.

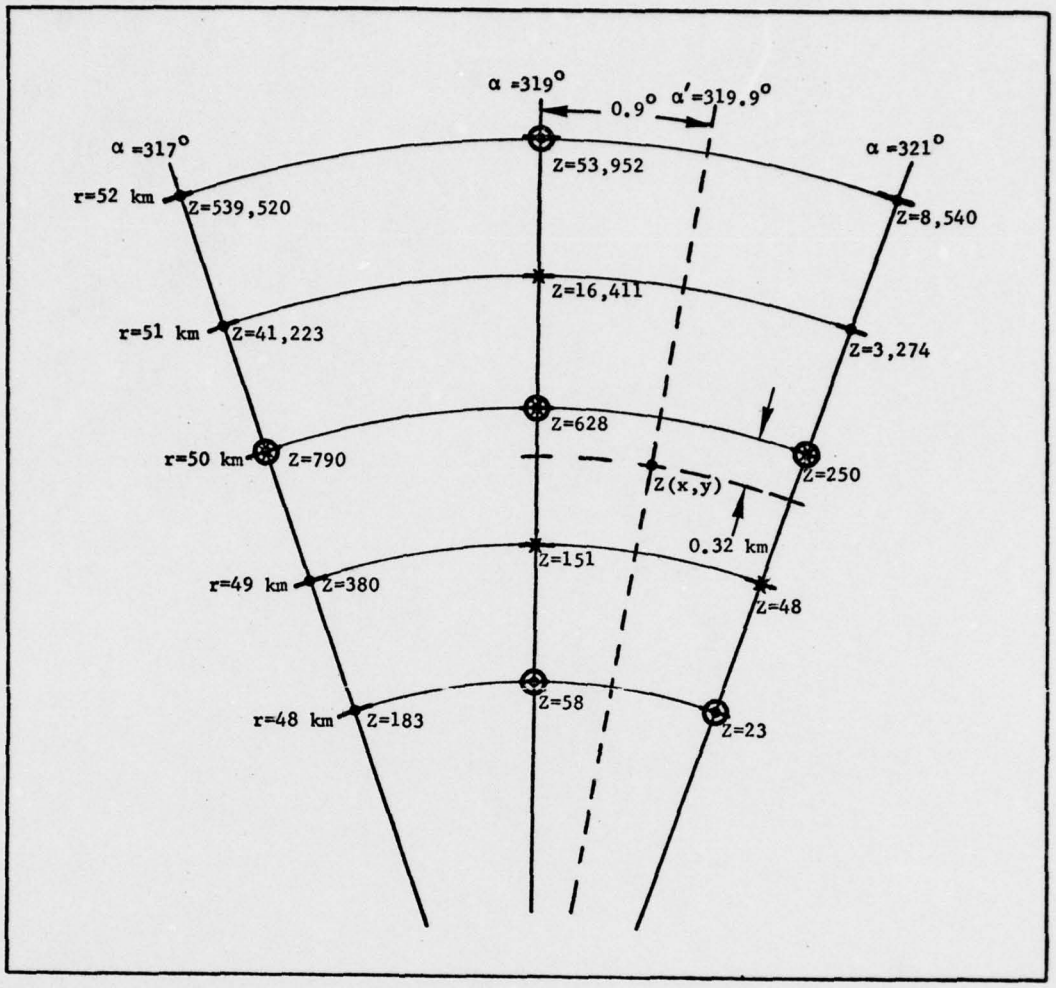

Fig. 40. The reflectivity (Z) data array used to interpolate the value of Z(x,y). Reflectivity values in mm^6/m^3.

If, however, we interpolate the value of Z(x,y) by using all of the reflectivity data, we get

$$Z(x,y) = -1{,}307 \text{ mm}^6 \text{ m}^{-3}$$

Of course, in either case, a negative reflectivity factor is not physically possible. Therefore, the next statement in the quadratic interpolation program set the value of Z(x,y) equal to the minimum value occurring at any of the six data points used in the interpolation. This means that Pittman [1976] gets

$$Z(x,y) = 23 \text{ mm}^6 \text{ m}^{-3}$$

or

$$Z(x,y) = 14 \text{ dBZ}$$

whereas, this investigator gets

$$Z(x,y) = 48 \text{ mm}^6 \text{ m}^{-3}$$

or

$$Z(x,y) = 17 \text{ dBZ}$$

The result is that Pittman's PVSZ map reflects a false BWER as indicated in Figure 38. In addition, if we use a linear interpolation scheme, we get

$$Z(x,y) = 345 \text{ mm}^6 \text{ m}^{-3}$$

or

$$Z(x,y) = 25 \text{ dBZ}$$

The result is an error of 93% $\left(\frac{345 \text{ mm}^6 \text{ m}^{-3} - 23 \text{ mm}^6 \text{ m}^{-3}}{345 \text{ mm}^6 \text{ m}^{-3}} \times 100\%\right)$

between the linearly interpolated value of Z(x,y) and the Z(x,y) for the quadratic technique as used by Pittman [1976], and 86% error for the quadratic technique using all of the data. In terms of dBZ this relates to an error of 44% and 32%, respectively. Note also the spurious wiggles in the reflectivity contours southeast of cell A. These wriggles appear to be noise created by the inaccuracies in the quadratic interpolation scheme. It should be noted, however, that these errors do not alter significantly the results of the Canipe and Pittman studies in that the major features of the analyses remain unaltered. In an attempt to reduce these errors, a new interpolation scheme was created that uses both the quadratic and linear interpolation schemes (QUAD/LIN).

Quadratic/Linear Interpolation Technique

The QUAD/LIN interpolation scheme will use the quadratic interpolation method to obtain the reflectivity factor, Z, at an x,y point. If, however, the quadratic interpolation results in Z(x,y) being negative, then a linear interpolation scheme which uses the four data points surrounding Z(x,y) is employed to obtain the interpolated value of Z(x,y). The data for 1800 CST, 23 May 1974, were reanalyzed by using this new interpolation scheme, with the results shown in Figures 41 through 43.

A comparison of the LAG-QUAD/LIN PVSZ maps with the maps generated by the other combinations of interpolation schemes (see Figures 17 through 28) reveals some interesting results. First, note that the lower-layer PVSZ map (LAG-QUAD/LIN) resembles more closely the lower-

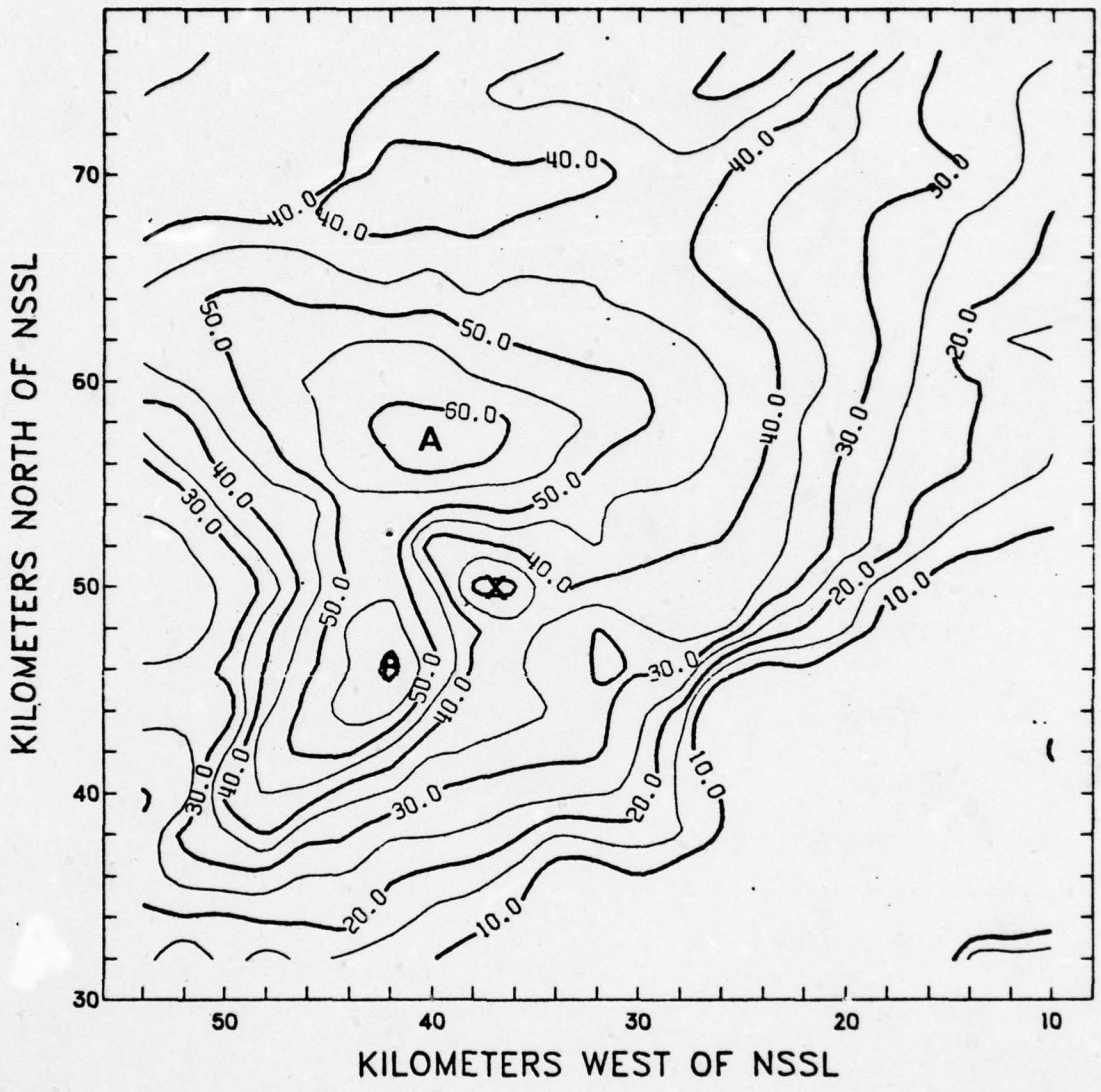

Fig. 41. Lower-layer PVSZ map (LAG-QUAD/LIN) for 1800 CST, 23 May 1974. Isopleths of reflectivity in dBZ.

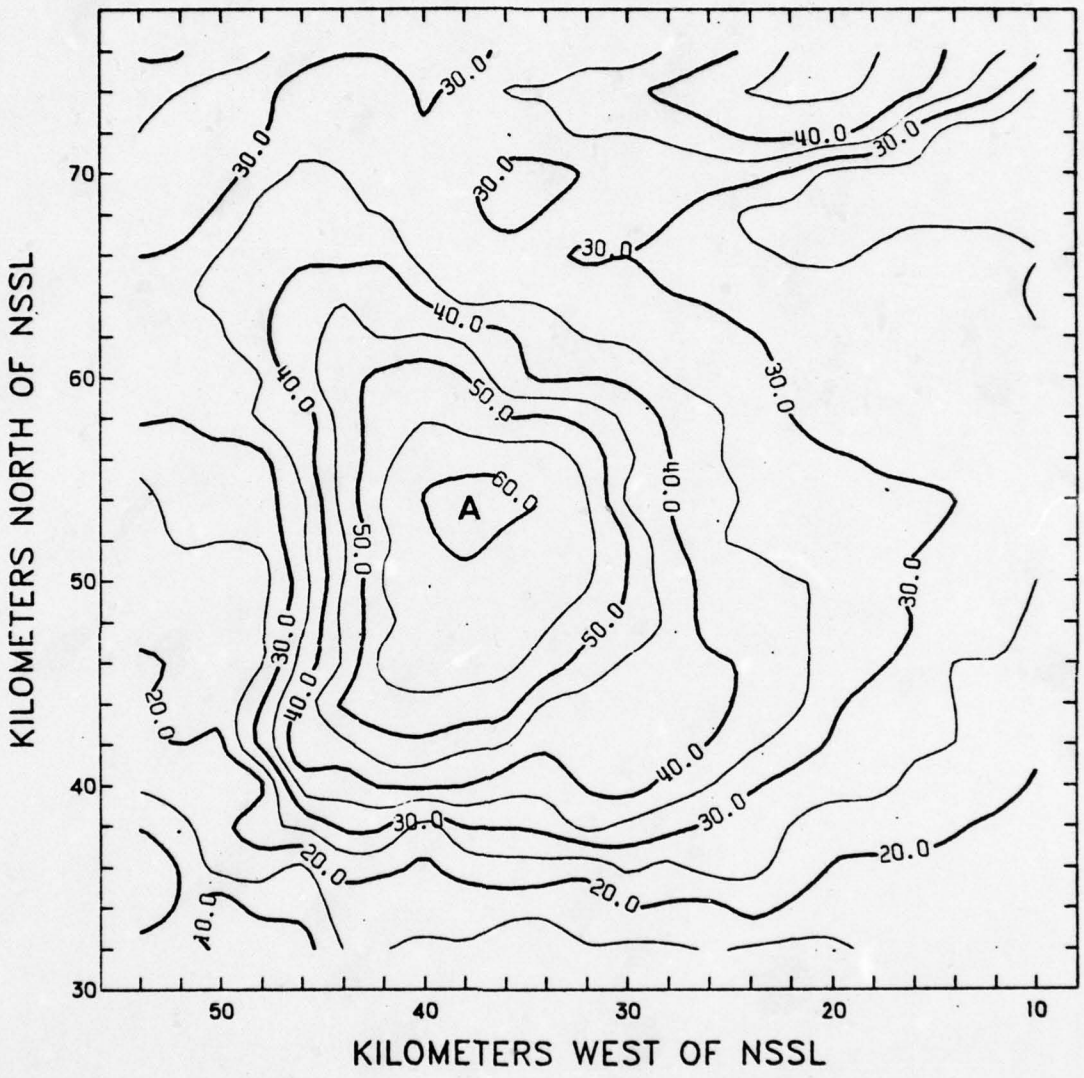

Fig. 42. Middle-layer PVSZ map (LAG-QUAD/LIN) for 1800 CST, 23 May 1974. Isopleths of reflectivity in dBZ.

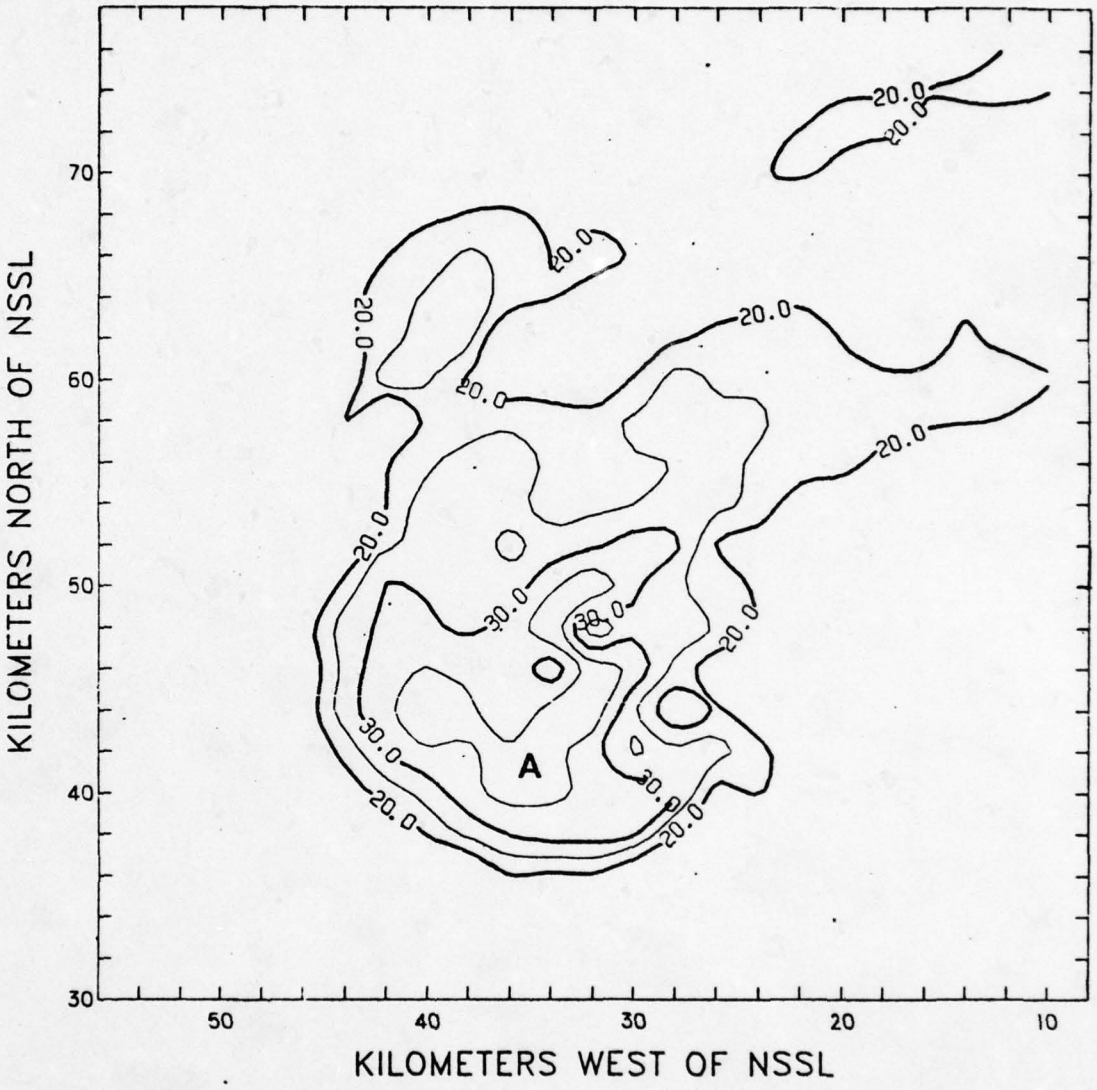

Fig. 43. Upper-layer PVSZ map (LAG-QUAD/LIN) for 1800 CST, 23 May 1974. Isopleths of reflectivity in dBZ.

layer PVSZ map produced by using the LAG-LIN or LIN-LIN combination. The location of the centers of maxima and minima are unchanged; however, the gradient of reflectivity between the BWER and the closest maximum is less for the LAG-QUAD/LIN case (∿5.5 dBZ/km) than for the LAG-QUAD case (∿6.8 dBZ/km). In fact the gradient is represented more closely by the LAG-LIN or LIN-LIN cases. It is obvious that, with unmodified quadratic interpolation, any time the quadratic tendencies in the data result in a negative value for Z(x,y) the minimum value of reflectivity of the six data points used in the interpolation is assigned to Z(x,y) which in turn may create a false gradient of reflectivity in the contoured PVSZ map. Therefore, it is evident that the LAG-LIN interpolation scheme adequately represents the significant features of the CAZMs, while requiring less computer time than the other combinations of techniques.

Finally, Pittman's program was rewritten to use all of the digital radar data in the interpolation schemes. The amount of computer memory required for the program was ∿896 Kbytes and the execution time increased to ∿22 sec. Pittman's new lower-, middle-, and upper-layer PVSZ maps produced by using all of the data and the QUAD/LIN interpolation scheme are shown in Figures 44 through 46. A comparison of these PVSZ maps with Pittman's previous PVSZ maps for this time period shows some interesting results.

The lower-layer PVSZ map (QUAD/LIN) shows the most significant differences. The magnitude of the reflectivity contours is reduced by 5 dBZ with the QUAD/LIN technique. Now, the magnitude of Pittman's reflectivity contours is the same as those of the CAZMs and the LAG-

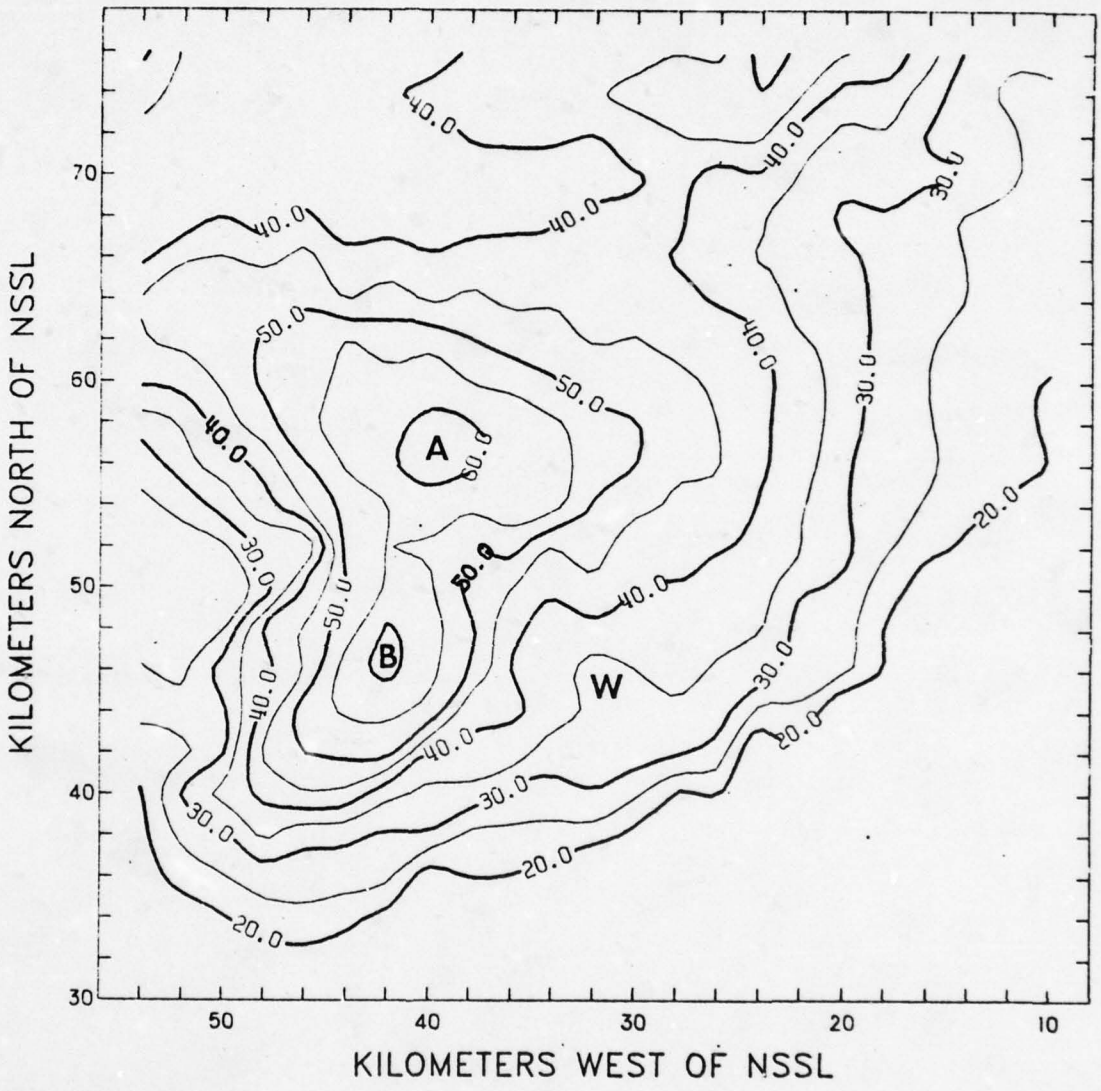

Fig. 44. Pittman's lower-layer PVSZ map (QUAD/LIN) for 1800 CST, 23 May 1974. Isopleths of reflectivity in dBZ.

AD-A050 155 TEXAS A AND M UNIV COLLEGE STATION DEPT OF METEOROLOGY F/G 17/9
REAL-TIME COMPUTER TECHNIQUES IN THE DETECTION AND ANALYSIS OF --ETC(U)
AUG 77 T E SIELAND AFOSR-77-3146

UNCLASSIFIED AFIT-CI-78-33 NL

2 OF 2
AD
A050 155

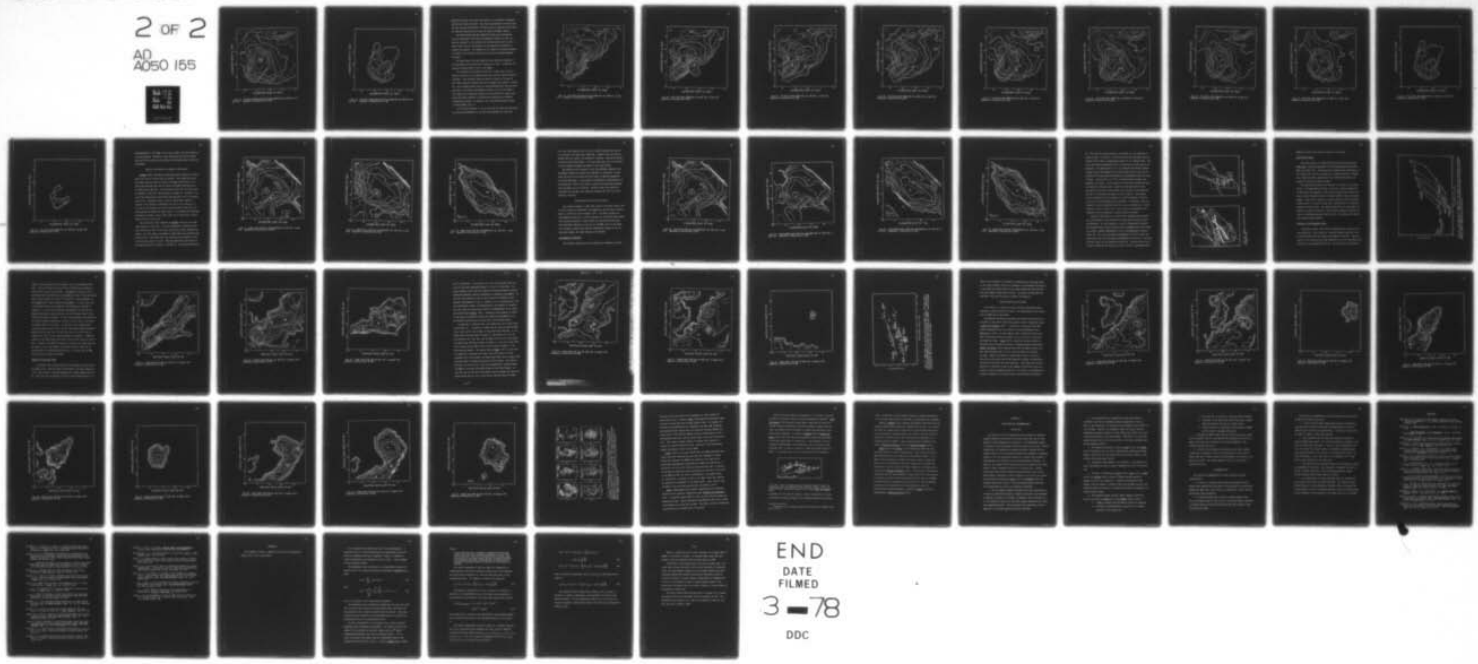

END
DATE
FILMED
3-78
DDC

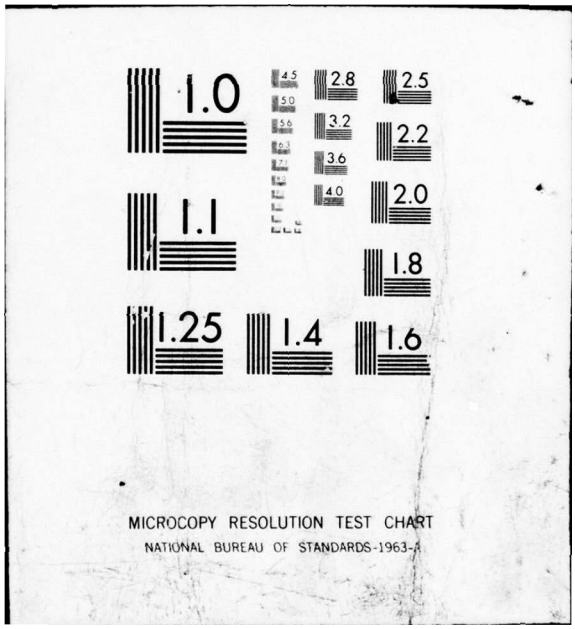
1.0
1.1
1.25
1.4
1.6
1.8
2.0
2.2
2.5
2.8
3.2
3.6
4.0
4.5
5.0
5.6
6.3
7.1
MICROCOPY RESOLUTION TEST CHART
NATIONAL BUREAU OF STANDARDS-1963-A

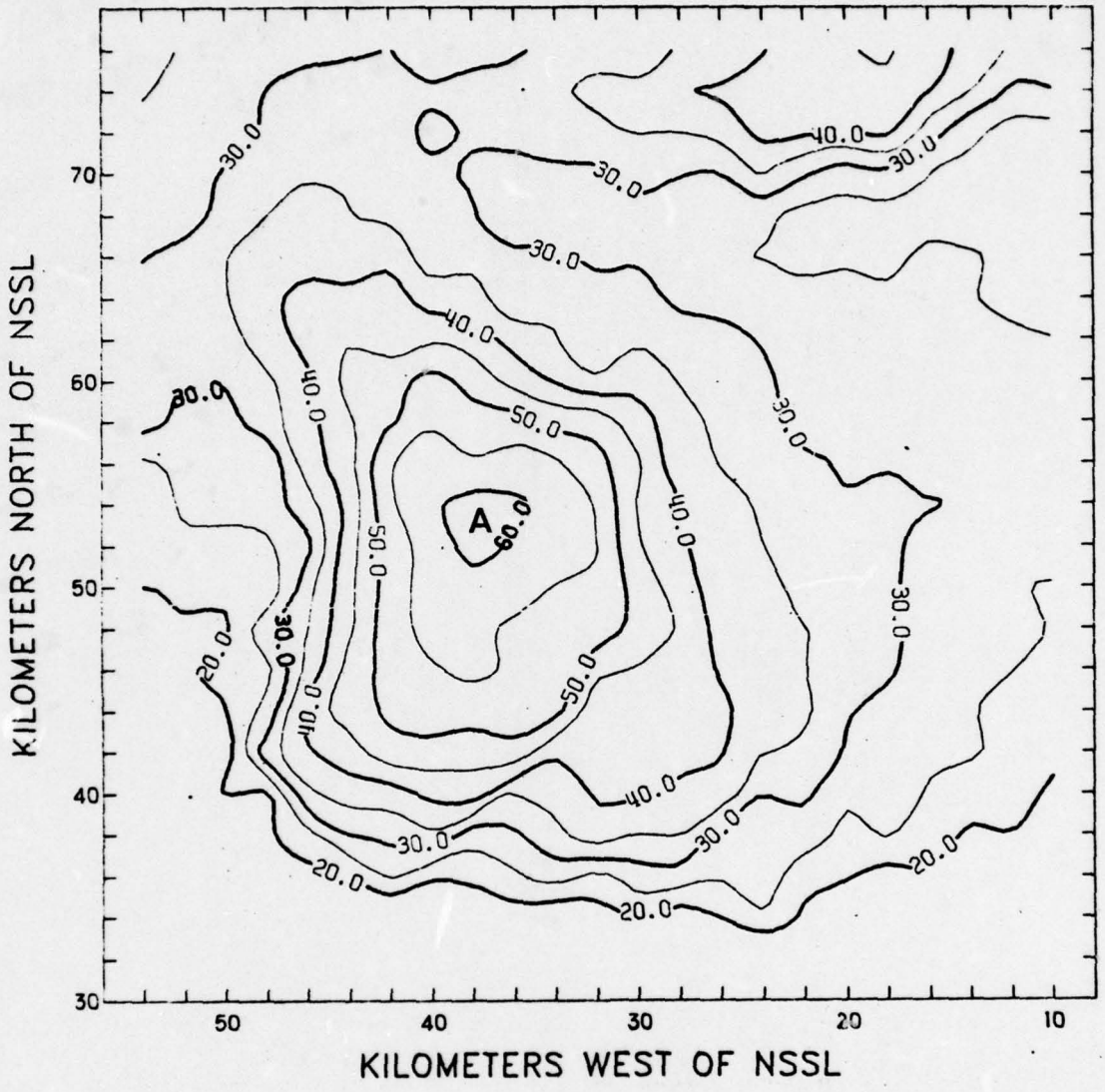

Fig. 45. Pittman's middle-layer PVSZ map (QUAD/LIN) for 1800 CST, 23 May 1974. Isopleths of reflectivity in dBZ.

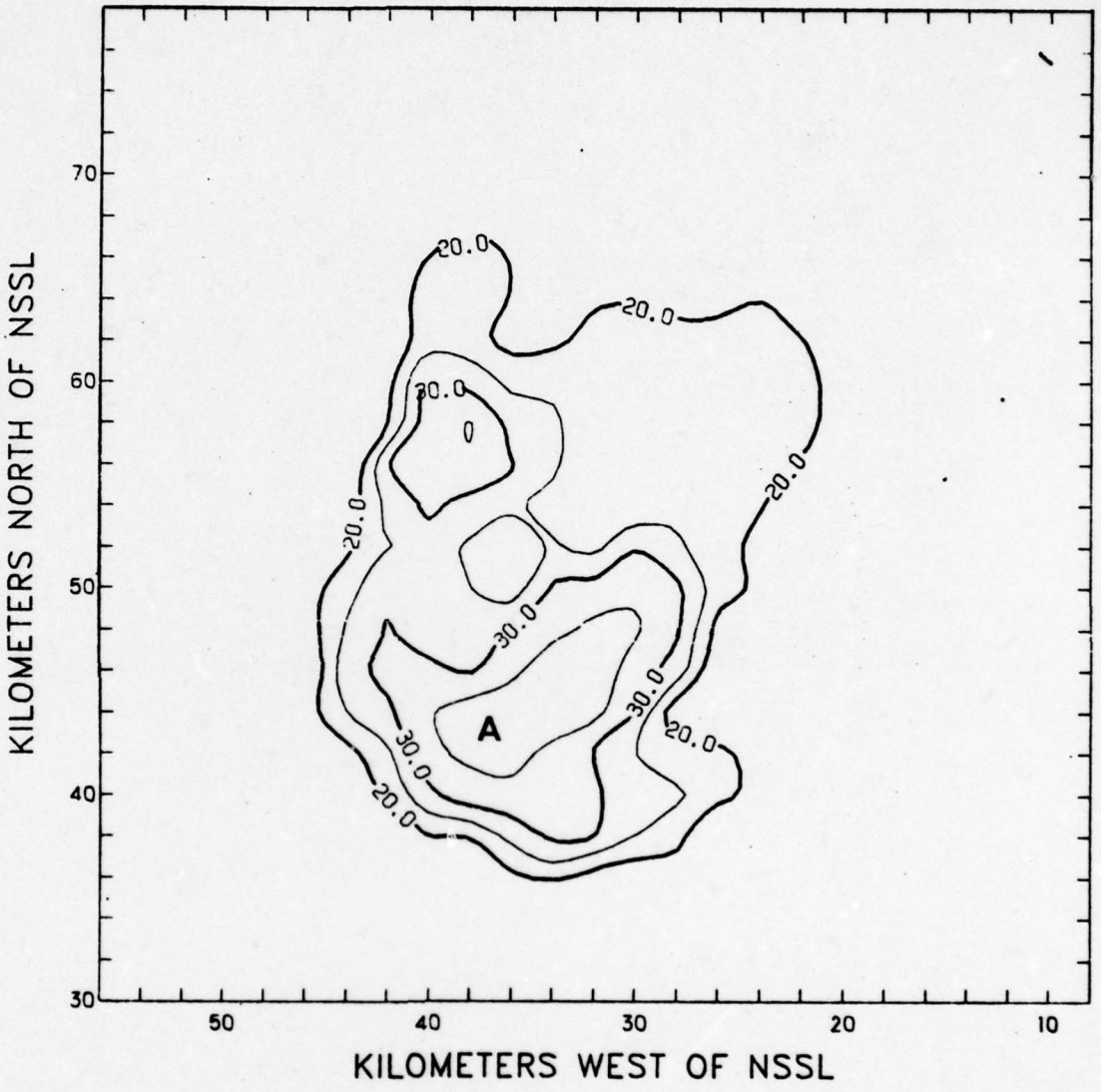

Fig. 46. Pittman's upper-layer PVSZ map (QUAD/LIN) for 1800 CST, 23 May 1974. Isopleths of reflectivity in dBZ.

QUAD/LIN PVSZ map. Note that the location of the centers of maximum reflectivity remain the same. This can be attributed to the fact that the area of high reflectivity (∿50 dBZ) covers a relatively large area. The improved technique still does not reflect the BWER, however.

The middle-layer PVSZ map (QUAD/LIN) shows minor differences . The main improvement from using the QUAD/LIN technique is that the spurious wriggles in the reflectivity contour pattern west of cell A which result from the inaccuracies of the quadratic interpolation schemes are removed. This damping out or removal of spurious wriggles is evident in all products generated by using the improved QUAD/LIN technique.

The upper-layer PVSZ map (QUAD/LIN) also reflects a decrease in the magnitude of the reflectivity contours of 5 dBZ. In addition, the spurious wriggles south of cell A are damped.

For comparison, the CAZMs for 1800 CST, 23 May 1974, were produced by using all of the digital-radar data and the improved QUAD/LIN technique. The resultant CAZMs are shown in Figures 47 through 56. When these CAZMs are compared with the old CAZMs (see Figures 5 through 14), the new CAZMs reflect much the same differences that the new PVSZ maps show. The primary improvements evident in all of the CAZMs is the elimination of spurious wriggles in the reflectivity contour patterns and false gradients of reflectivity created by the quadratic interpolation scheme. In addition, the 0-deg reflectivity map shows a definite BWER (cell X).

In the final analysis, it can be seen that the PVSZ maps generated by using the LAG-QUAD/LIN or the LAG-LIN techniques are very good

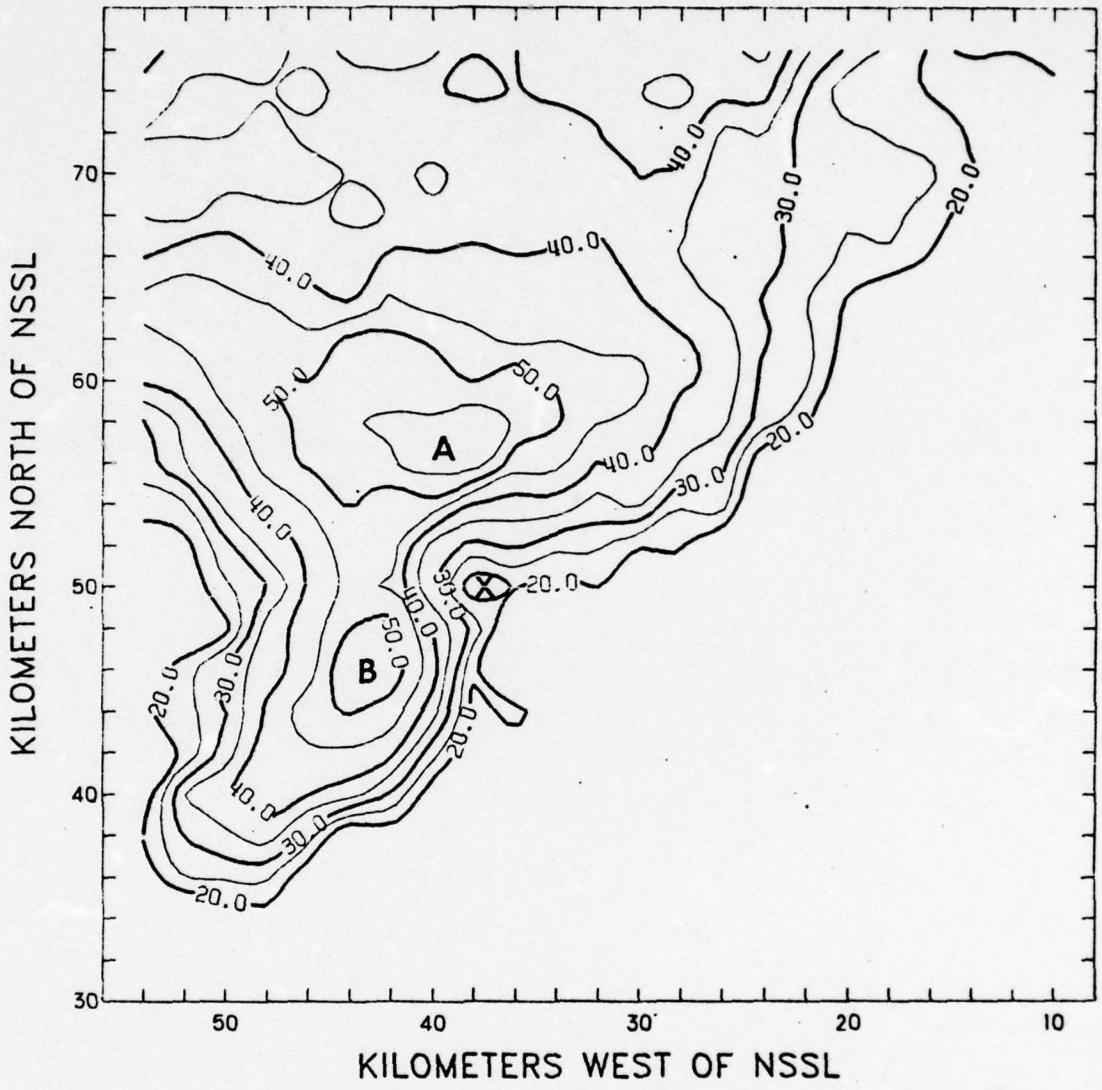

Fig. 47. The 0-deg reflectivity map (QUAD/LIN) for 1800 CST, 23 May 1974. Isopleths of reflectivity in dBZ.

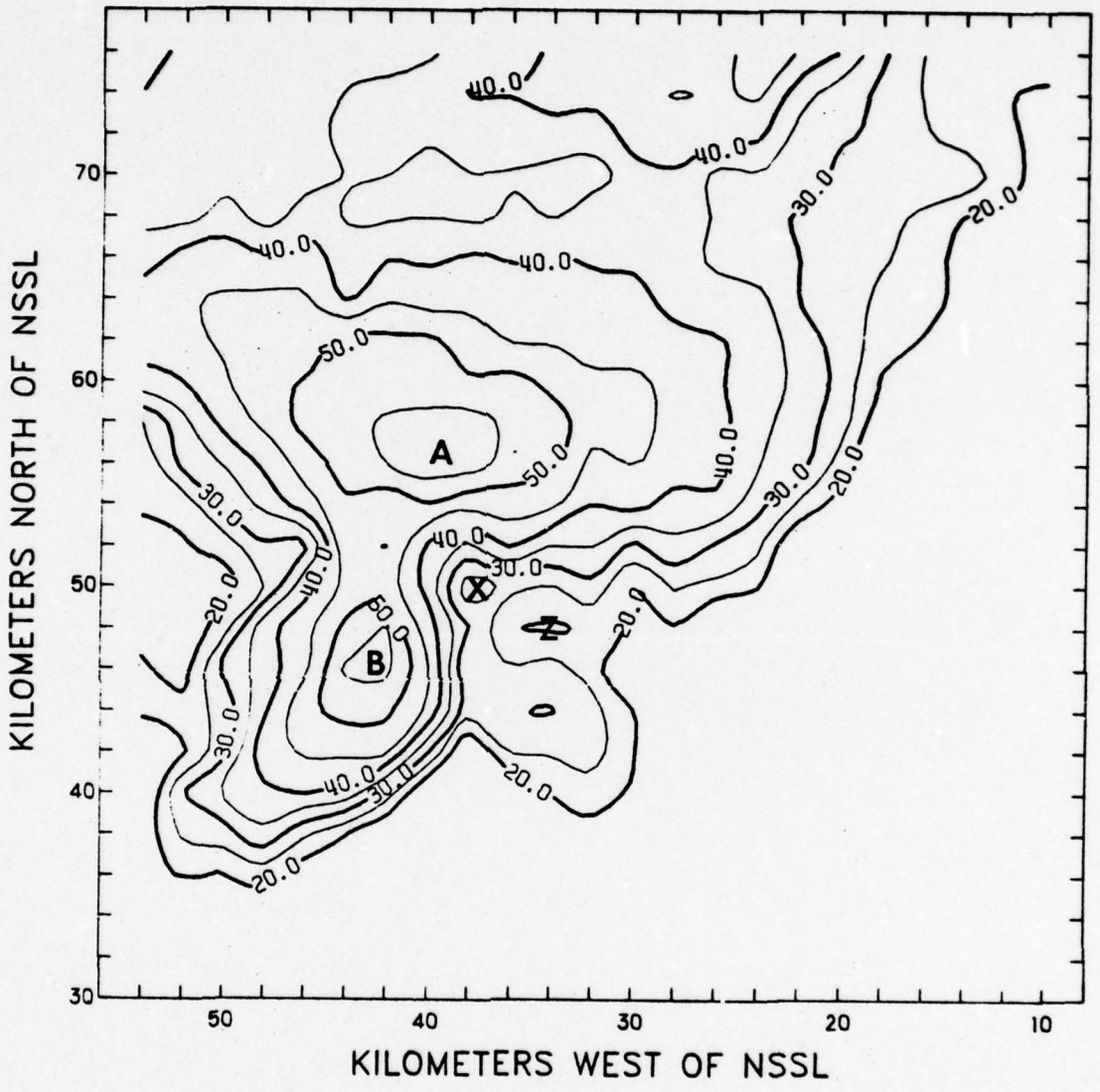

Fig. 48. The 5-kft CAZM (QUAD/LIN) for 1800 CST, 23 May 1974. Isopleths of reflectivity in dBZ.

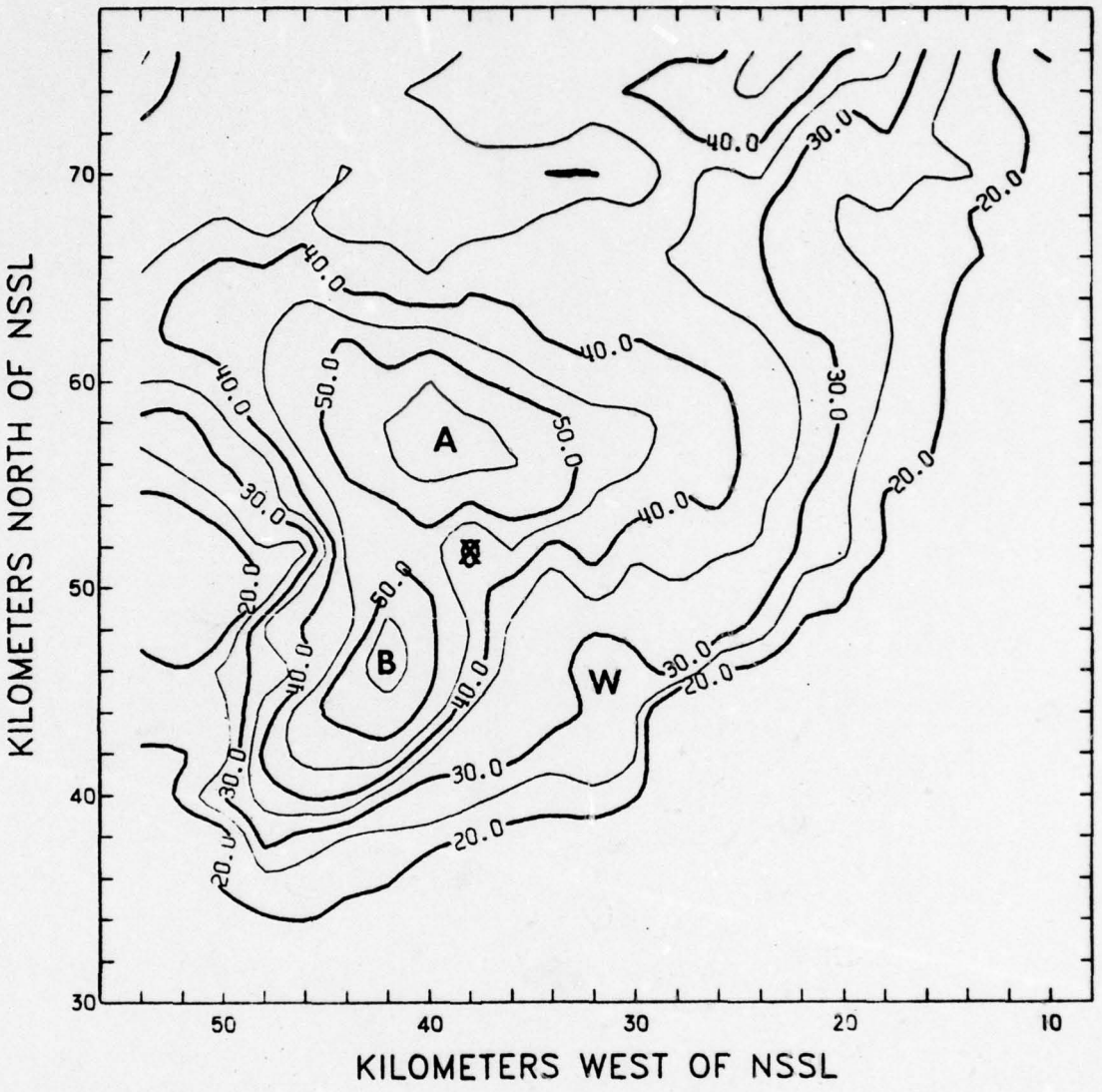

Fig. 49. The 10-kft CAZM (QUAD/LIN) for 1800 CST, 23 May 1974. Isopleths of reflectivity in dBZ.

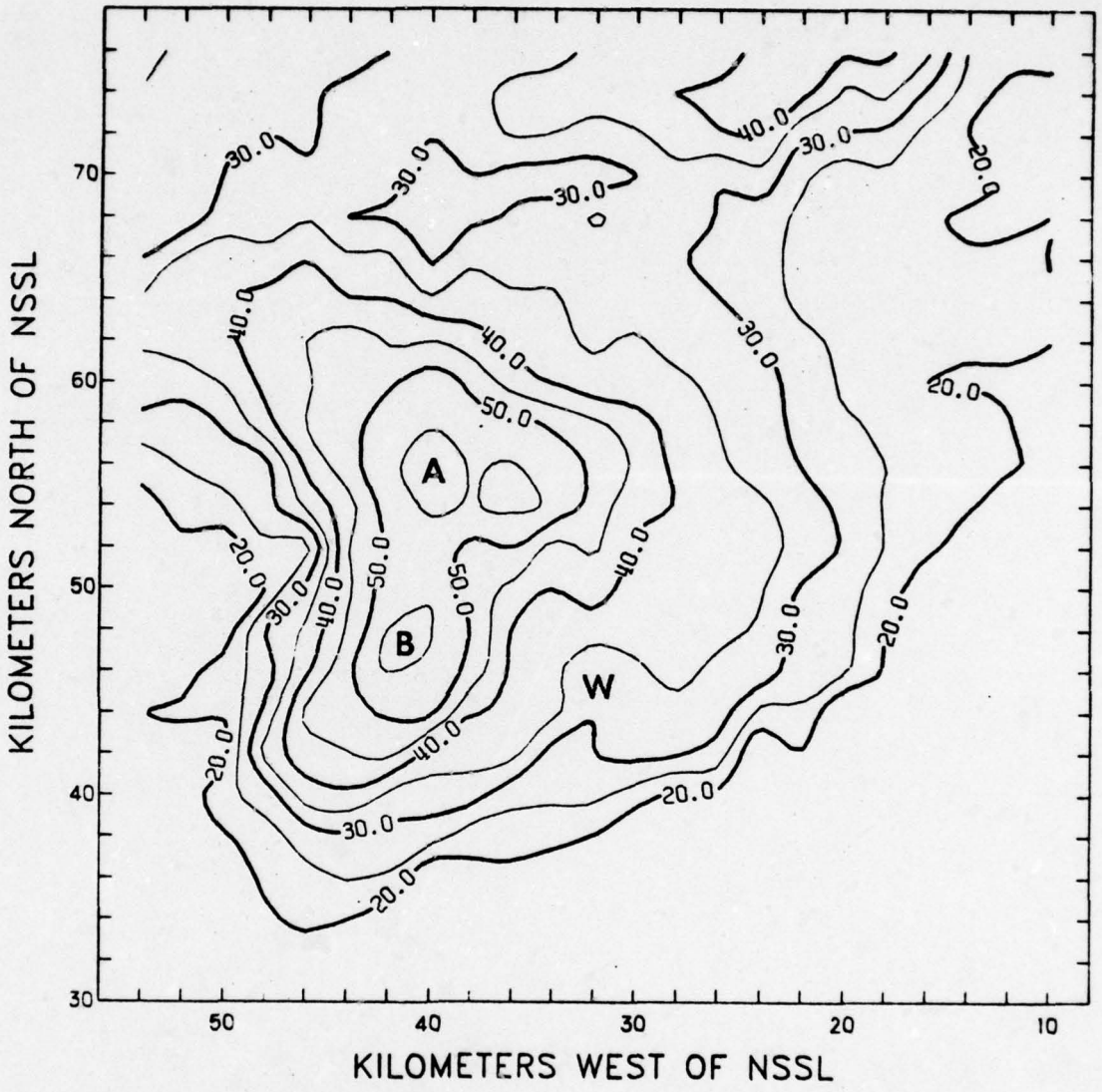

Fig. 50. The 15-kft CAZM (QUAD/LIN) for 1800 CST, 23 May 1974. Isopleths of reflectivity in dBZ.

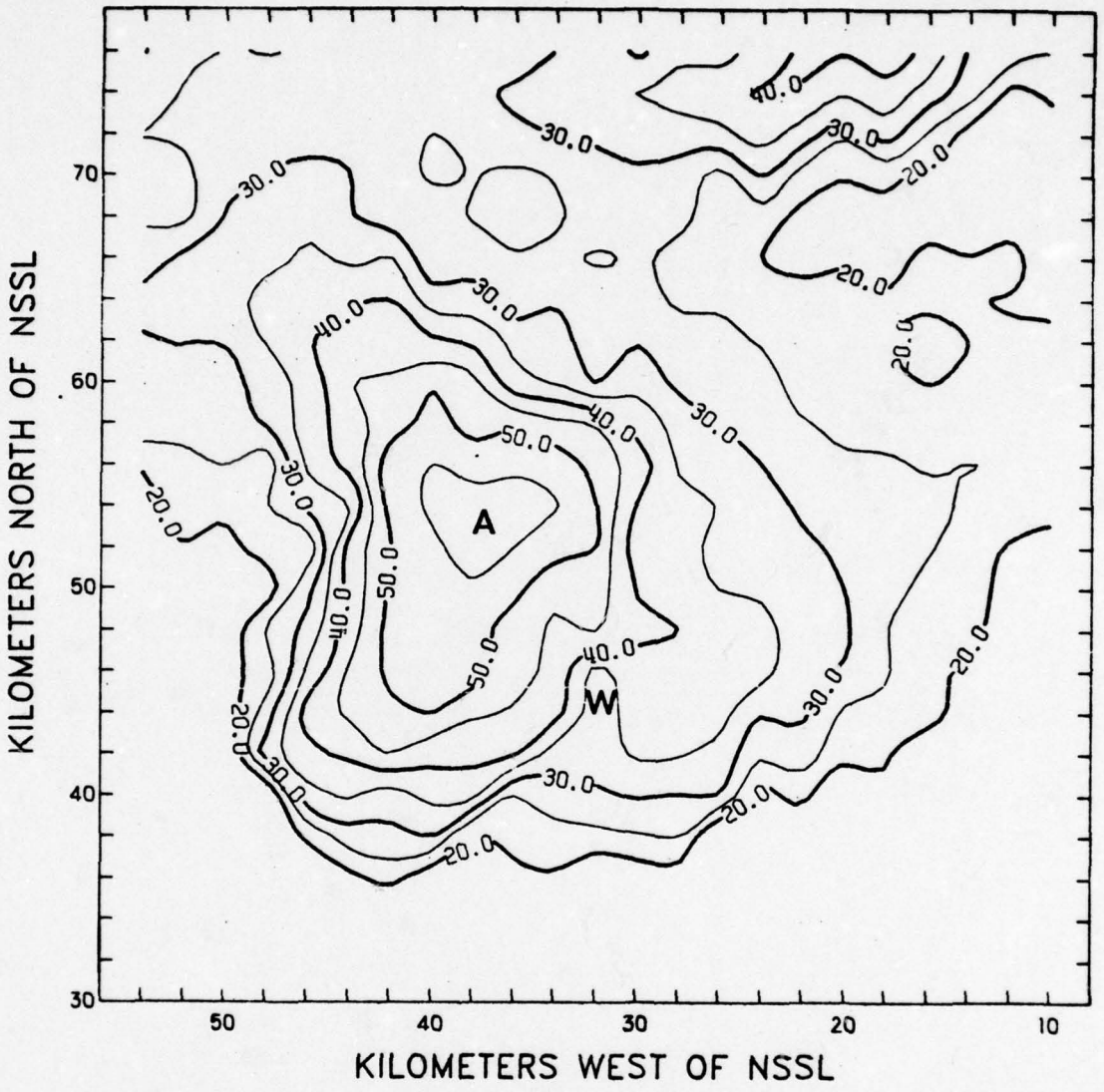

Fig. 51. The 20-kft CAZM (QUAD/LIN) for 1800 CST, 23 May 1974. Isopleths of reflectivity in dBZ.

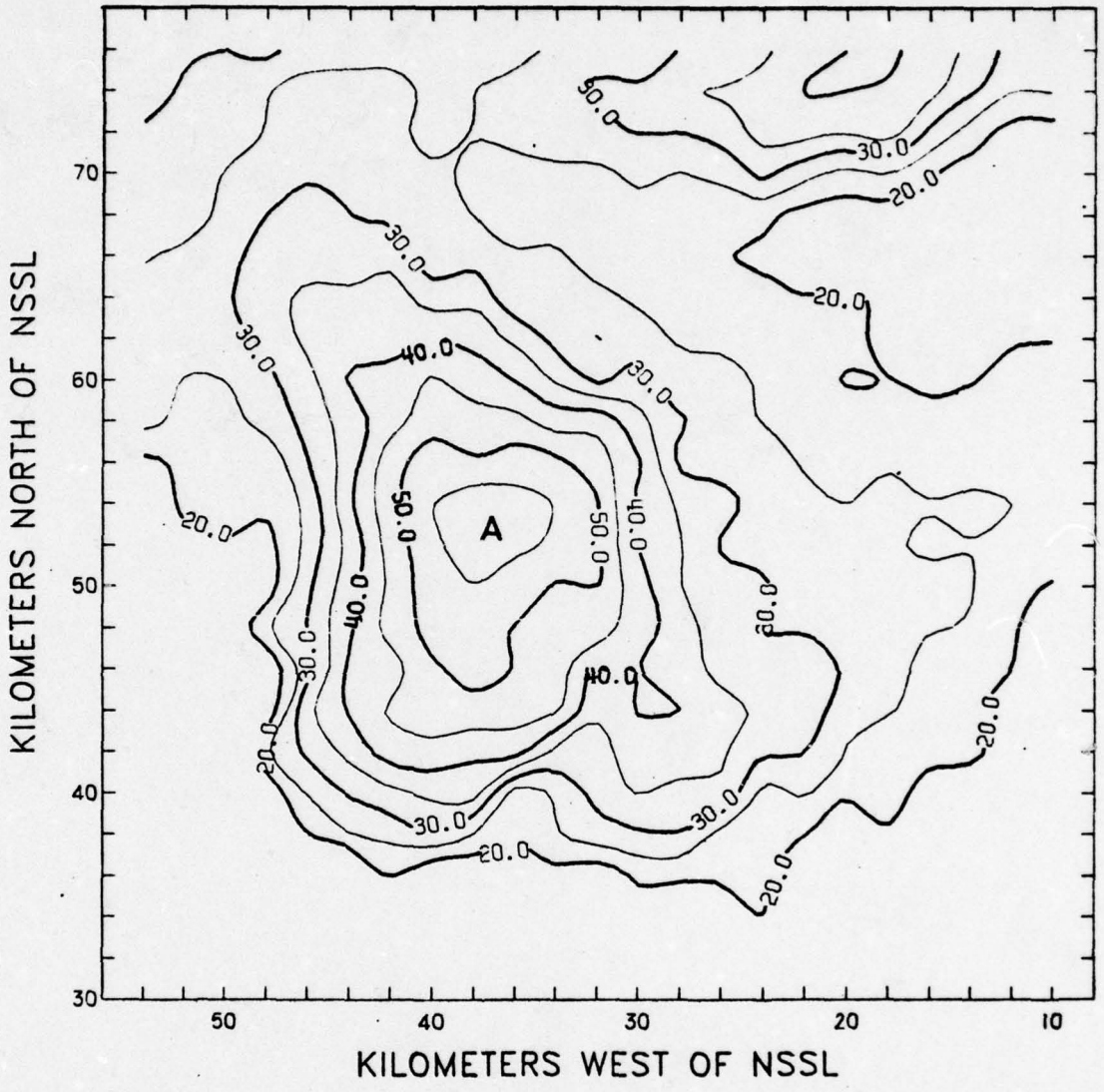

Fig. 52. The 25-kft CAZM (QUAD/LIN) for 1800 CST, 23 May 1974. Isopleths of reflectivity in dBZ.

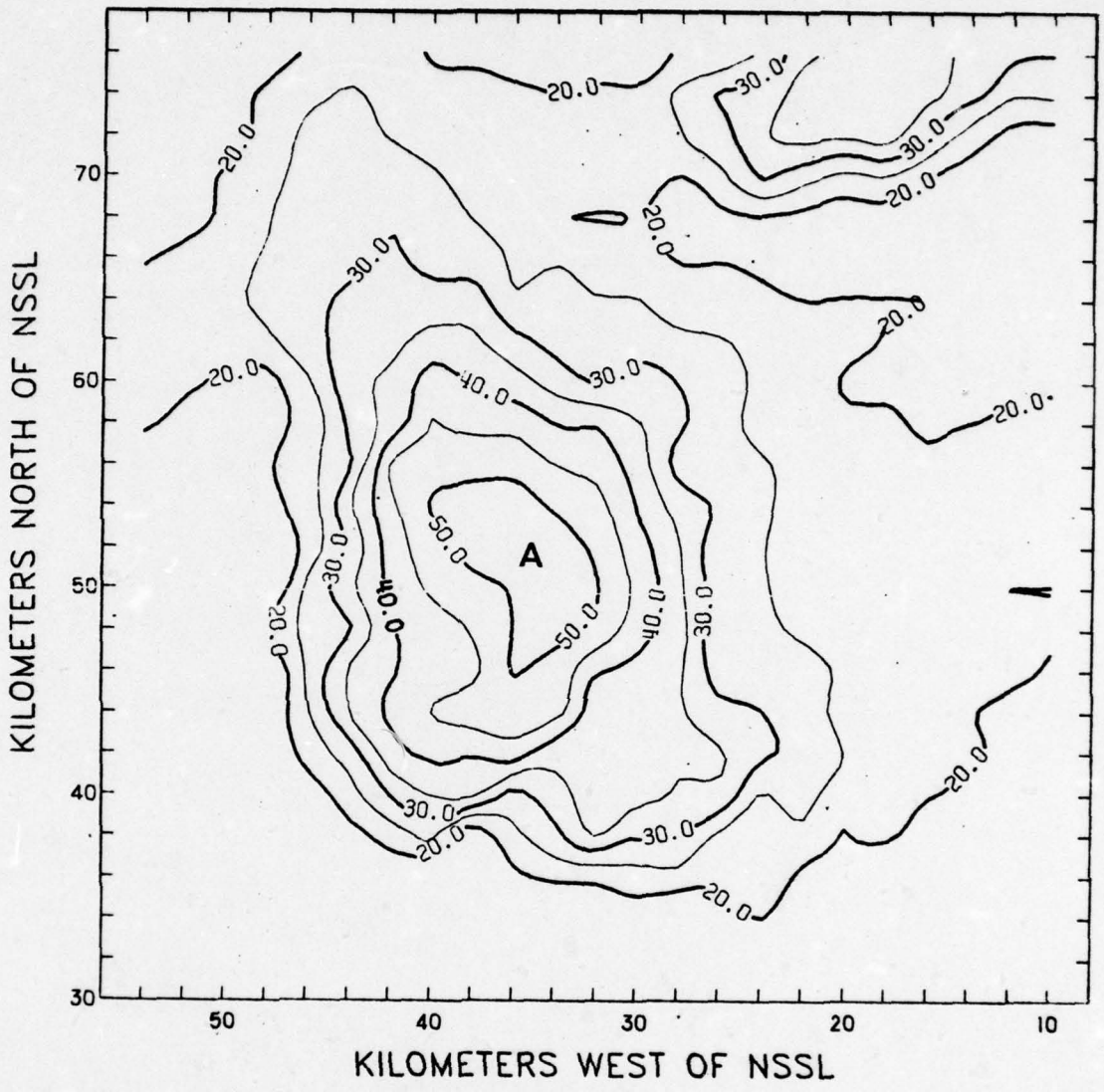

Fig. 53. The 30-kft CAZM (QUAD/LIN) for 1800 CST, 23 May 1974. Isopleths of reflectivity in dBZ.

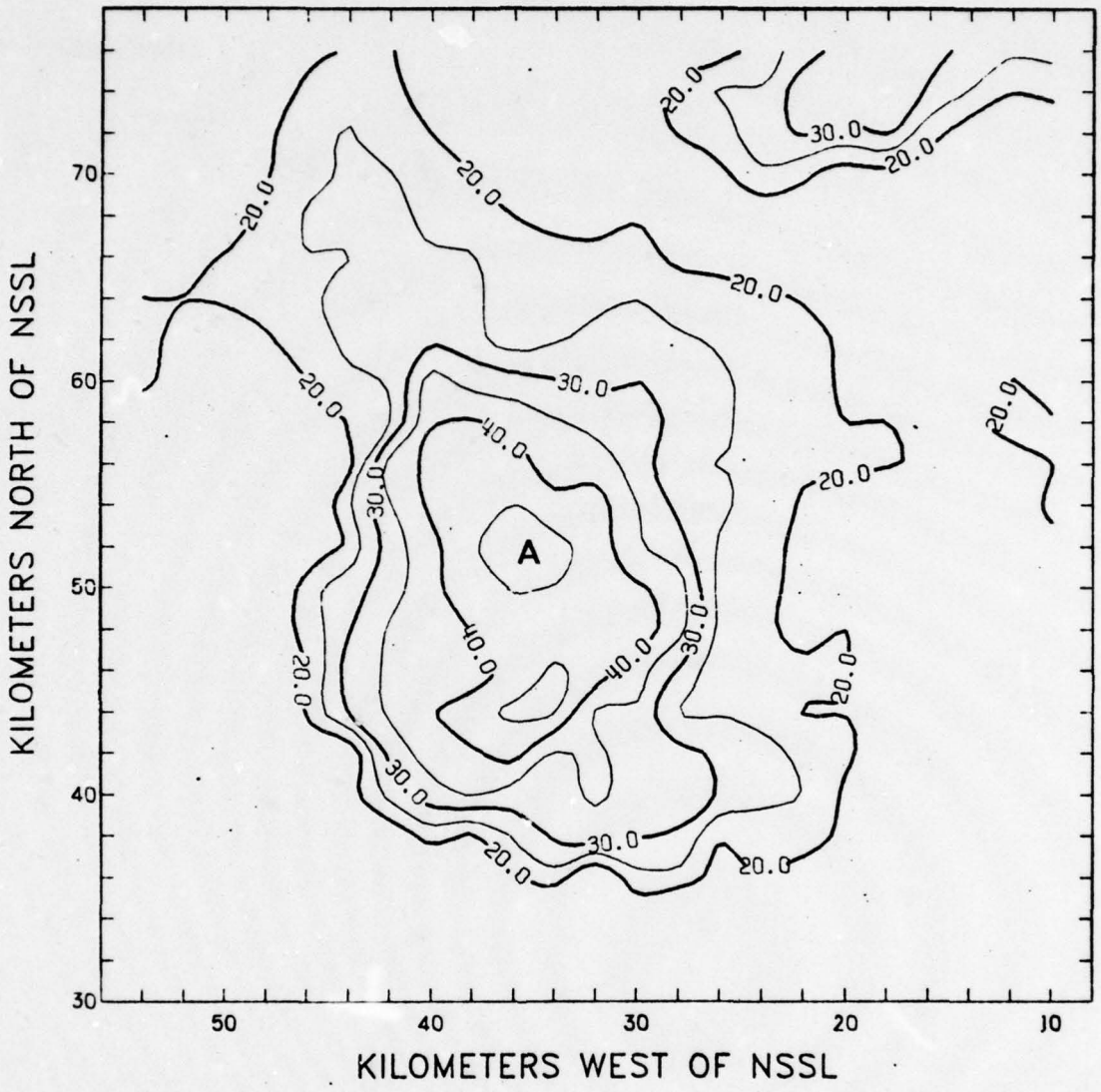

Fig. 54. The 35-kft CAZM (QUAD/LIN) for 1800 CST, 23 May 1974. Isopleths of reflectivity in dBZ.

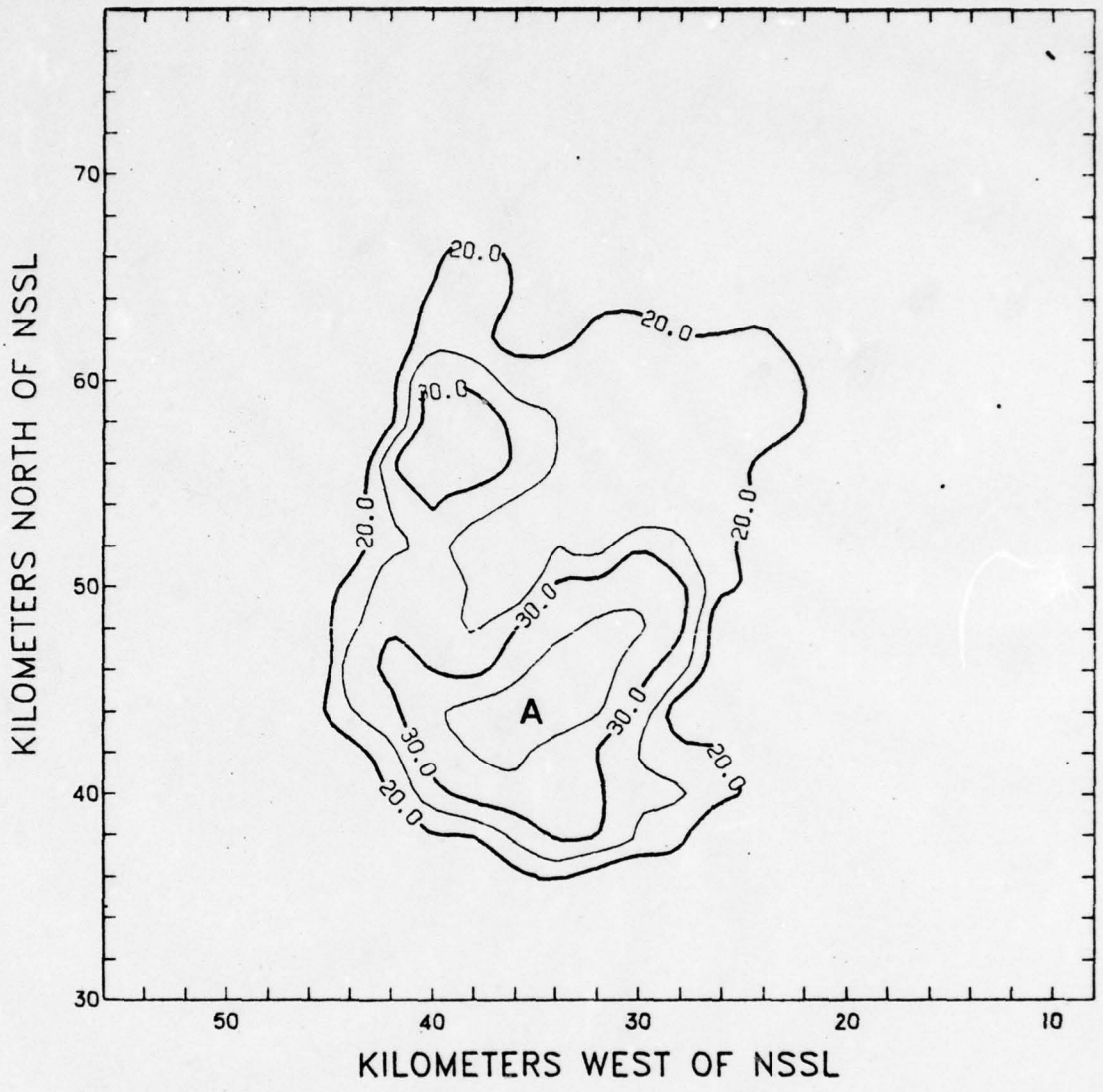

Fig. 55. The 40-kft CAZM (QUAD/LIN) for 1800 CST, 23 May 1974. Isopleths of reflectivity in dBZ.

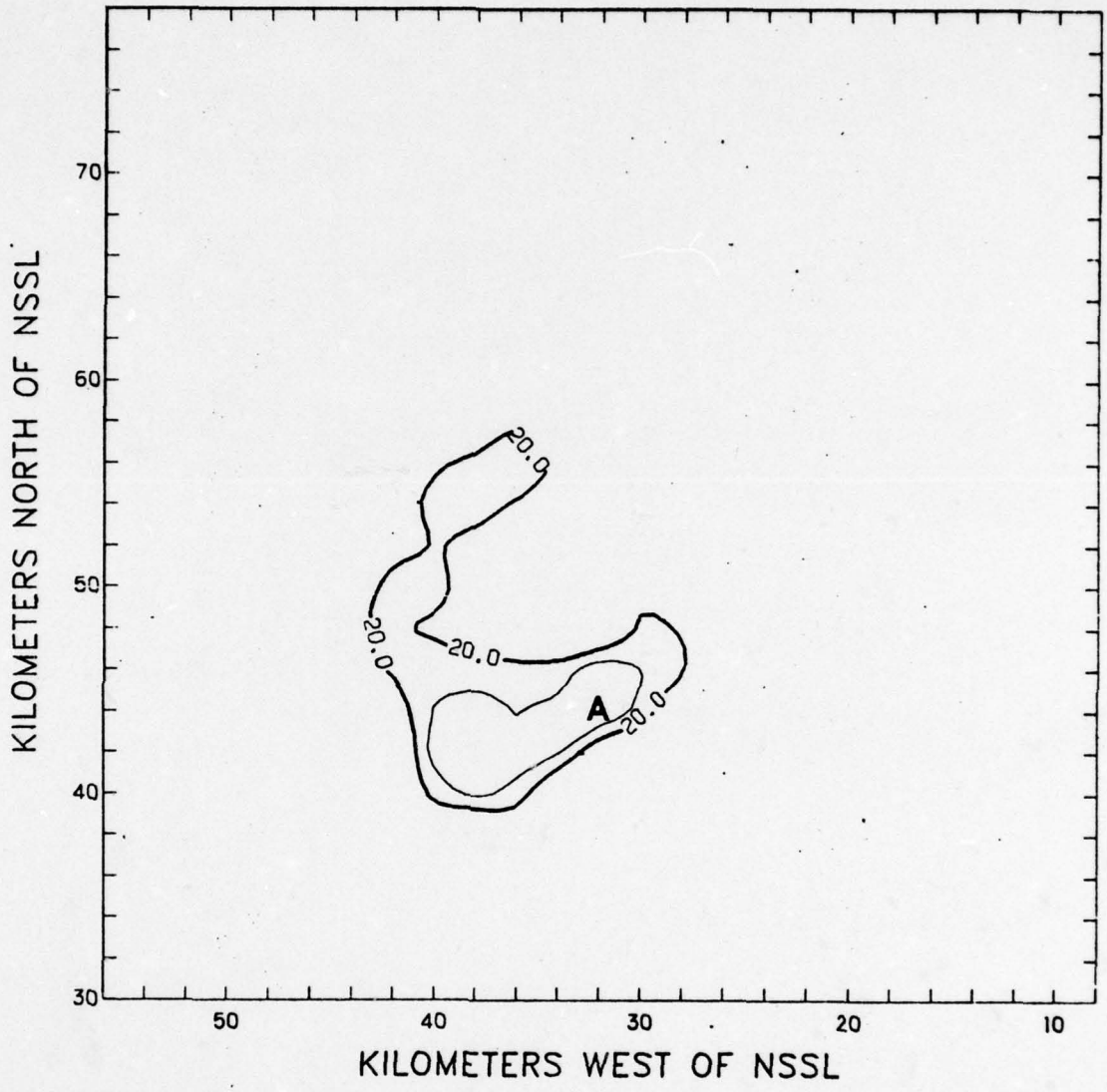

Fig. 56. The 45-kft CAZM (QUAD/LIN) for 1800 CST, 23 May 1974. Isopleths of reflectivity in dBZ.

representations of the CAZMs in the lower, middle, and upper layers of the storm complex. Therefore, these techniques will be the primary ones used for any further data reduction and analyses used in this investigation.

Results from Varying the Number of PVSZ Layers

Pittman [1976] occasionally experienced some difficulty in determining the tilt of a storm core with height. This difficulty arose when there was more than one center of maximum reflectivity in the lower-layer PVSZ map and only one center of maximum reflectivity in the middle-layer PVSZ map. This situation occurs for the Yukon storm at 1800 CST, 23 May 1974 (see Figures 41 through 43). However, it is clear from observing the lower-layer PVSZ map that cell A is stronger than cell B. Therefore, when one has to decide which centers to connect in the vertical to determine the tilt of the storm core, it is clear to one familiar with severe-storm structure that cell A extends through the middle and upper layers. In reviewing the PVSZ maps generated by Pittman, in most cases there was no difficulty in determining the tilt of the core.

The second case study conducted by Pittman [1976] was the Drumright storm on 8 June 1974. This storm presented a difficult situation in which the tilt of the storm core was not clearly defined with height. For this reason, the number of PVSZ layers was increased from three to four. The middle layer was divided into two layers, 15 kft to 25 kft and 25 kft to 35 kft. PVSZ maps depicting three layers of the storm are shown in Figures 57 through 59. In these presentations,

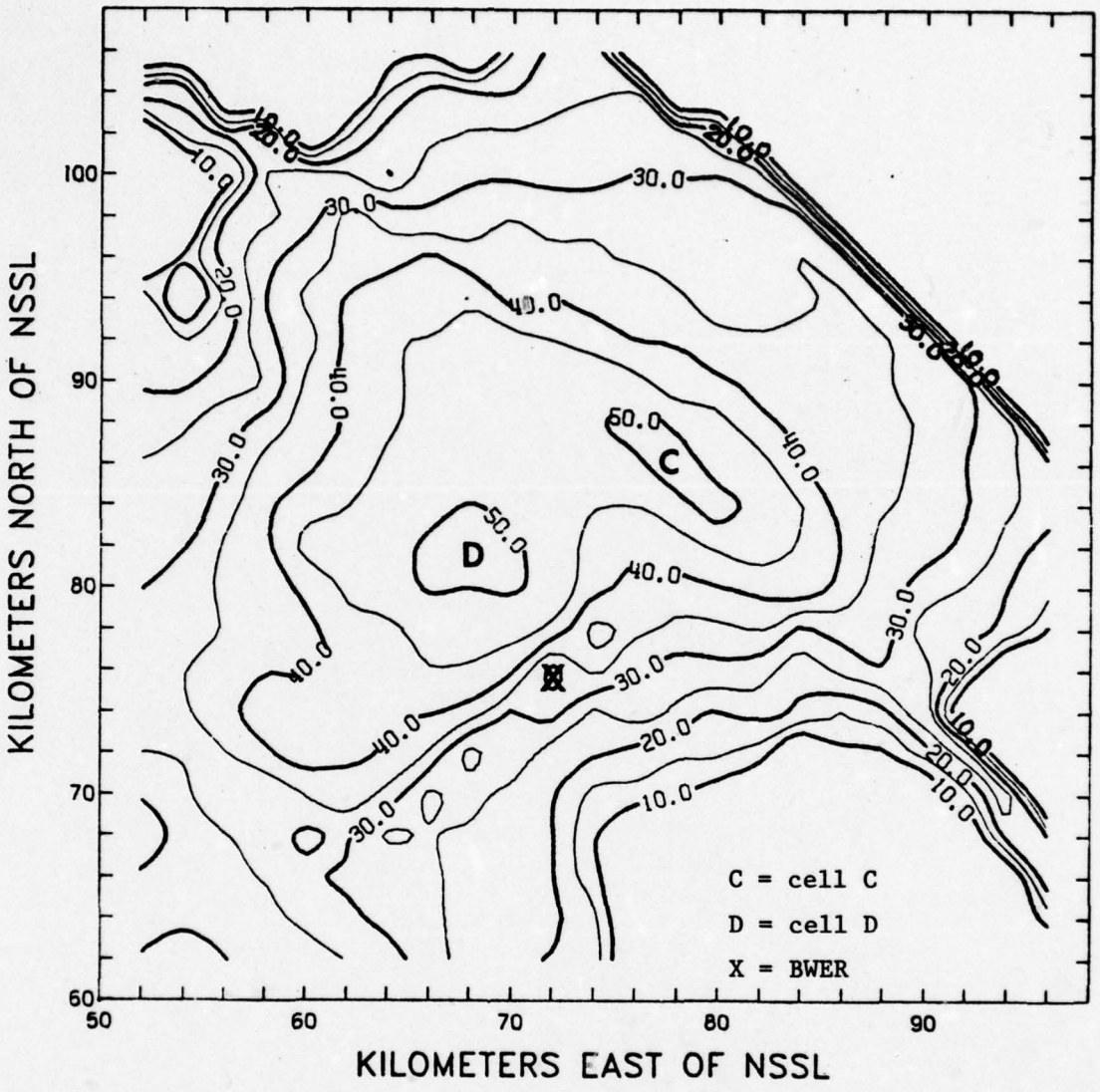

Fig. 57. Lower-layer PVSZ map (LAG-QUAD/LIN) for 1540 CST, 8 June 1974. Isopleths of reflectivity in dBZ.

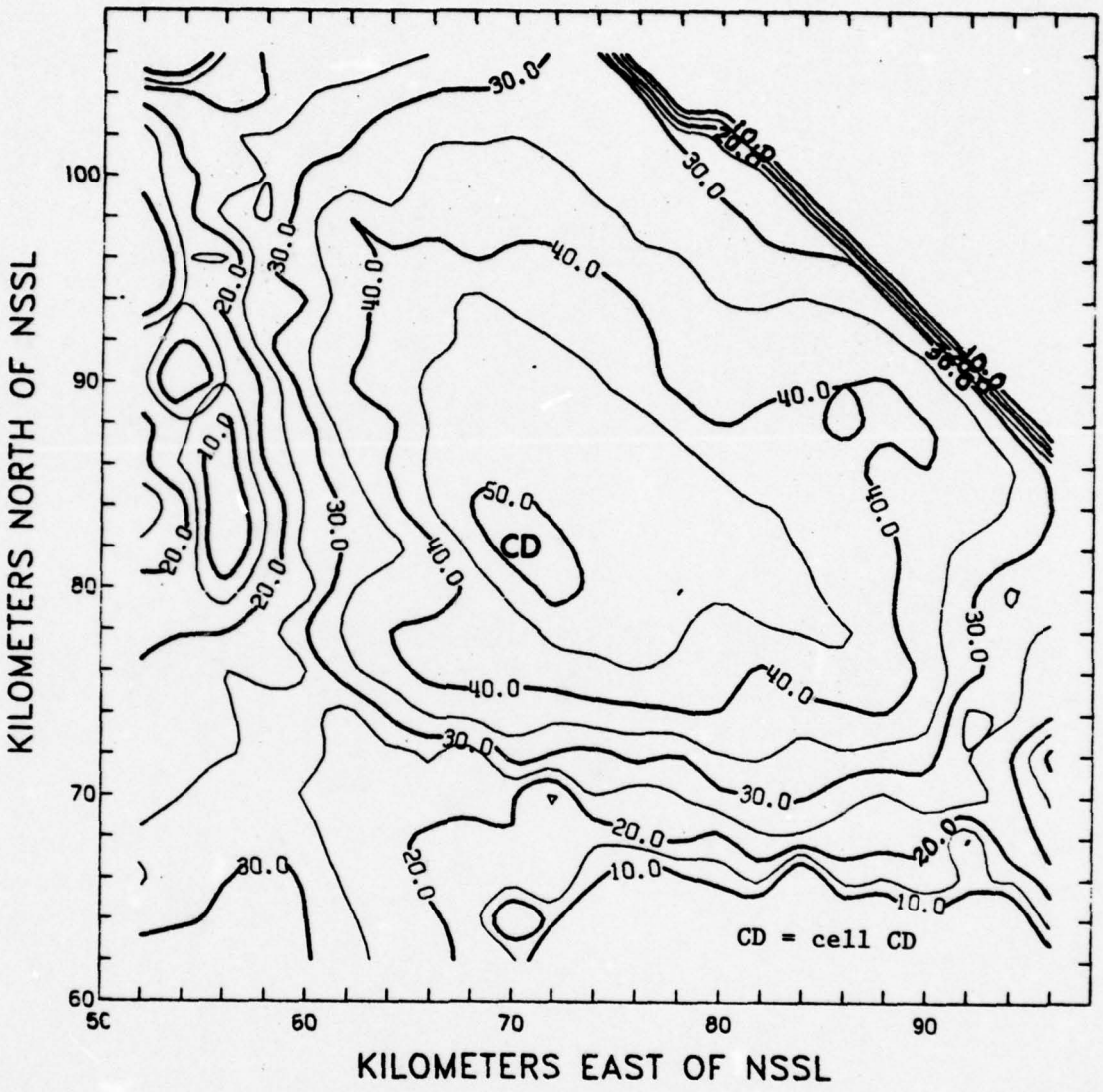

Fig. 58. Middle-layer PVSZ map (LAG-QUAD/LIN) for 1540 CST, 8 June 1974. Isopleths of reflectivity in dBZ.

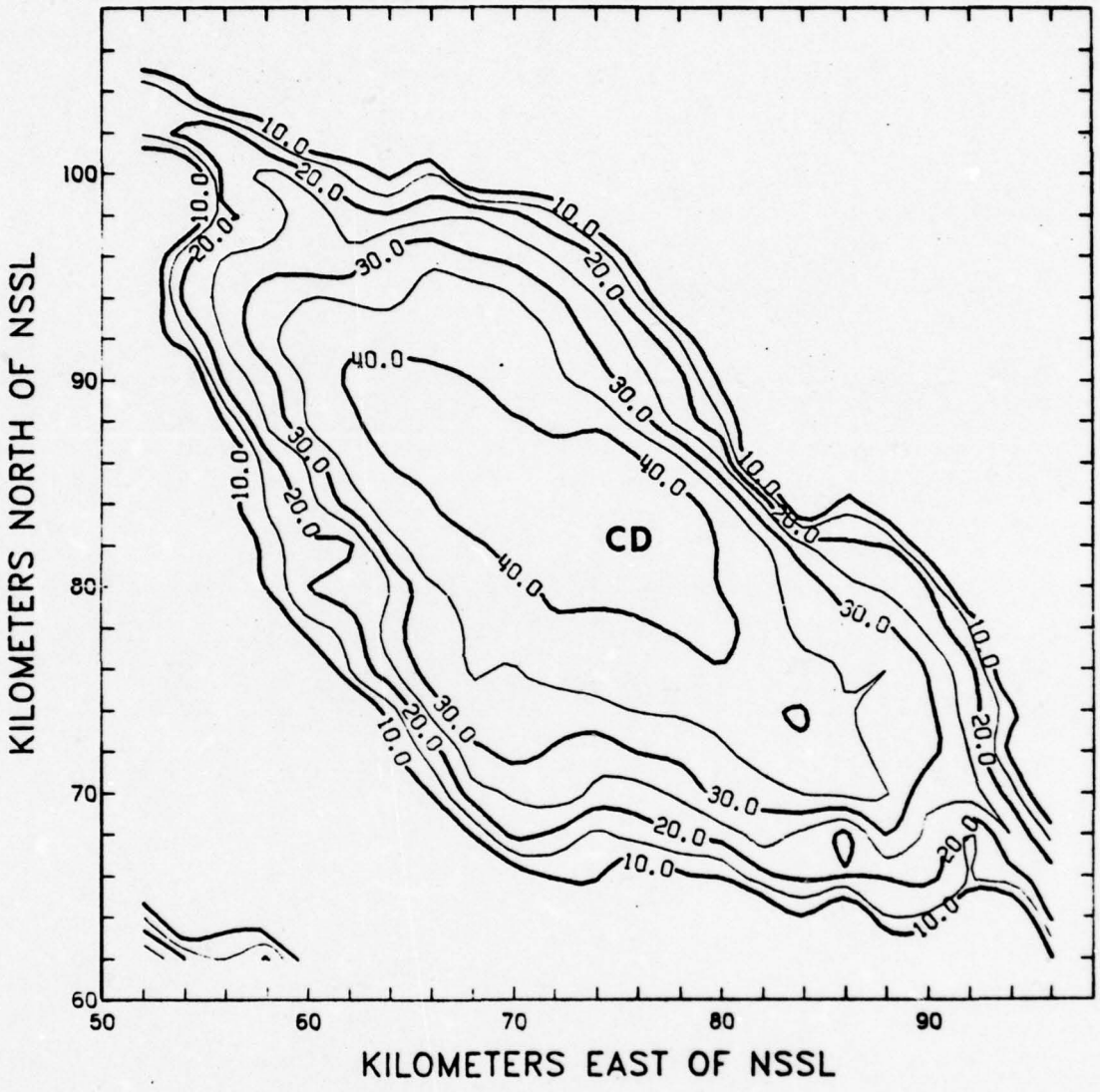

Fig. 59. Upper-layer PVSZ map (LAG-QUAD/LIN) for 1540 CST, 8 June 1974. Isopleths of reflectivity in dBZ.

it is not clear whether cell C or cell D should connect with cell CD in the middle- and upper-layer PVSZ maps. However, when the storm is divided into four layers, the problem is resolved. Figures 60 through 63 show the four PVSZ layers. It is now clear that cell D is the main cell and extends throughout the depth of the storm system.

The question now is whether or not the additional computer time and memory required to produce four PVSZ maps is justified. In most cases the tilt of the storm core with height is depicted adequately with three PVSZ maps. If the sample investigated is representative of the population, then in this author's opinion the additional computer time and memory are not justified. However, before any definitive conclusion can be made, more extensive research will have to be conducted in this area.

New England Severe Storm Case Study

This section contains a radar case study of two severe storms, one of which occurred in Kensington, New Hampshire, and the other in Wells, Maine, on Friday the 13th of August, 1976. The study includes the environmental conditions, a brief discussion of the severe-storm events, and a detailed analysis of these events by using PVSZ and VIL maps. The significant features to look for are the BWER, tilt of the storm core, changes in upper-layer mass as indicated by changes in the reflectivity maxima, and rapid changes in VIL maxima.

Environmental Conditions

The synoptic conditions for this system are presented in Figure

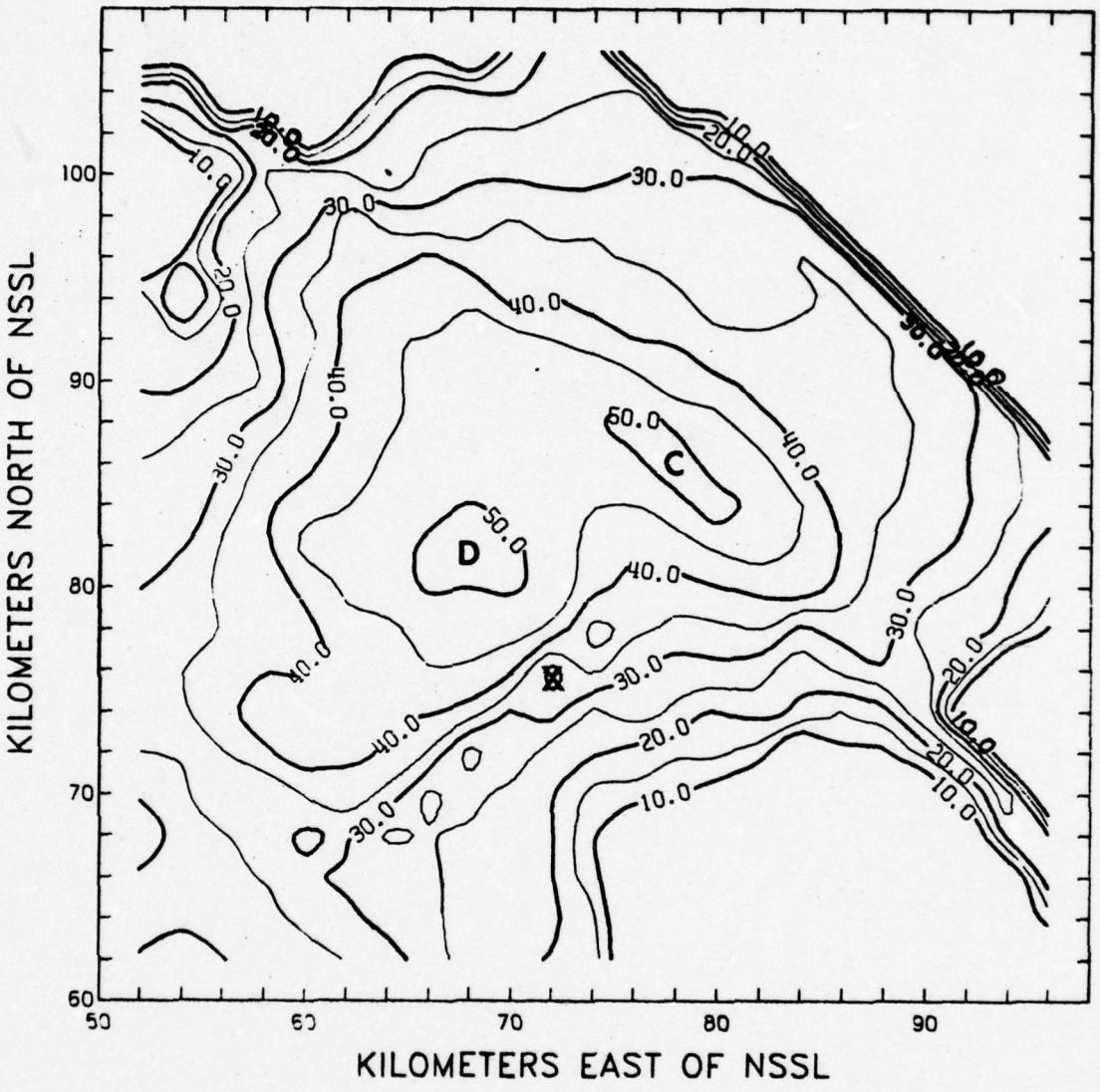

Fig. 60. Lower-layer PVSZ map (LAG-QUAD/LIN) for 1540 CST, 8 June 1974. Isopleths of reflectivity in dBZ.

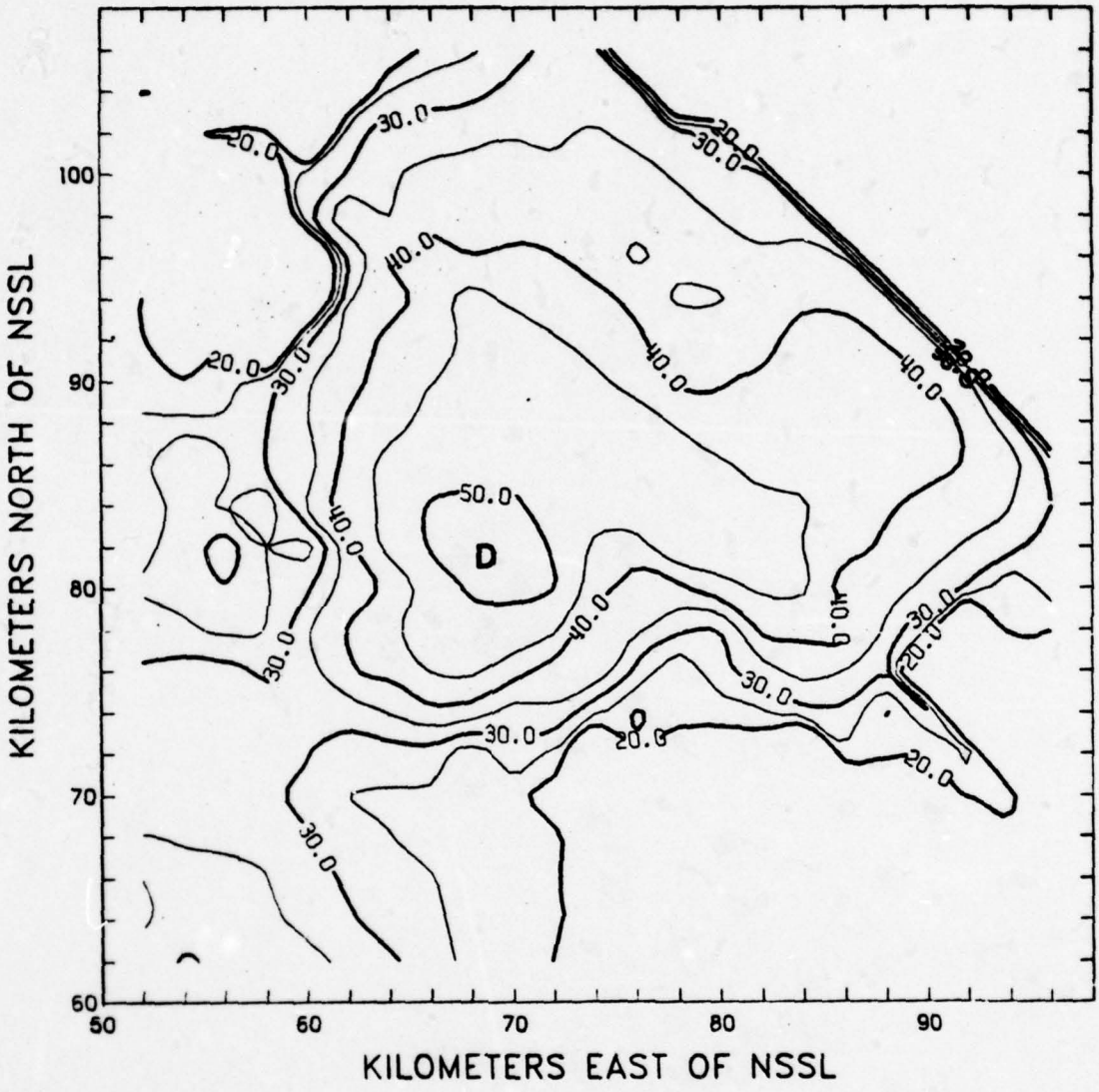

Fig. 61. Lower-middle-layer PVSZ map (LAG-QUAD/LIN) for 1540 CST, 8 June 1974. Isopleths of reflectivity in dBZ.

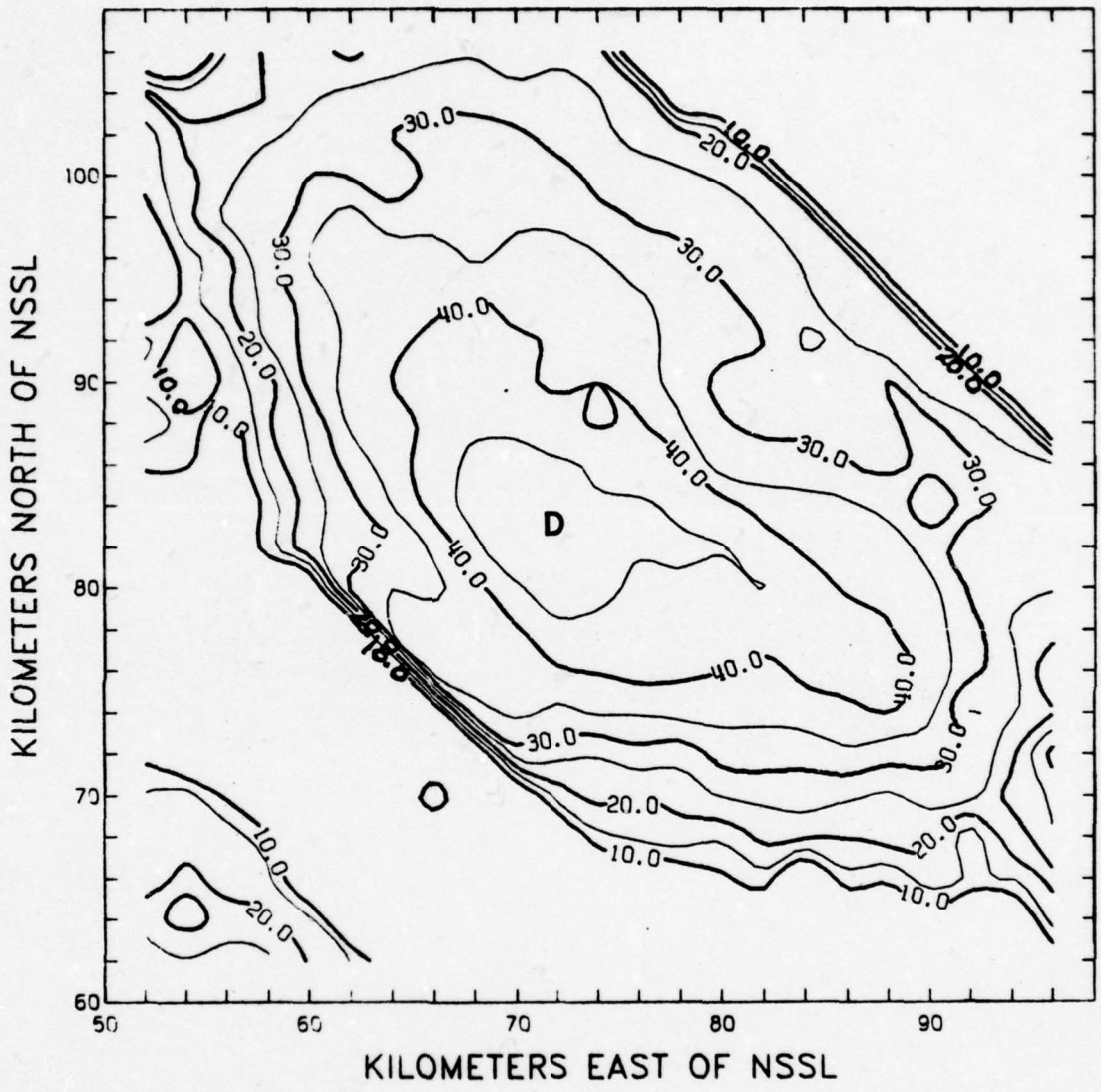

Fig. 62. Upper-middle-layer PVSZ map (LAG-QUAD/LIN) for 1540 CST, 8 June 1974. Isopleths of reflectivity in dBZ.

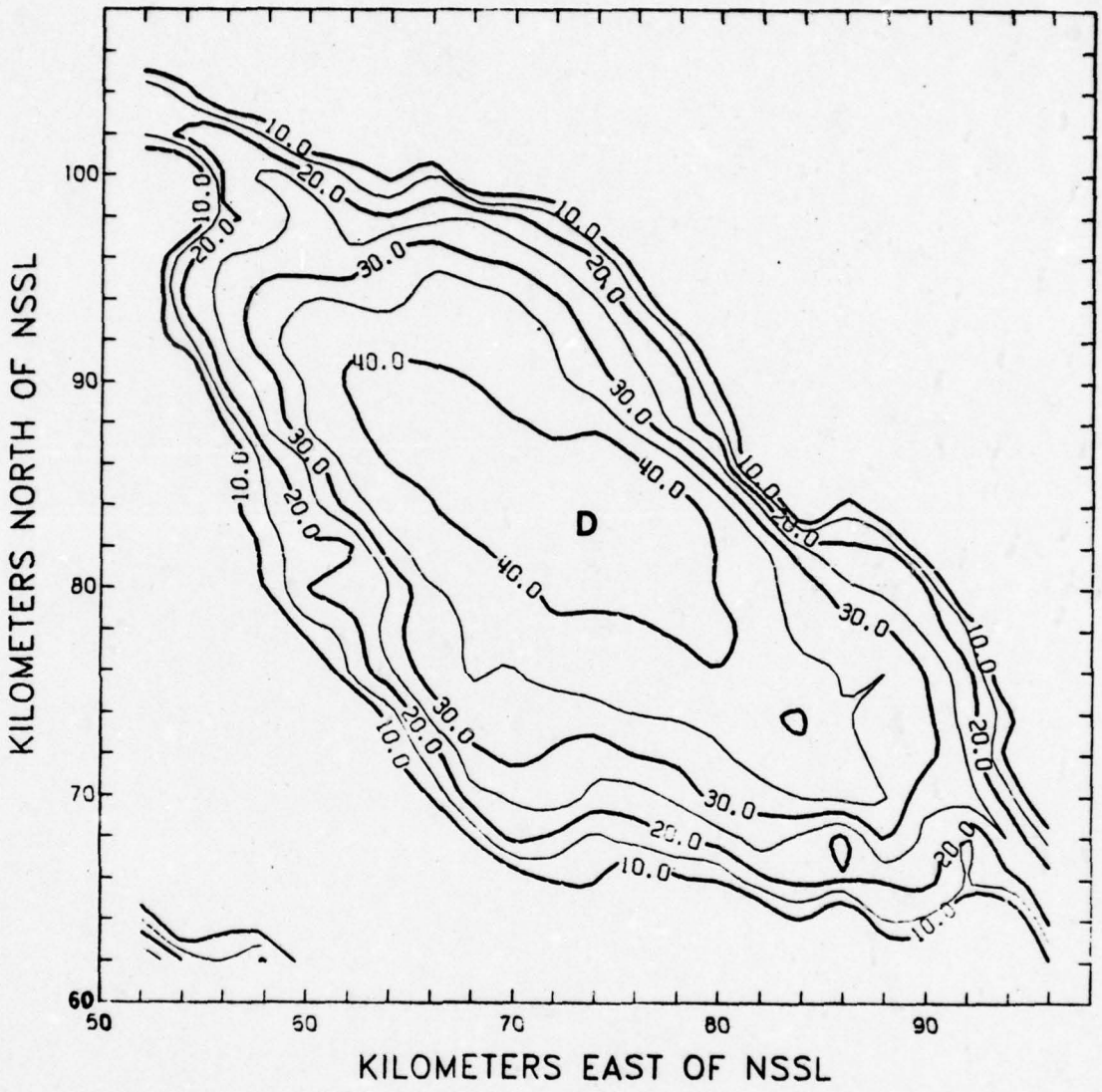

Fig. 63. Upper-layer PVSZ map (LAG-QUAD/LIN) for 1540 CST, 8 June 1974. Isopleths of reflectivity in dBZ.

64. This type of synoptic pattern is favorable for the formation of severe storms. At 1600 EST a slow moving cold front extended from the northern tip of Maine, southwestward along the U.S.-Canada border. The front was moving southeastward with a surface-level trough east of the mountains. The upper-level jet (70 kt) extended from western Vermont through central New Hampshire and southern Maine with a low-level jet extending from southwestern Massachusetts northeastward along the coast of Maine. The mid-level jet (40 kt) crossed southern Vermont, New Hampshire, and Maine. The intersection of the low- and mid-level jets was located in southern Maine. Ample low-level moisture also was available as indicated by the dashed line in Figure 64 that encloses an area of 2 deg dew-point spread or less at 850 mb. The average relative humidity from the surface to 500 mb was between 70 and 80% with 1.67 in. of precipitable water available. In addition, there was moderate to strong instability over the area as indicated by a lifted index of -4 and a K index of 35. Thus, all of the ingredients were available for the production of severe convective weather.

During the afternoon of 13 August 1976, thunderstorms developed over the mountains of New England and slowly moved eastward to east-northeastward. By late afternoon, a line of thunderstorms extended from northern Maine through south-central New Hampshire and into southern Vermont, western Massachusetts, and on southwestward as shown in Figure 65. This line was moving southeastward at 20-25 kt while the cells within the line were moving northeastward at 25-40 kt. The three strongest cells are as indicated in Figure 65. The cell with a top at 38 kft in Maine and the cell with a top at 52 kft in southeastern New

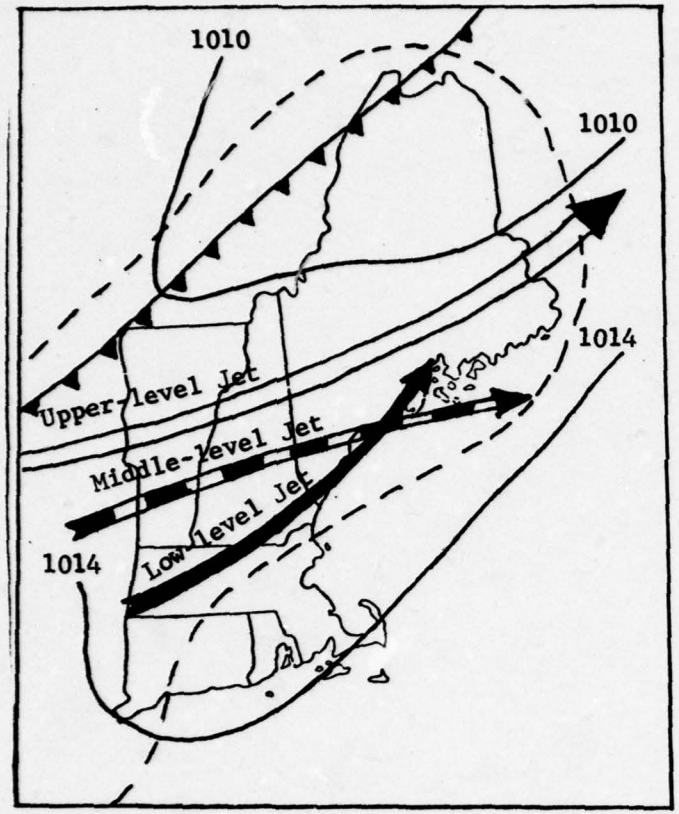

Fig. 64. Synoptic pattern for 1600 EST, 13 August 1976.

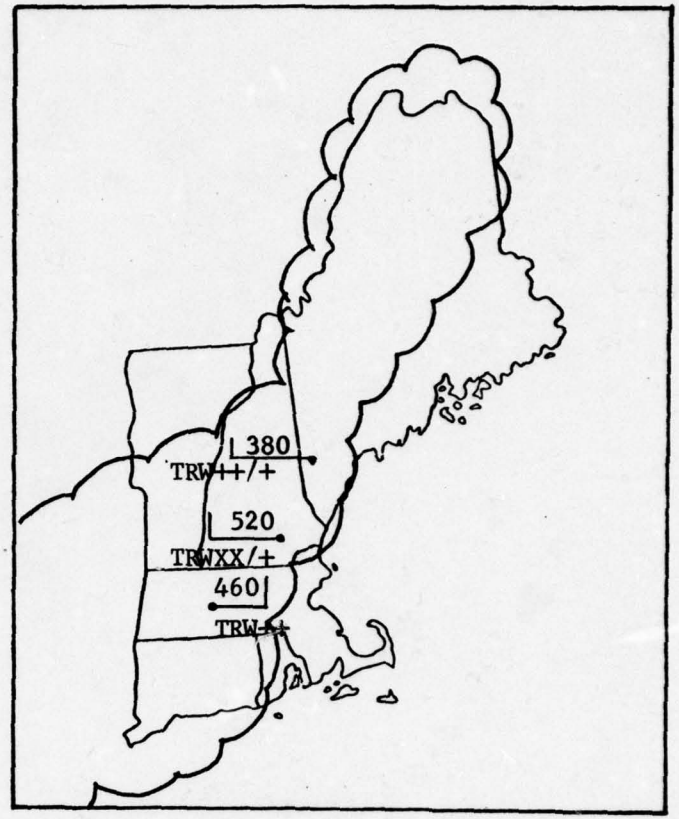

Fig. 65. Radar summary for 1830 EST, 13 August 1976.

Hampshire are the two storms of interest in this study.

Severe-Storm Events

The actual reports of severe-storm events were extracted from Storm Data, a monthly publication of the Environmental Data Service, NOAA, for August 1976. This publication contains such information as the location and time of occurrence of a severe-storm event, tornado path length and width, maximum hail size, maximum wind speed, and reports of injury and property damage.

Two severe-storm events were reported as a result of this storm system. At approximately 1915 EST, there was a severe thunderstorm at Kensington, New Hampshire, which caused a major power outage, many fires, severe lightning activity, and some moderate crop and property damage. There were no reports of serious injury and only one traffic related injury. At about the same time, 1900-1930 EST, a tornado was reported at Wells, Maine. The tornado touched down in the harbor and moved in an easterly direction, finally making landfall, destroying a house, and severely damaging several boats. Two persons were injured and required hospitalization.

Analysis of the Kensington Storm

From early evening, cell A was the dominant cell in terms of VIL (see Figure 66). Cell A moved in a general easterly direction at 25 kt from 1744 EST until the squall line formed at 1832 EST. From this time on, cell A moved to the east-northeast at 35 kt as the squall line moved to the east-southeast at 26 kt. New cells (cell D and cell E)

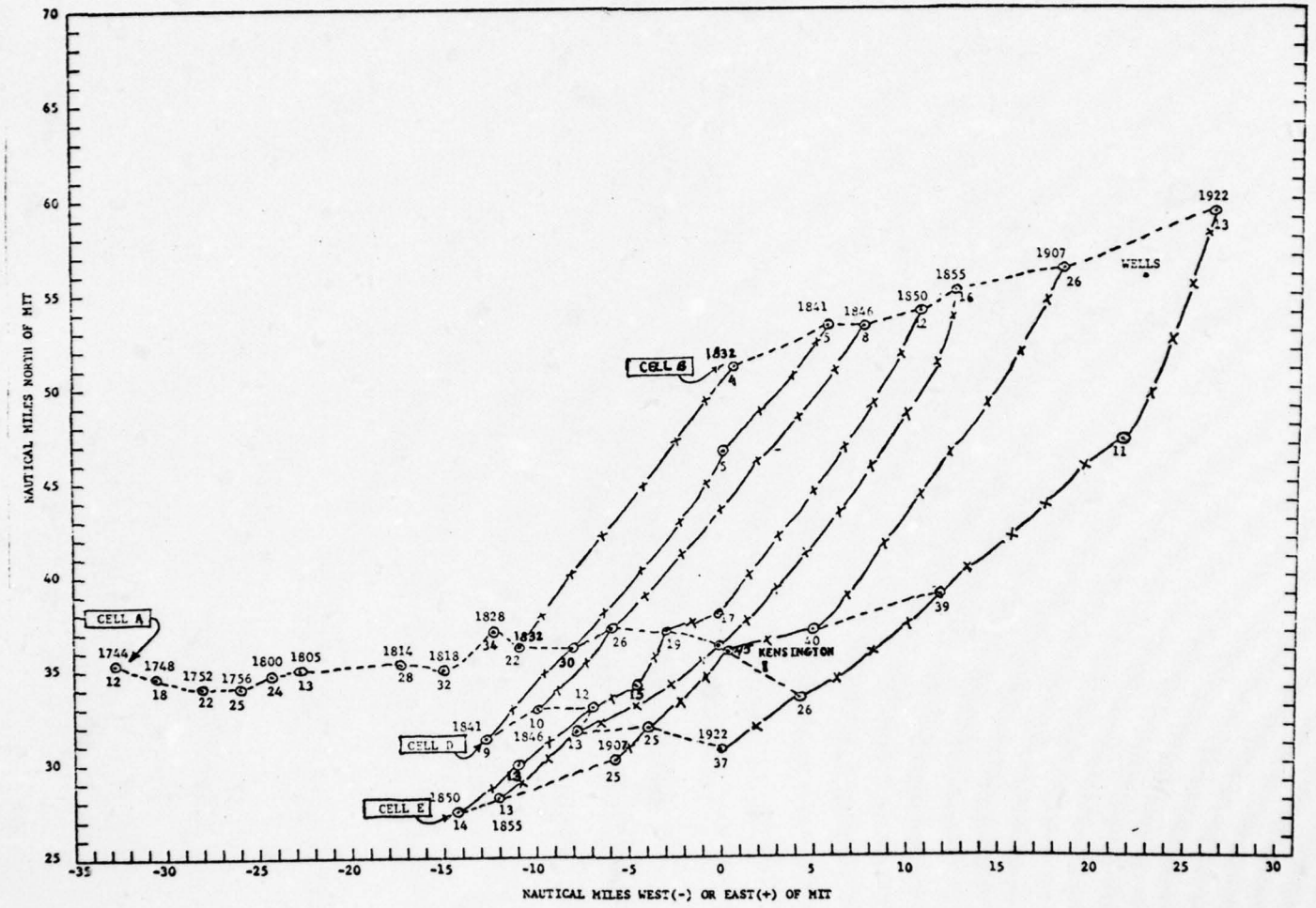

Fig. 66. VIL centers for 13 August 1976. The dashed lines show individual cell movement while the intermittent dash - x lines are the approximate position of the squall line at specific times. Values of VIL are in kg m^{-2}.

formed on the southern end of the squall line, thus lengthening the line. The VIL of cell A was 12 kg m^{-2} at 1744 EST and increased to greater than 20 kg m^{-2} by 1752 EST. Subsequently, the VIL of cell A fluctuated until 1850 EST when it decreased to 19 kg m^{-2} and then underwent a rapid increase to 45 kg m^{-2} at 1907 EST. This phenomenon is what Greene [1971] terms "explosive development." At this time, cell A was nearly vertical as indicated by the PVSZ maps in Figures 67 through 69. At the time of explosive development, not only did the maximum reflectivity values increase, but the horizontal area of the reflectivity maxima increased. In fact, the horizontal area bounded by the 45 dBZ isopleth increased by a factor of two or more in the lower and middle layers of the storm. In addition, cell A became quasi-stationary between 1855 and 1907 EST and then moved through Kensington between 1907 and 1922 EST. By 1922 EST, the VIL of cell A had decreased to 26 kg m^{-2} as the storm decreased in intensity. A BWER was evident in the middle-layer PVSZ map at 1907 EST just north of cells E and D. However, this BWER was located to the rear (as viewed from the MIT radar) of the storm complex and therefore may be caused by attenuation due to intervening precipitation. This same type of BWER also was noted in some earlier maps.

Analysis of the Wells Storm

At 1832 EST cell B formed (Figure 66) and became the north end of the squall line. While the squall line moved to the east-southeast at 26 kt, cell B moved to the east-northeast at a speed between 28 and 35 kt. The VIL of cell B started at 4 kg m^{-2} and increased slowly to 12

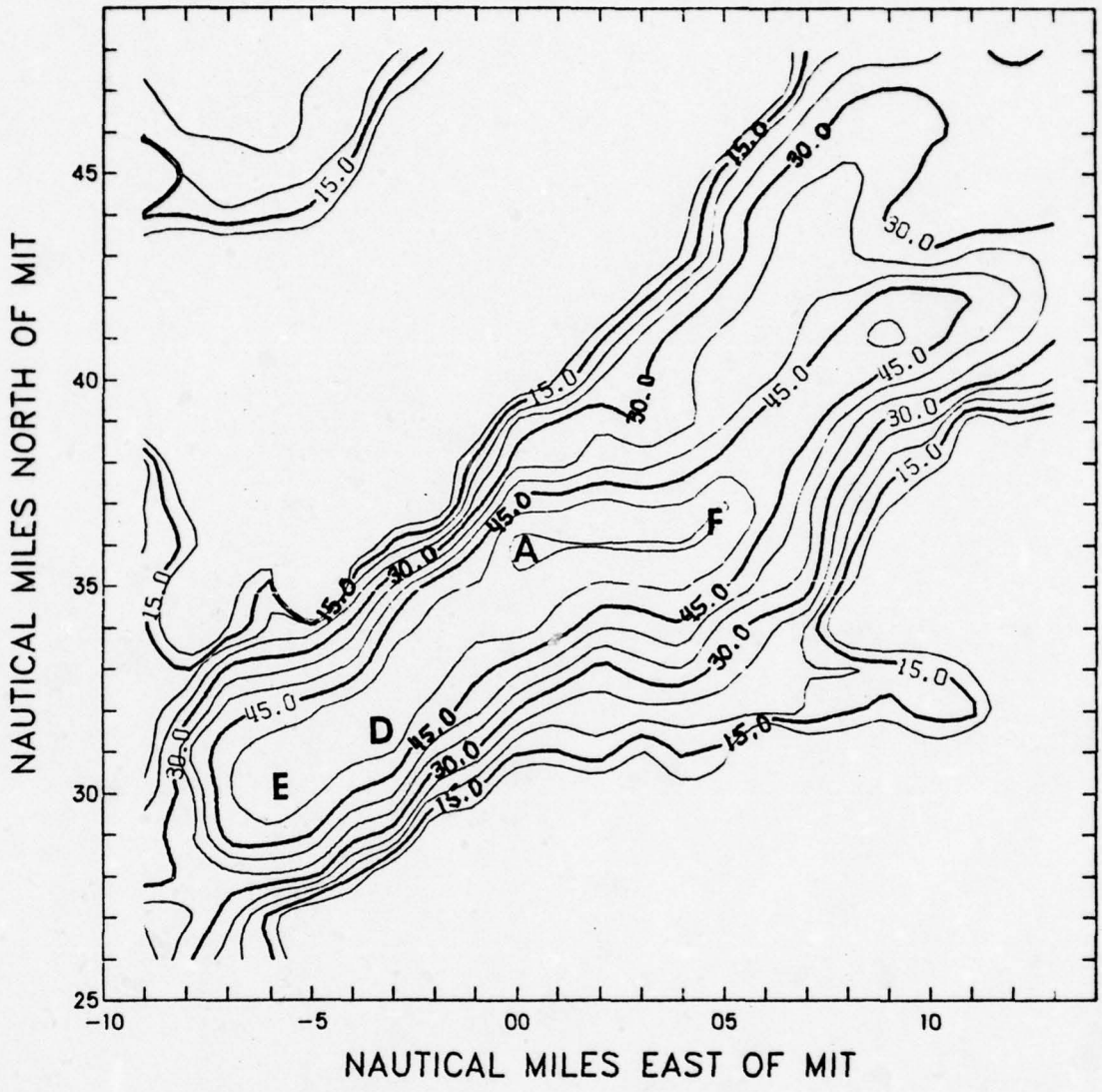

Fig. 67. Lower-layer PVSZ map for 1907 EST, 13 August 1976. Isopleths of reflectivity in dBZ.

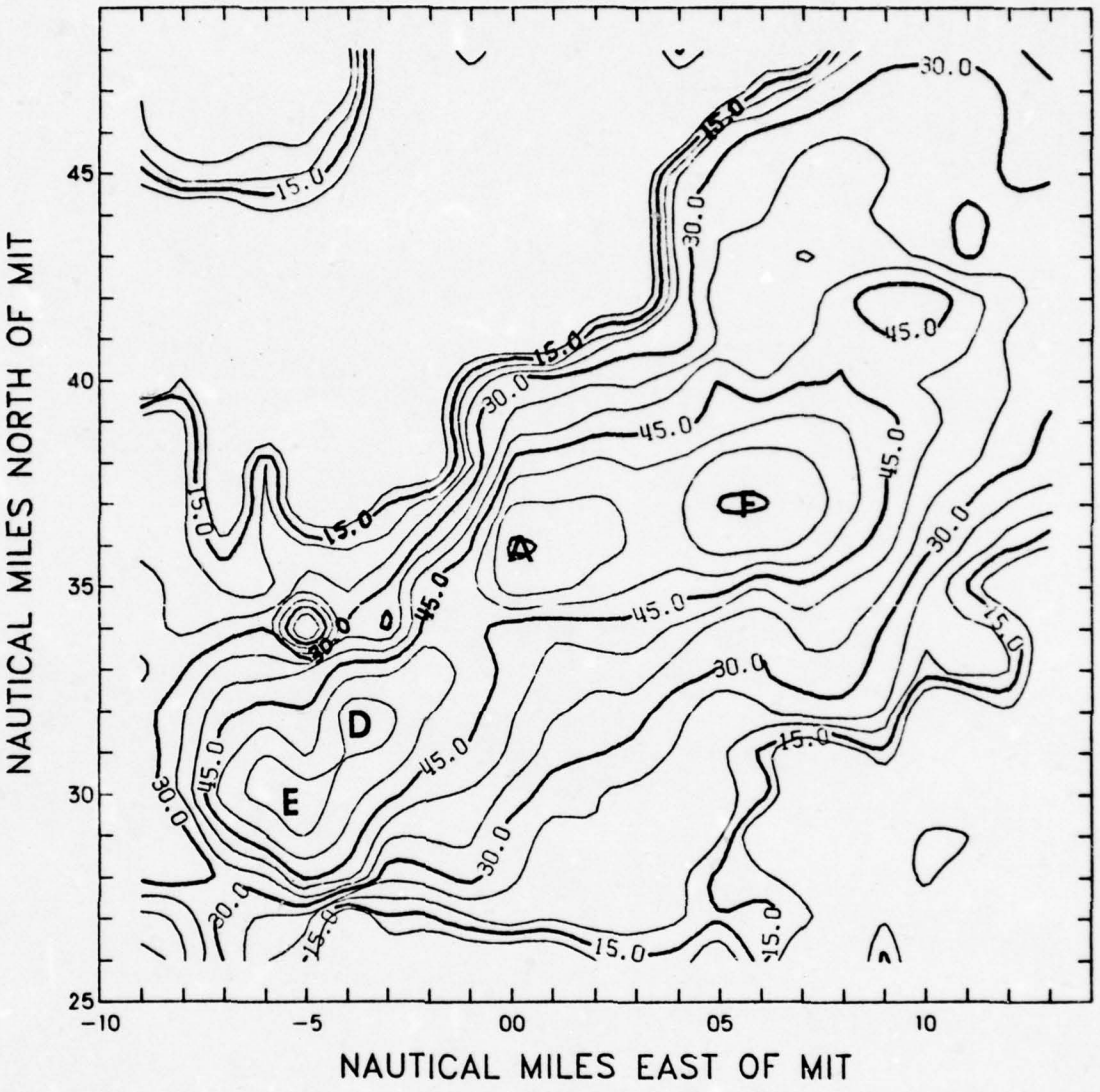

Fig. 68. Middle-layer PVSZ map for 1907 EST, 13 August 1976. Isopleths of reflectivity in dBZ.

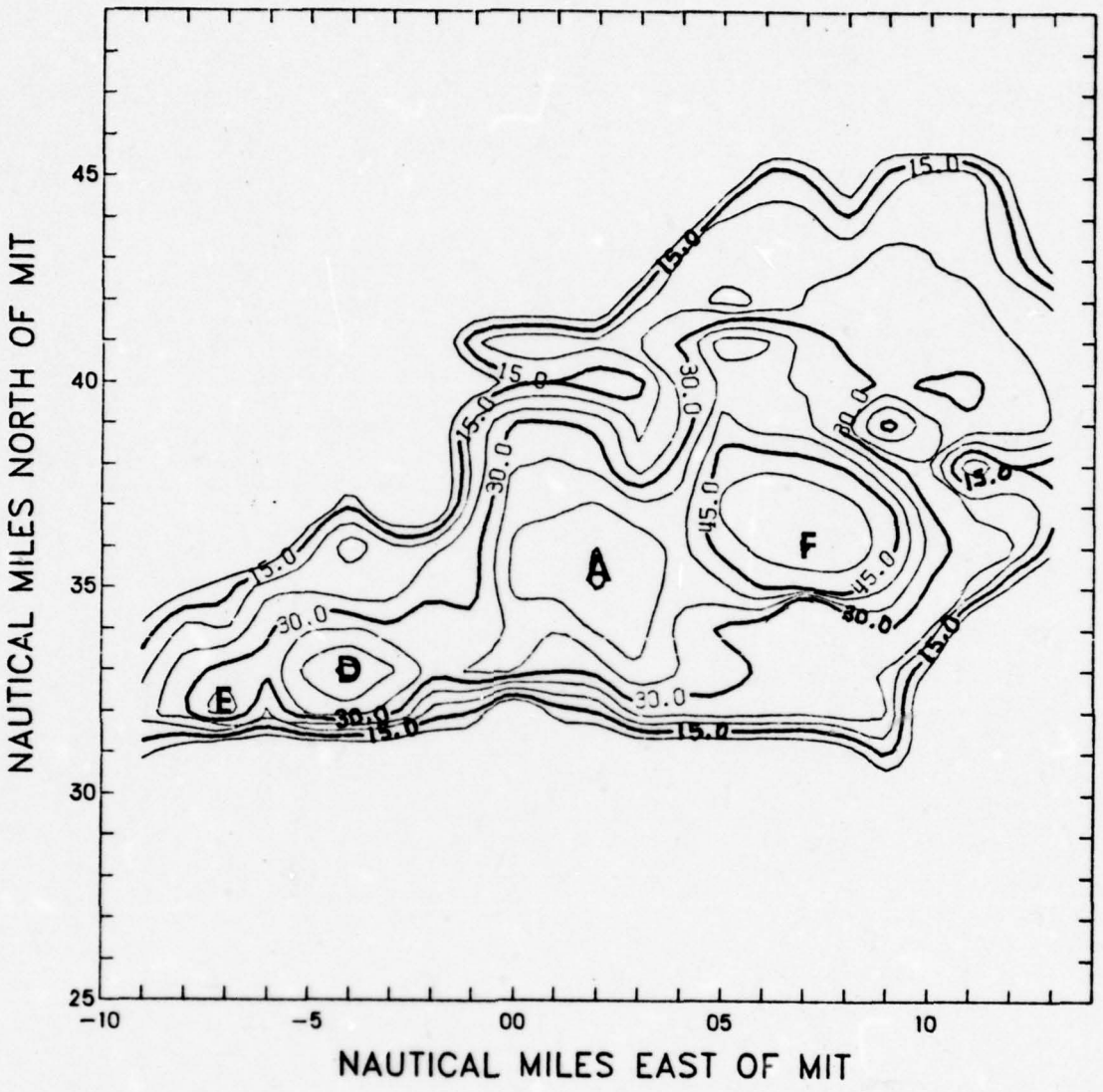

Fig. 69. Upper-layer PVSZ map for 1907 EST, 13 August 1976. Isopleths of reflectivity in dBZ.

kg m^{-2} at 1850 EST. In the next 17 min, the VIL increased from 12 to 26 kg m^{-2} and then decreased sharply to 13 kg m^{-2} by 1922 EST. The sharp increase at 1907 EST was caused by the storm becoming vertically stacked and possibly could be interpreted as explosive development. At any rate, the increase in VIL of cell B was not as dramatic as the explosive development of cell A. However, it is a well-known fact that the liquid water content of thunderstorms in New England is considerably less than the liquid water content of thunderstorms in the southern United States [Whiton, 1971]. Therefore, more research is needed in this area to establish criteria for explosive development in the New England states as well as other areas of the United States.

By 1846 EST, a satellite cell, BB, formed near cell B (the parent cell)(Figure 70). In addition, a BWER (cell R) with two smaller BWERs (cell Y and cell Z) were evident in the lower-layer PVSZ map. In the middle-layer PVSZ map shown in Figure 71, the parent cell (cell B), the satellite cell (cell BB), and the BWER (cell R) still are evident. The upper-layer PVSZ map is shown in Figure 72. The tilt of the storm core is away from the BWER at this time as shown in Figure 73, the PVSZ analysis summary. The system used by Canipe [1973] is used here. The symbol, ⊙ , represents the lower-layer PVSZ center, and each succeeding dot is the middle- and upper-layer PVSZ center, respectively. Canipe provides a complete description of this system. From 1846 to 1855 EST, the tilt of cell B and cell BB became more inclined toward the BWERs in the lower and middle layers of the storm complex. By 1907 EST, the tilt of cell B had become vertical between the lower and middle levels and the tilt of cell BB was inclined toward the BWER.

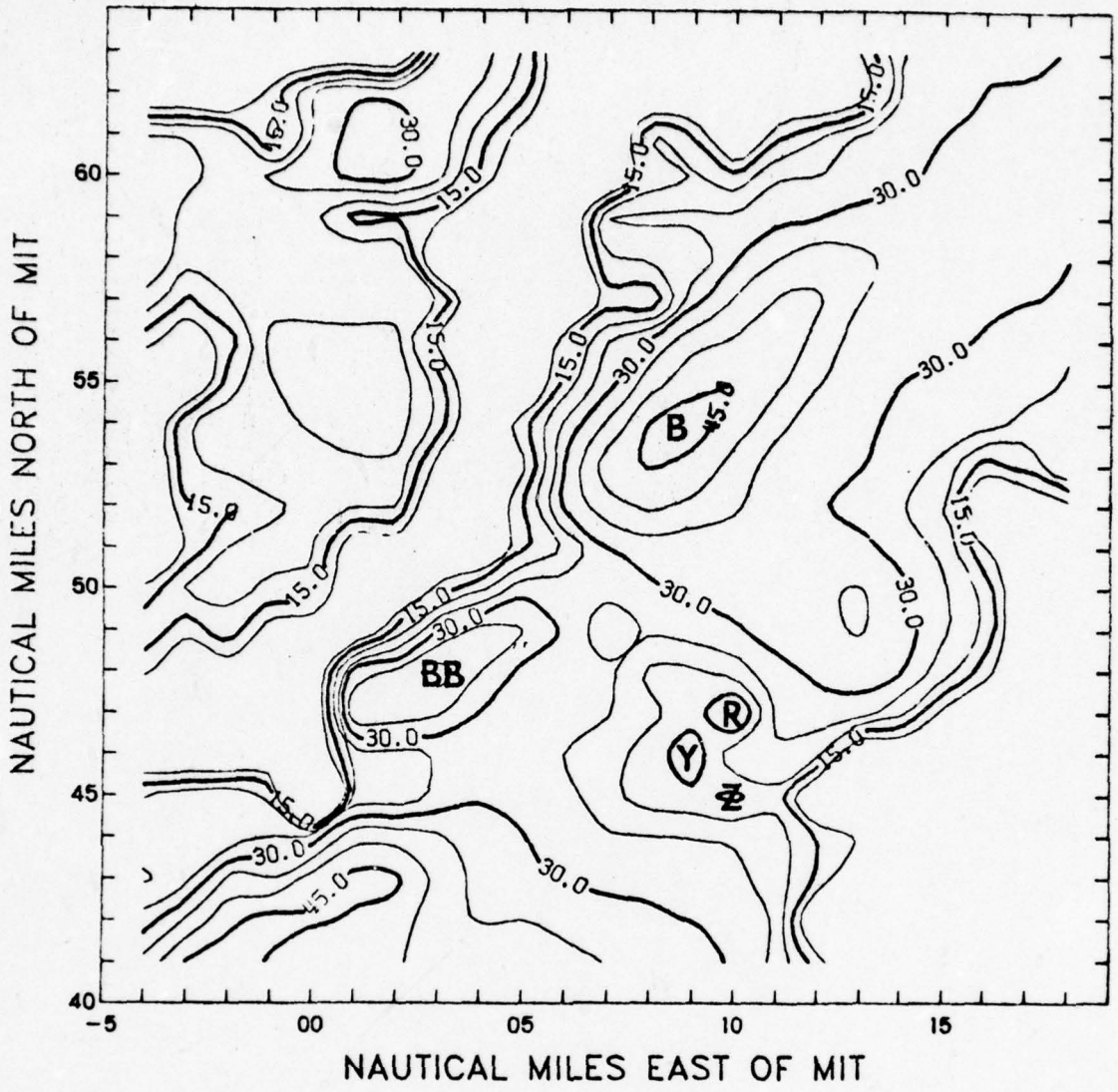

Fig. 70. Lower-layer PVSZ map for 1846 EST, 13 August 1976. Isopleths of reflectivity in dBZ.

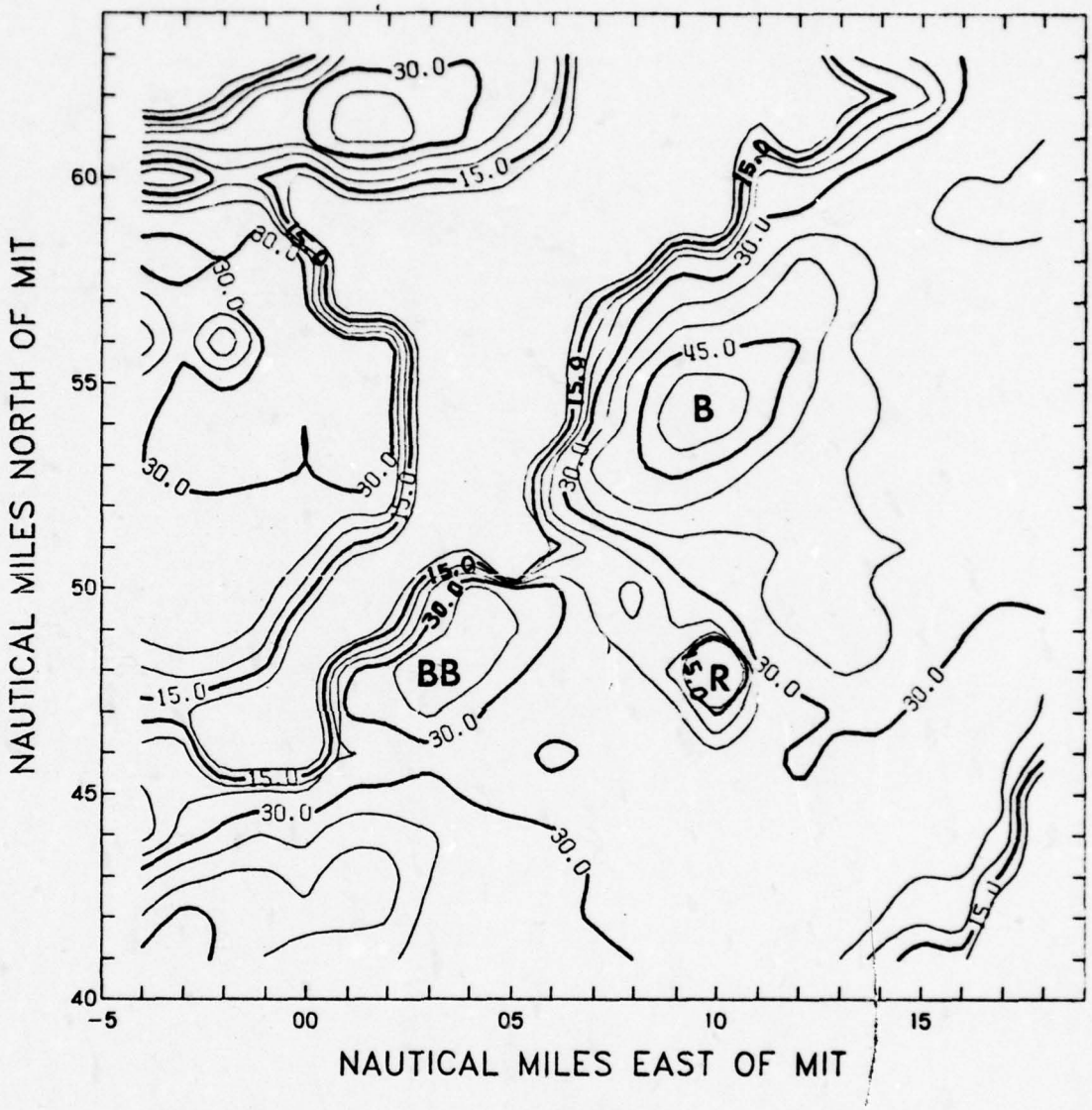

Fig. 71. Middle-layer PVSZ map for 1846 EST, 13 August 1976. Isopleths of reflectivity in dBZ.

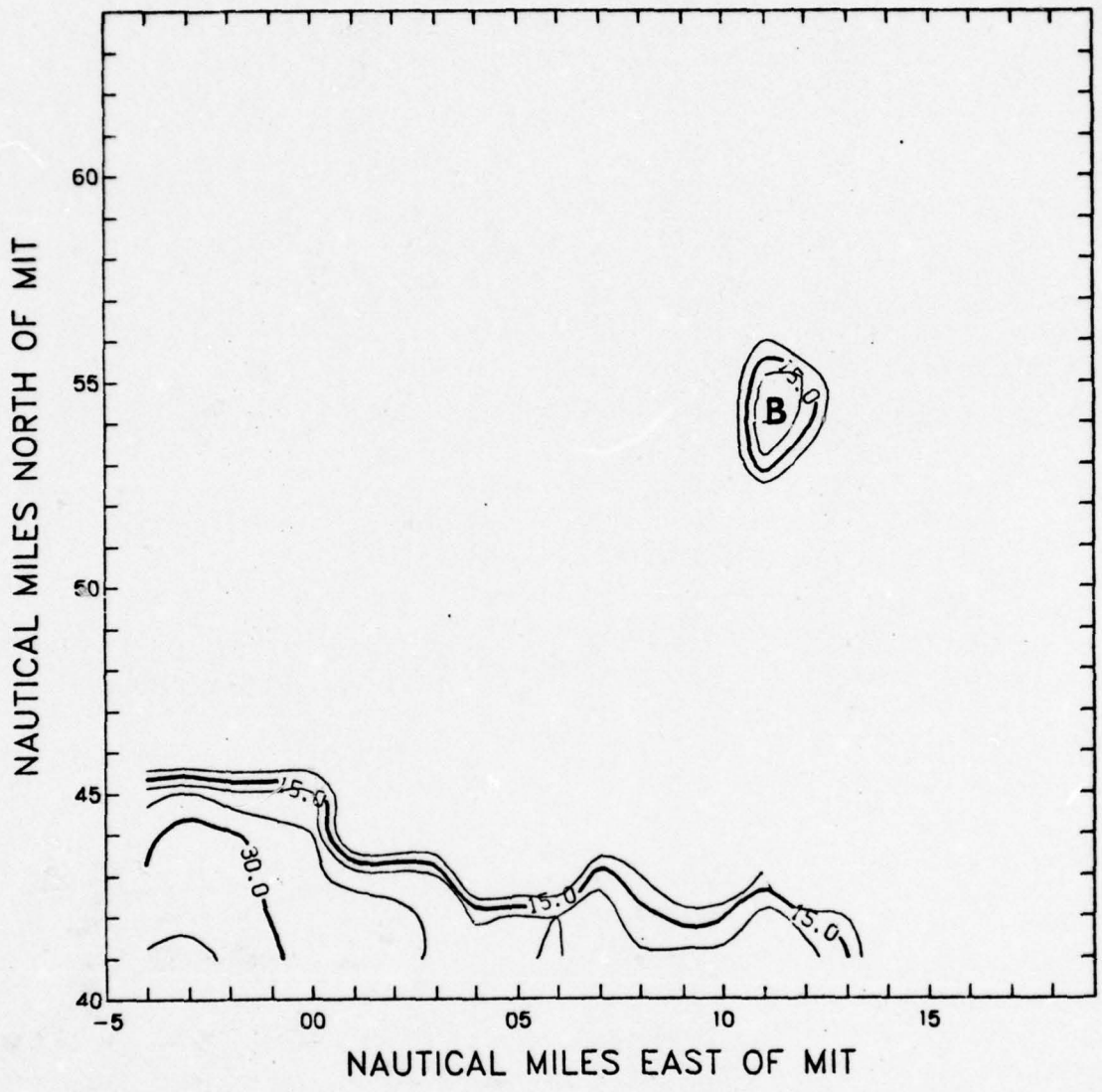

Fig. 72. Upper-layer PVSZ map for 1846 EST, 13 August 1976. Isopleths of reflectivity in dBZ.

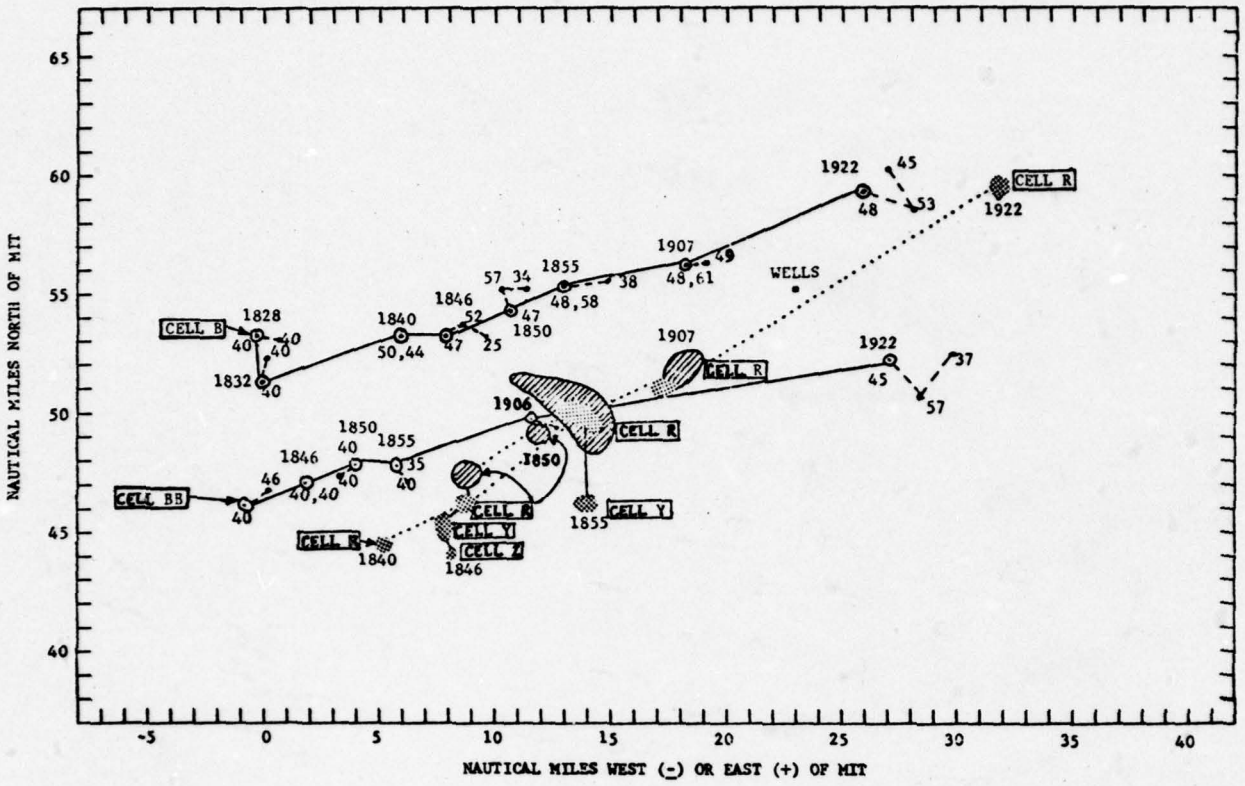

Fig. 73. PVSZ summary for the Wells storm of 13 August 1976. The solid lines show cell movement while the dotted lines show BWER cell movement. Stippled areas are lower-layer BWERs and hatched areas are middle-layer BWERS. Values of maximum reflectivity in dBZ are shown below cell positions.

There is no evidence of a decrease in reflectivity in the upper layer at this time; however, there was a decrease in the maximum reflectivity in the upper and middle layers of the storm between 1907 and 1922 EST when the tornado touched down at Wells. The series of PVSZ maps for 1855 EST to 1922 EST are shown in Figures 74 through 82.

Vortex Formation and the BWER

This section is a review of various theories concerning vortex formation in severe convective storms. The relationship of the vortex with the BWER also is discussed.

Hydrodynamic laboratory experiments have shown that vortices can be formed in the wake of fluid flow around a solid, cylindrical object [Prandtl and Tietjens, 1957]. In addition, it has been shown that severe thunderstorms act as a barrier to the environmental winds. Brown et al. [1973], by using doppler radar, found that both the updraft and tornado cyclone circulation act as a barrier to mid-level environmental winds. Jessup [1972] found much the same results by analyzing chaff trajectories around a tornado-producing thunderstorm. Kropfli and Miller [1976] analyzed data from two doppler radars that were used simultaneously to scan a large hailstorm in northeast Colorado. Kropfli and Miller's results show a region of cyclonic vorticity on the right side of the storm and a region of anticyclonic vorticity on the left side (see Figure 83). They imply that the generation of a vorticity is due to the updraft of the storm acting as a barrier to the environmental wind flow. The result is a generation of cyclonic curvature on the right flank of the storm and anticyclonic

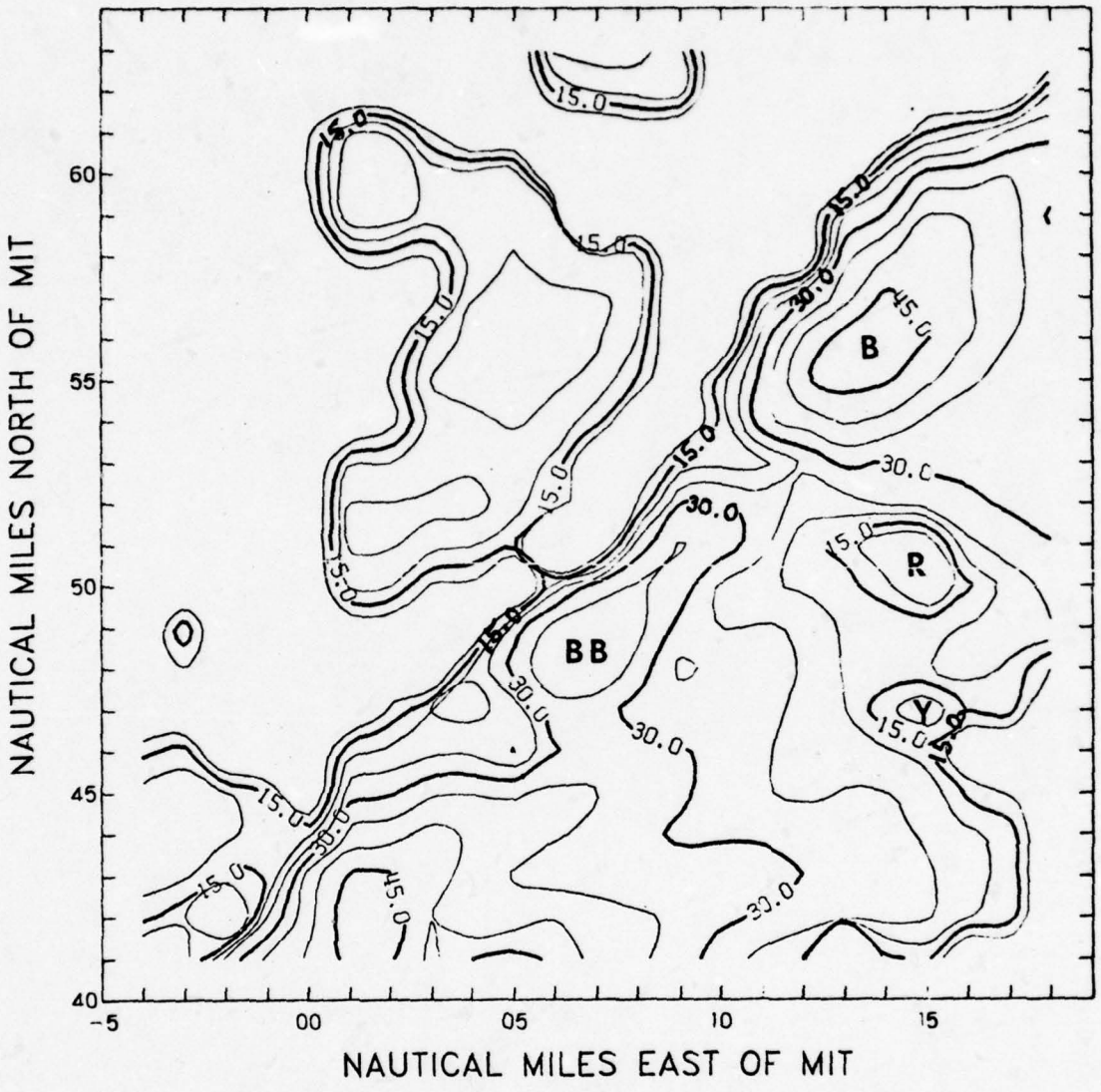

Fig. 74. Lower-layer PVSZ map for 1855 EST, 13 August 1976. Isopleths of reflectivity in dBZ.

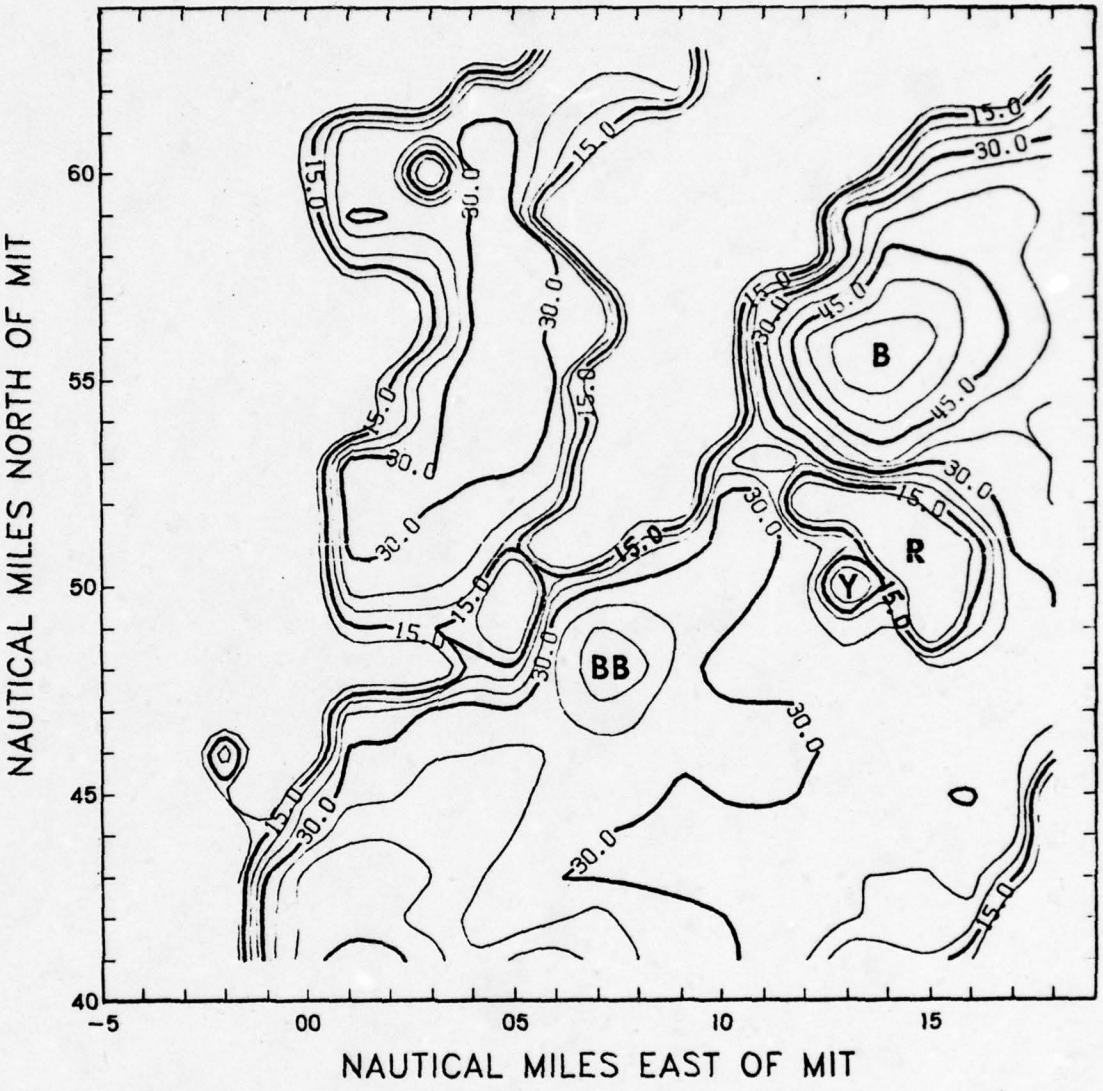

Fig. 75. Middle-layer PVSZ map for 1855 EST, 13 August 1976. Isopleths of reflectivity in dBZ.

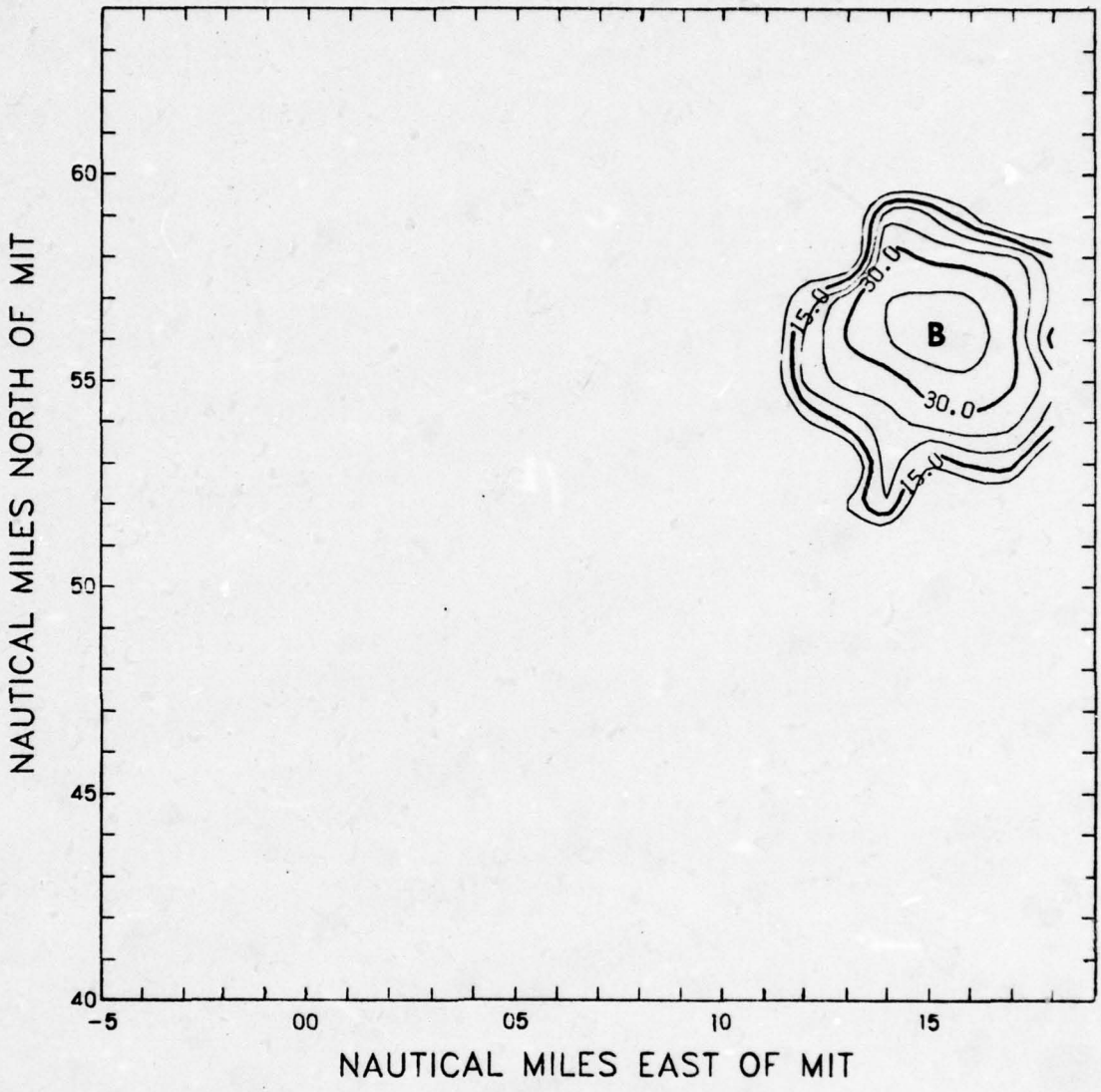

Fig. 76. Upper-layer PVSZ map for 1855 EST, 13 August 1976. Isopleths of reflectivity in dBZ.

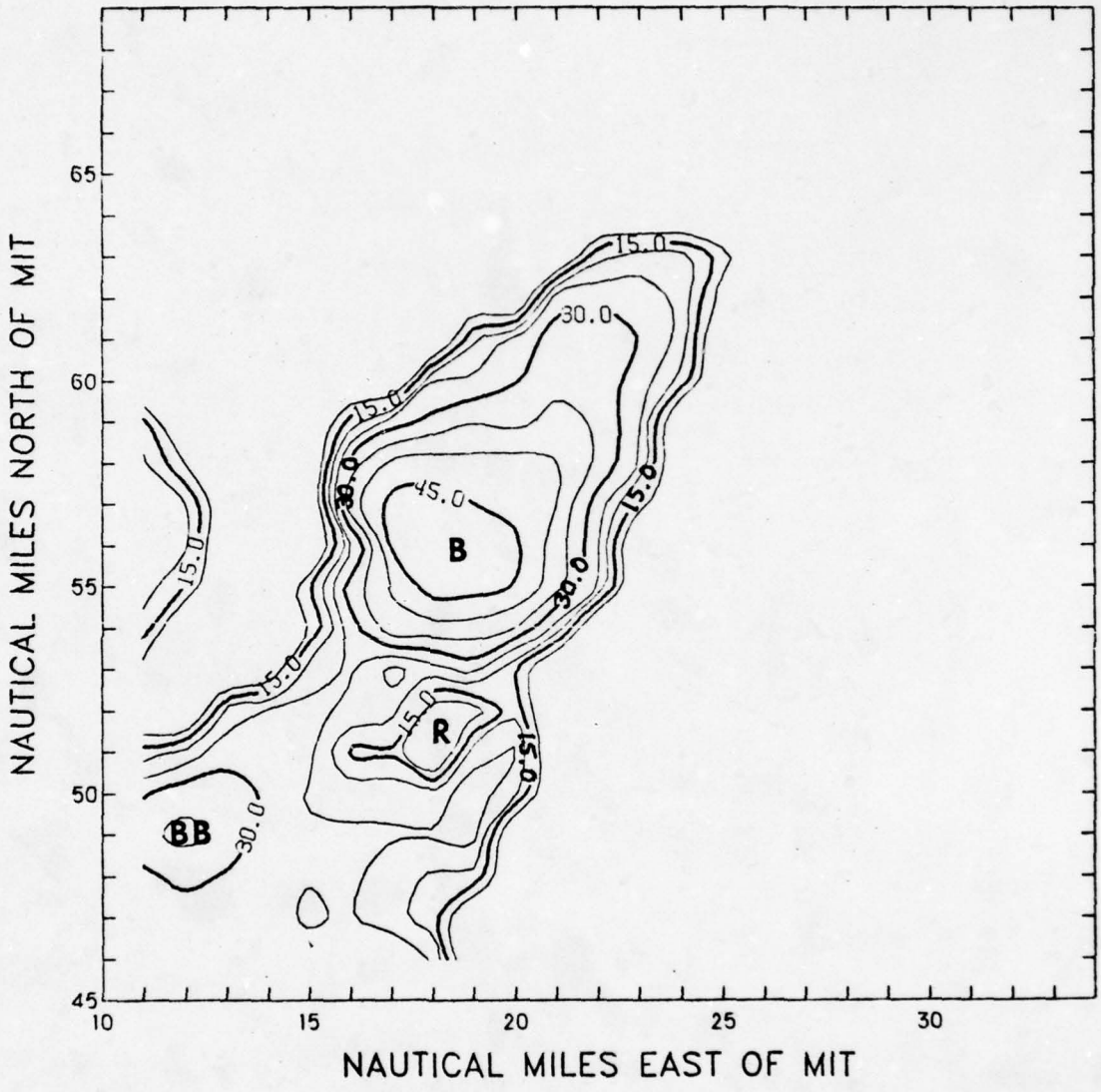

Fig. 77. Lower-layer PVSZ map for 1907 EST, 13 August 1976. Isopleths of reflectivity in dBZ.

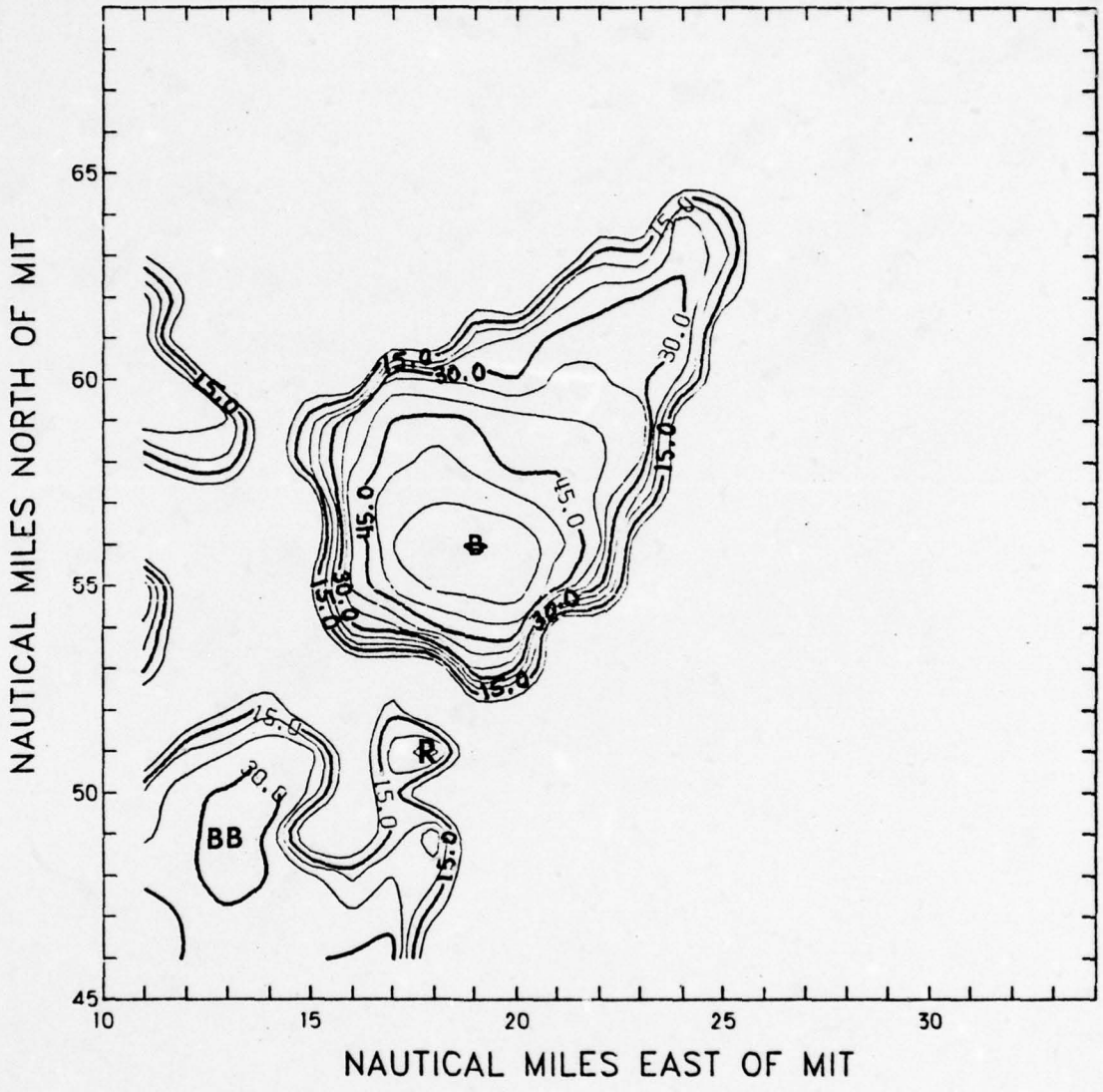

Fig. 78. Middle-layer PVSZ map for 1907 EST, 13 August 1976. Isopleths of reflectivity in dBZ.

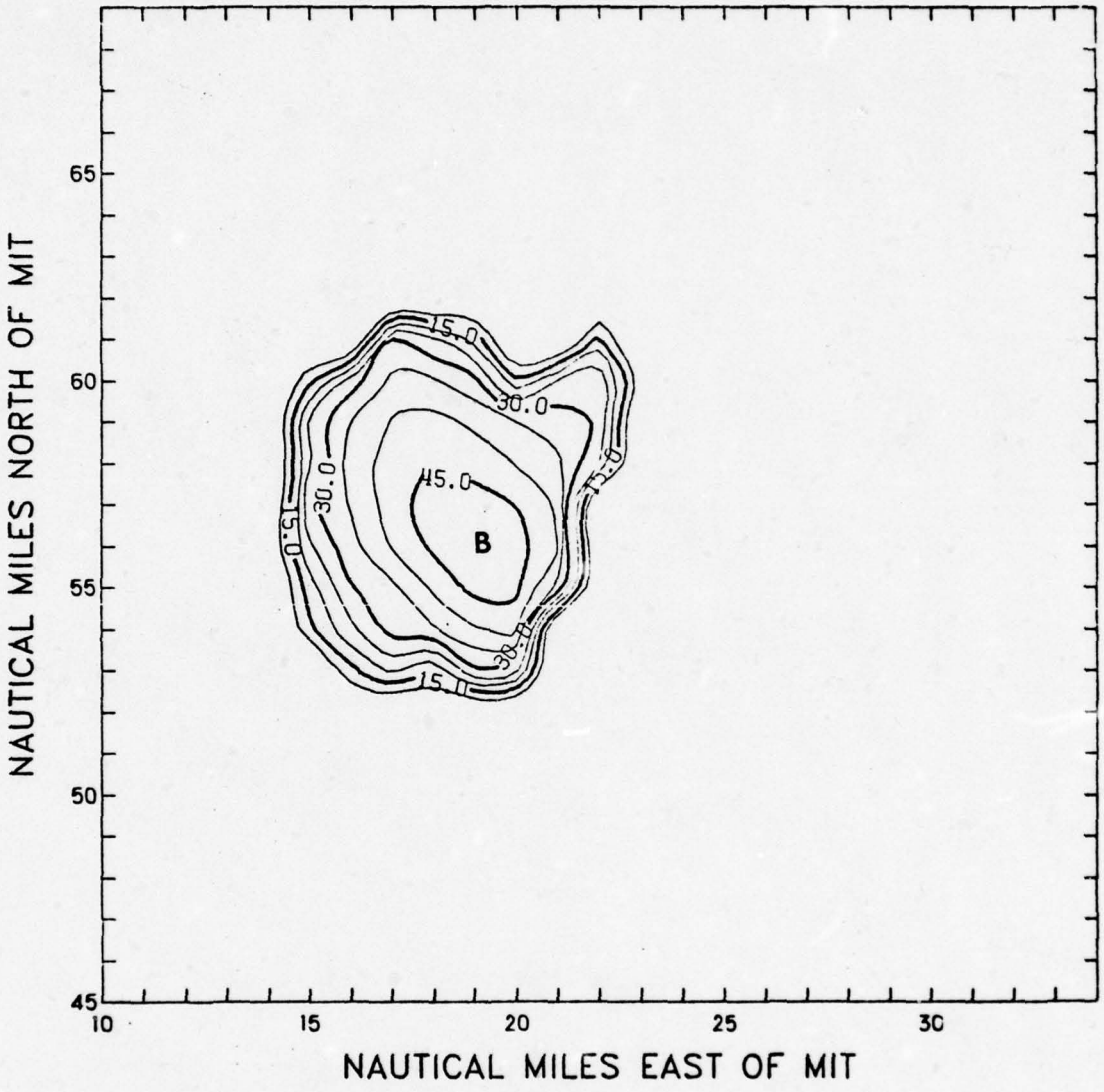

Fig. 79. Upper-layer PVSZ map for 1907 EST, 13 August 1976. Isopleths of reflectivity in dBZ.

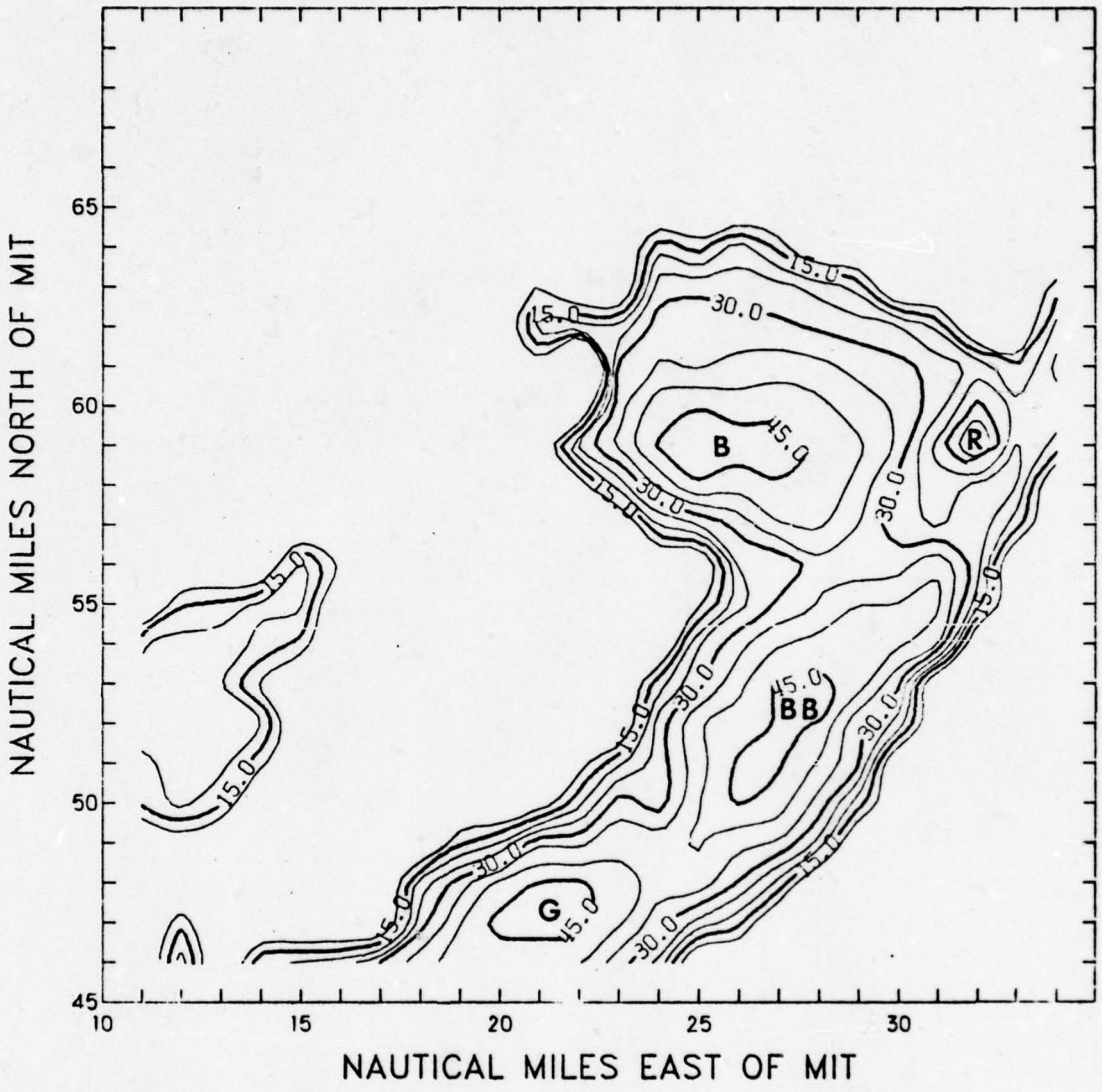

Fig. 80. Lower-layer PVSZ map for 1922 EST, 13 August 1976. Isopleths of reflectivity in dBZ.

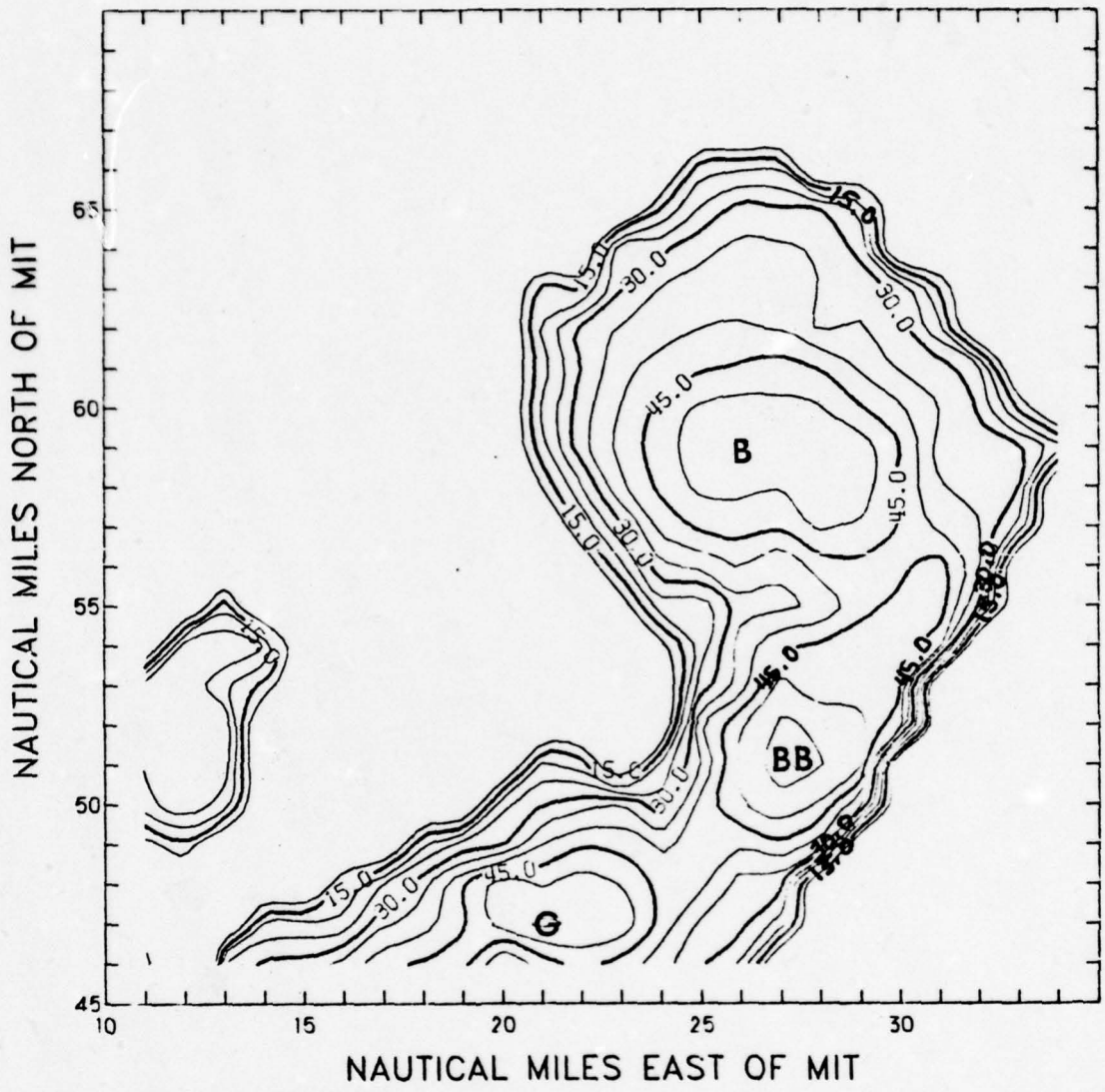

Fig. 81. Middle-layer PVSZ map for 1922 EST, 13 August 1976. Isopleths of reflectivity in dBZ.

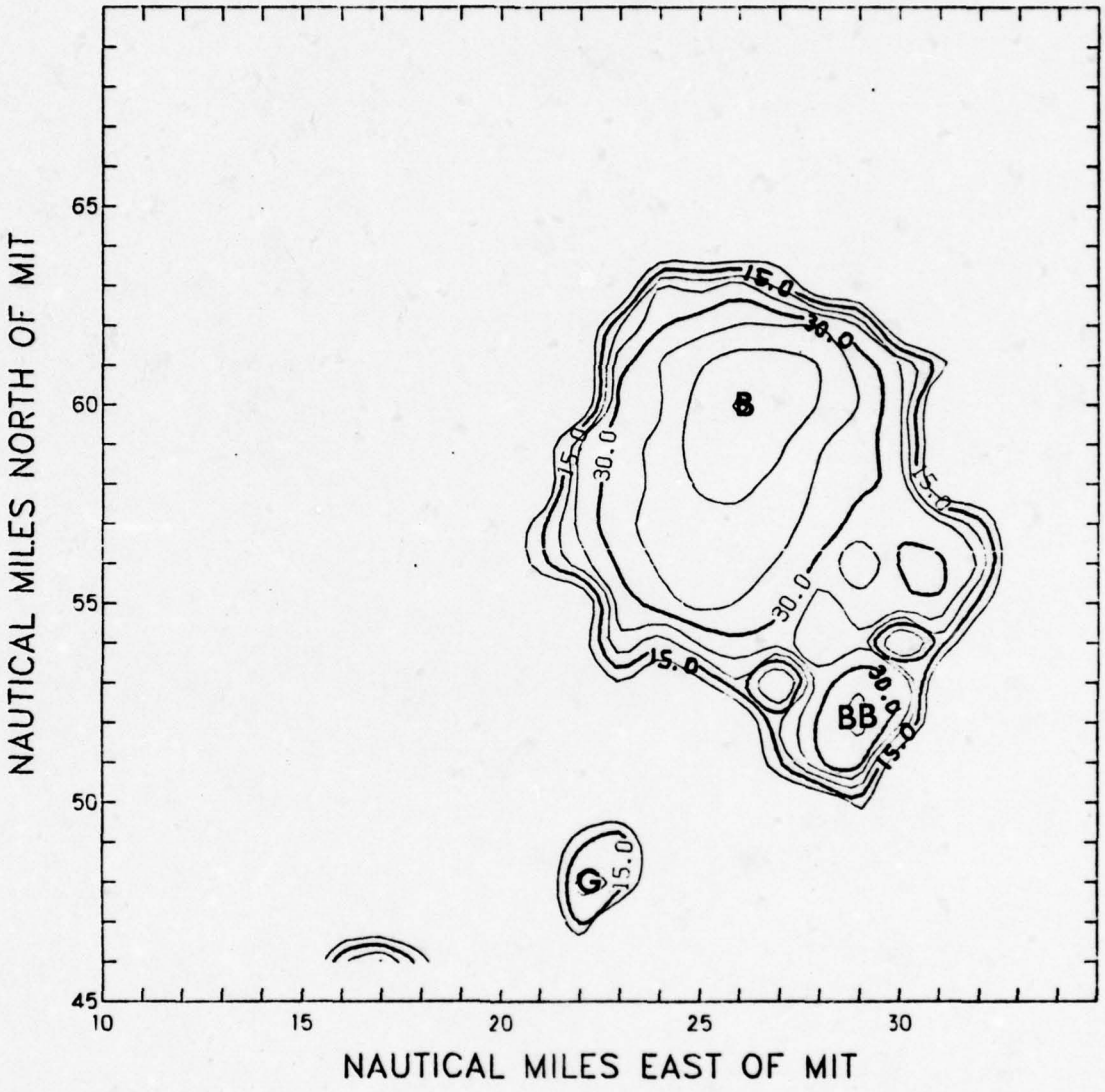

Fig. 82. Upper-layer PVSZ map for 1922 EST, 13 August 1976. Isopleths of reflectivity in dBZ.

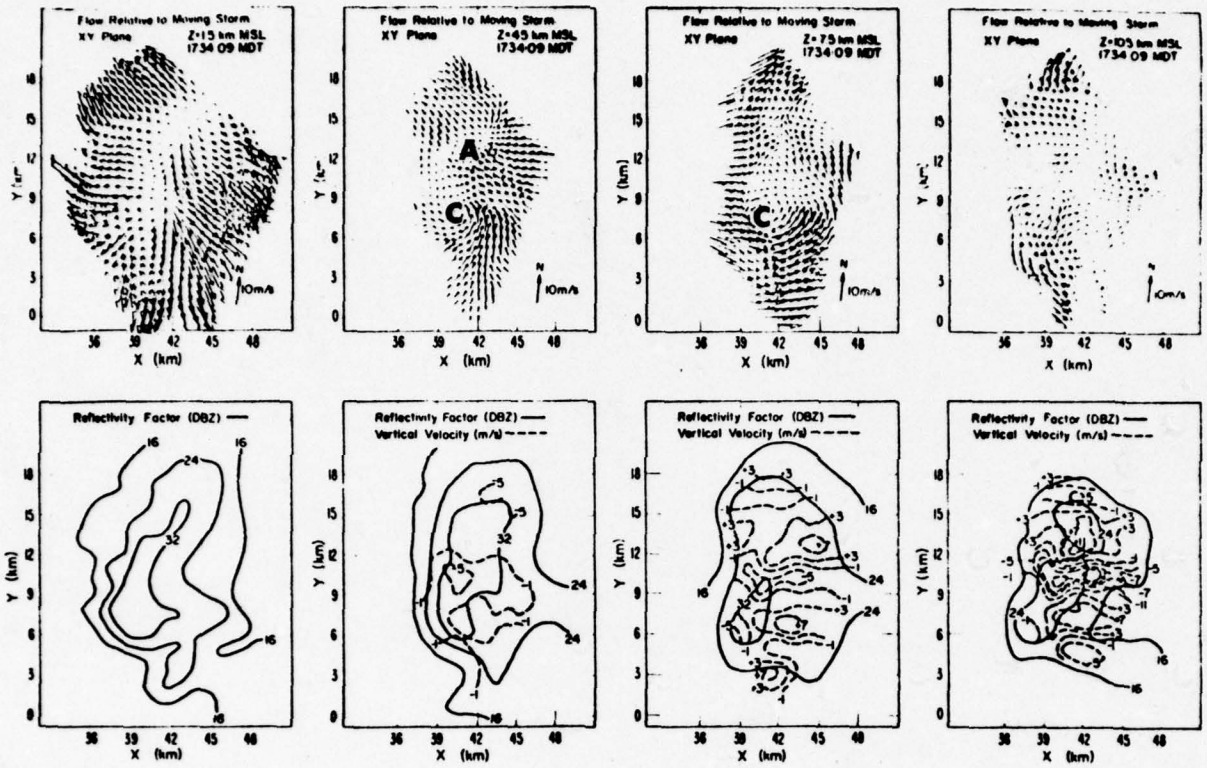

Fig. 83. Two-dimensional relative airflow in horizontal planes at heights 1.5 (surface), 4.5 (∿cloud base), 7.5, and 10.5 km MSL. At the bottom are reflectivity contours at 16, 24, 32, and 40 dBZ. The vertical velocity contours (dashed lines) are -5, -1, +3, +7, and +11 m s^{-1}. An A represents an area of anticyclonic vorticity and a C represents an area of cyclonic vorticity. [After Kropfli and Miller, 1976].

curvature on the left flank as environmental air flows around the storm from the rear. Finally, Lemon [1976a] observed anticyclonic wake vortices by using data from the NSSL doppler radar. He proposes the starting vortex mechanism as an explanation for wake eddy formation. The starting vortex results from a cyclonically rotating updraft in a severe storm. This rotating updraft acts as a solid barrier to the environmental wind flow, and the vortex forms in the lee of the storm core. Thus, there is ample evidence to support the formation of vortices in severe convective storms. Now what is the relationship between these wake vortices and the BWER?

Canipe [1973] in his study showed that the BWERs associated with single cells were observed when and where the tornadoes or funnel clouds were reported; the BWERs were observed in the wake of VIL maxima where hydrodynamic considerations suggest the generation of vorticity; the tilt of the storm core was such that hail- or precipitation-induced downdrafts could concentrate the vorticity in the area of the BWER and that the loss of hydrometeors in the upper levels (as indicated by a decrease in PVIL in the upper layer) may indicate the presence of a downdraft in the upper levels. Thus, Canipe links the BWER to the area where wake vortices are known to occur.

Lemon [1976b] examined an Oklahoma thunderstorm which exhibited features of the supercell thunderstorm type [Browning and Donaldson, 1963]. A weak echo region (WER) or vault (in ther vertical plane) was observed on radar. Visual observation confirmed the fact that a funnel cloud formed in the area near the WER. This WER or vault was definitely associated with the updraft area of the storm.

Perhaps the most extensive documentation of a tornadic storm ever produced is contained in NOAA Technical Memorandum ERL NSSL-80.[6] Lemon and Burgess [1976] analyzed single doppler radar data to derive the tornadic storm airflow patterns and have presented evidence that supports the contention that the BWER is created and sustained by organized intense updrafts. In addition, Browning [1964], Marwitz and Berry [1971], and others also have presented theoretical and observational data supporting this contention. A time sequence of the relationship between BWERs, the mesocyclone, and the tornadic vortex signature (TVS) is shown in Figure 84. Lemon and Burgess state that BWER A is coincident with the core circulation and most probably

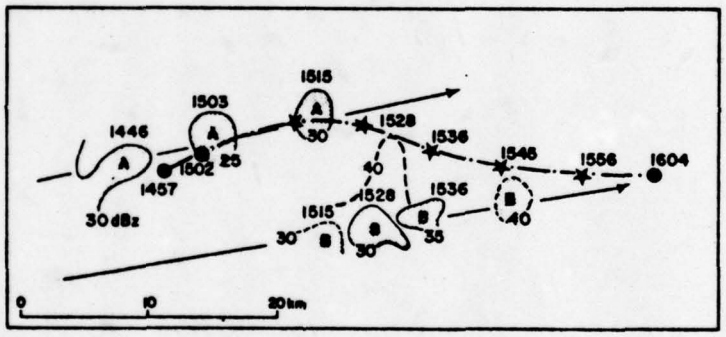

Fig. 84. Paths of bounded weak echo regions (arrows) as well as mesocyclone (dot) and tornadic vortex signature (star). Solid contours are from 6 km height; dashed, 5 km. [After Lemon and Burgess, 1976].

coincident with the updraft (based on visual observations of lowered cloud base and rapidly ascending cloud fragments beneath the circula-

---

[6] "The Union City, Oklahoma, Tornado of 24 May 1973," Rodger Brown, Editor, 1976.

tion). In addition, strong evidence supports an updraft with BWER B. It can be seen from Figure 84 that BWERs are associated with tornadoes.

Recently, Brandes [1977] analyzed dual-doppler radar data from two tornadic storms that occurred near Oklahoma City in 1974. His results show that the tornado vortex forms within the mesocyclone associated with the principal rotating updraft, and further, that the tornado is located on the right flank of the storm where environmental air is flowing around the updraft. These observations are compatible with those of Kropfli and Miller [1976] and Lemon and Burgess [1976].

Canipe [1973] and Pittman [1976] observed the BWER with every confirmed tornado in their investigations. This author also found a BWER associated with the tornado which struck Wells, Maine. If the BWER at Wells represents an updraft acting as a solid, cylindrical barrier to the environmental wind flow, then areas of cyclonic and anticyclonic vorticity should have been created in the relative wake of the storm [Kropfli and Miller, 1976]. The mid-level environmental winds were from the west-southwest at speeds near 40 kt, thus an area of cyclonic vorticity should have occurred to the right of the BWER. The mechanism which concentrates this vorticity to form the tornado may well be the convergence field associated with a hail- or precipitation-induced downdraft, as implied by Canipe [1973] and demonstrated by Eskridge and Das [1976].

CHAPTER IV

CONCLUSIONS AND RECOMMENDATIONS

Conclusions

The objective of this investigation was to develop an improved computer method by which multi-tilt digital radar data can be interpolated in three dimensions and reduced to a two-dimensional display of partially vertically-summed reflectivity maps in real time. Various combinations of interpolation schemes were used to develop the new computer method, and the resultant products were compared to determine whether or not the significant features of a severe storm evident in CAZM analyses are retained by the new data-reduction technique. In addition, the number of PVSZ layers was varied to determine the number needed to depict adequately the tilt of the storm core. Finally, severe-storm data from New England were processed by using the new data-reduction technique to find out whether or not any of the severe-storm signatures observed by Canipe [1973] and Pittman [1976] for Oklahoma storms were evident in the New England digital radar data. The investigation has led to the following conclusions.

1. The new computer method developed during this investigation resulted in significant savings of computer processing time and memory as compared to Canipe's or Pittman's techniques, while retaining all of the significant features of the storm complex revealed by the other, more cumbersome methods. This new method very conceivably could be adapted to a real-time operation with mini-computers.

2. The Lagrangian cubic interpolation along each radial of information and then the quadratic/linear interpolation in the x,y plane is the combination of techniques that provides the most detail in the PVSZ maps. However, the Lagrangian cubic and linear (LAG-LIN) combination provides virtually the same results and retains all of the significant features of the storm complex. Therefore, in a real-time operation where time is the critical factor, the latter technique will provide adequate results.

3. The quadratic technique as used by Canipe [1973] and Pittman [1976] introduced error into their resultant PVIL, CAZM and PVSZ maps. However, these errors do not significantly alter their results or conclusions concerning severe storms.

4. Three PVSZ layers appear to be sufficient, in the majority of cases investigated to date, to depict adequately the tilt of the storm core.

5. VIL maps, as indicated by Greene [1971], Vogel [1973], Canipe [1973], and Pittman [1976], provide a simple and quick method to display a storm in two dimensions. "Explosive development" alone, however, does not appear to correlate well with tornadic activity, and therefore should be used only to identify areas where the potential for severe activity exists.

6. The observed tornado at Wells, Maine, appears to meet the criteria set forth by Canipe [1973] and Pittman [1976], such as:

   a. A BWER is present when and where a tornado is reported.

   b. The BWER is associated with a large cell or a smaller satellite of the larger cell.

c. The storm core is vertical or inclined toward the BWER.

d. A decrease in the upper-layer PVSZ reflectivity maximum takes place during the time the tornado occurs.

e. Strong gradients of reflectivity exist between the BWER and the center of maximum reflectivity.

7. Although the BWER itself cannot be used as a positive identifier of tornadic activity, the BWER and the conditions set forth in 6 above can be used as an indication of the high probability that tornadic activity will occur.

8. The Wells storm parallels observations from other tornadic storms where an updraft, acting as a solid barrier to the environmental wind flow, creates cyclonic and anticyclonic vorticities in the wake of the storm. The tornado appears to occur in the region of cyclonic vorticity.

Recommendations

The following recommendations are made concerning tornado identification.

1. A study of a tornadic storm should be conducted by using doppler data combined with PVSZ maps to define better the relationship between the BWER, tilt of the storm core, production of wake vortices, and tornado vortex signatures.

2. A concerted effort must be made to analyze digital radar data of tornadic storms in other areas of the United States, especially in southern Texas by using the newly digitized radar system at Texas A&M University (TAMU).

The following recommendations are made concerning the processing of additional digital radar data.

1. A study of heavy Texas thunderstorms should be conducted by using PVSZ and VIL maps to determine what applicability VIL has to identify areas of very heavy precipitation. This type of study could be useful in terms of flash flood warnings.

2. Dual wavelength digital radar data should be recorded by using the TAMU radar system. The storm data should be recorded in the four collection modes available, (1 deg or 2 deg of azimuth and 1 km or 2 km in range) at various ranges, to determine the optimum data-collection mode based on the distance of a storm from the radar, and those differences, if any, that exist in the appearance of a storm based on the wavelength of the radar used.

3. The computer method developed during this investigation should be programmed and tested on a mini-computer to determine the time required to produce PVSZ maps. Both the Lagrange-quadratic/linear and the Lagrange-linear schemes should be tested.

4. An investigation of large hailstorms should be conducted by using digital radar data to produce PVSZ maps. The changes of maximum reflectivity in the middle-layer PVSZ maps should be analyzed for a time sequence in order to determine whether or not the initial stages of hail formation can be observed in the middle levels of a hailstorm.

REFERENCES

Appleton, E., The influence of tropospheric conditions on ultra-shortwave propagation, 17 pp., London; Physical Society, London, England, 1946.

Battan, L. J., Radar Meteorology, 161 pp., University of Chicago, IL, 1959.

_____, Radar Observation of the Atmosphere, 324 pp., University of Chicago, IL, 1973.

Bigler, S. G., An analysis of tornado and severe weather echoes, Proc. 5th Radar Meteorol. Conf., pp. 167-175, Asbury Park, NJ, 1955.

Brandes, E. A., Gust front evolution and tornado genesis as viewed by doppler radar, J. Appl. Meteorol., 16, 333-338, 1977.

Brown, R. A., Burgess, D. W., and Crawford, K. C., Twin tornado cyclones within a severe thunderstorm; single-doppler radar observations, Weatherwise, 26, pp. 63-71, 1973.

Browning, K. A., Airflow and precipitation trajectories within severe local storms which travel to the right of the winds, J. Atmos. Sci., 4, 634-639, 1964.

_____, and Donaldson, R. J., Jr., Airflow and structure of a tornadic storm, J. Atmos. Sci., 20, 533-545, 1963.

Canipe, Y. J., Temporal variability in intensity-height profiles of a severe storm using digital radar data, M. S. Thesis, Texas A&M University, College Station, TX, 78 pp., 1972..

_____, On the structure and development of severe local storms as revealed by digital radar observations, PH.D. Dissertation, Texas A&M University, College Station, TX, 142 pp., 1973.

_____, and Das, P., Partial vertical integration of liquid water (PVIL), an improved radar-analytical tool, Proc. 16th Radar Meteorol. Conf., pp. 328-332, Houston, TX, 1975.

Carnahan, B., Luther, H. A., and Wilkes, J. O., Applied numerical methods, 604 pp., John Wiley & Sons, NY, 1969.

Clark, R. A., and Y. J. Canipe, Applications of digital radar in both meteorology and hydrology, Proc. 15th Radar Meteorol. Conf., pp. 93-98, Champaign-Urbana, IL, 1972.

Elvander, R. C., The relationship between digital radar data and reported severe weather occurrences, Proc. 16th Radar Meteorol. Conf., pp. 333-336, Houston, TX, 1975.

Eskridge, R. E., and Das, P., Effect of a precipitation-driven downdraft on a rotating wind field: a possible trigger mechanism for tornadoes?, J. Atmos. Sci., 33, 70-84, 1976.

Greene, D. R., An investigation of precipitation attenuation and its application in a dual-doppler frequency radar morphology of subtropical precipitation, M.S. Thesis, Texas A&M University, College Station, TX, 109 pp., 1964.

_____, Numerical techniques for the analysis of digital radar data with applications to meteorology and hydrology, Ph.D., Dissertation, Texas A&M University, College Station, TX, 124 pp., 1971.

Jessup, E. A., Interpretation of chaff trajectories near a severe thunderstorm, Mon. Wea. Rev., 100, pp. 653-661, 1972.

Kropfli, R. A., and L. J. Miller, Kinematic structure and flux quantities in a convective storm from dual-doppler radar observations, J. Atmos. Sci., 33, 520-529, 1976.

Lemon, L. R., Wake vortex structure and aerodynamic origin in severe thunderstorms, J. Atmos. Sci., 33, 678-685, 1976a.

_____, The flanking line, a severe thunderstorm intensification source, J. Atmos. Sci., 33, 686-694, 1976b.

_____, and D. W. Burgess, Tornadic storm airflow and morphology derived from single-doppler radar measurements, NOAA Tech. Mem. ERL NSSL-80, pp. 85-106, Norman, OK, 1976.

Marshall, J. S., The constant-altitude presentation of radar weather patterns, Proc. 6th Radar Meteorol. Conf., pp. 321-324, Cambridge, MA, 1957.

Marwitz, J. D., and E. X. Berry, The airflow within the weak echo region of an Alberta hailstorm, J. Appl. Meteorol., 10, 487, 1971.

Morgan, M. M., and E. A. Mueller, The total liquid water mass of large convective stroms, Proc. 15th Radar Meteorol. Conf., pp. 39-40, Champaign-Urbana, IL, 1972.

Pautz, M., and F. Doloresco, On the relation between radar echo tops, the tropopause and severe weather occurrences, Proc. 10th Radar Meteorol. Conf., pp. 51-56, Washington, D.C., 1963.

Phillips, J. F., Cloud structure from defense meteorological satellite data, M. S. Thesis, Texas A&M University, College Station, 142 pp., 1975.

Pittman, D. W., Tornado identification from analyses of digital radar data, M. S. Thesis, Texas A&M University, College Station, TX, 93 pp., 1976.

Prandtl, L., and O. G. Tietjens, Applied hydro- and aeromechanics, 306 pp., Dover Publications, New York, NY, 1957 edition.

Probert-Jones, J. R., The radar equation in meteorology, Quart. J. Roy. Meteorol. Soc., 88, 485, 1962.

Vogel, J. E., Applications of digital radar in the analysis of severe local storms, M.S. Thesis, Texas A&M University, College Station, TX, 94 pp., 1973.

Whiton, R. C., On the use of radar in identifying tornadoes and severe thunderstorms: a diagnostic guide for radar-scope interpretation, USAF Technical Report 243, 18 pp., Scott AFB, IL, 1971.

Wilk, D. E., W. L. Watts, D. W. Sirmans, R. M. Lhermitte, E. Kessler, and K. C. Gray, Weather radar data systems at the National Severe Storms Laboratory, Proc. 5th Radar Meteorol. Conf., pp. 14-23, Boston, 1967.

_____, and K. C. Gray, Processing and analysis techniques used with NSSL weather radar systems, Proc. 14th Radar Meteorol. Conf., pp. 369-374, Boston, 1970.

_____, and E. Kessler, Quantitative radar measurements of precipitation, Meteorol. Monographs, 11, Boston, 1970.

Yates, J. M., The association of vertical radar echo protrusions with hail, Progress Report No. 12, WSR-57 Radar Program, pp. 47-51, U.S. Weather Bureau, 1963.

APPENDIX A

This appendix contains a summary of the various interpolation schemes used in this investigation.

Five interpolation schemes were used in this investigation. A Lagrangian cubic or linear interpolation was accomplished along each radial of information and then a quadratic, linear, or quadratic/linear interpolation was performed in the x,y plane. A brief summary of each technique follows.

The Lagrangian cubic interpolation is accomplished by using the general form of the Lagrange interpolating polynomial [Carnahan et al., 1969]

$$P_n(x) = \sum_{i=0}^{n} L_i(x)\, f(x_i), \tag{A1}$$

where

$$L_i(x) = \prod_{\substack{i=0 \\ i \neq j}}^{n} \frac{(x - x_j)}{(x_i - x_j)}, \quad i = 0,1,\ldots,n. \tag{A2}$$

and n is the degree of the interpolating polynomial.

The Lagrangian cubic interpolation scheme uses the four data points (two on either side) nearest the interpolation point (see Figure 16) and generates a cubic equation through these four points. This cubic equation is then evaluated at the interpolation point to provide the interpolated value of the reflectivity factor.

For this investigation, n was chosen to be 3, which yields the Lagrangian cubic interpolation polynomial. Of course, we could have chosen n to be greater, but one must realize that an n^{th} degree interpolating polynomial will have n inflection points. If n is large, the chances are greater that the interpolated value of the reflectivity factor may be in error. In fact, Carnahan et al. [1969]

states:

> On the reassuring side, low-degree interpolating polynomials usually have very good convergence properties, that is, most of the functional value can be represented by low-order terms. In practice, we can almost always achieve the desired accuracy with low-degree polynomial approximations, provided that the base-point functional values are available on the interval of interest.

The linear interpolation along the radial of information is accomplished by using the two points on either side of the interpolation point and the distance, δr, from the first data point to the interpolation point. For example, in Figure 16 we would get

$$Z_e(r',h)_\alpha = Z_e(r_i)_\alpha + \left[Z_e(r_{i+1})_\alpha - Z_e(r_i)_\alpha\right] \frac{\delta r}{\Delta r} \tag{A3}$$

The quadratic interpolation in the x,y plane (h = constant) is basically a finite-difference form of the Taylor series expansion in two dimensions truncated after the second order terms and is given by

$$Z_e(x,y)_{h=\text{constant}} = a_1 + a_2\delta\alpha + a_3\delta s + a_4(\delta\alpha)^2 + a_5(\delta s)^2 + a_6\delta\alpha\delta s \tag{A4}$$

The coefficients a_1 through a_6 are determined by relationships between the six nearest data points in the horizontal plane of α (see Figure 4).

The linear interpolation in the x,y plane (h = constant) uses the four $(s,\alpha)_h$ grid points that encompass the $(x,y)_h$ point in question. In Figure 6 the four points are $Z_e(\alpha_{i-1},s_{i+1})$, $Z_e(\alpha_i,s_{i+1})$, $Z_e(\alpha_{i-1},s_i)$, and $Z_e(\alpha_i,s_i)$. First, the linearly interpolated value of $Z_e(\alpha',s_{i+1})$ and $Z_e(\alpha',s_i)$ are calculated and are given by

$$Z_e(\alpha', s_{i+1}) = Z_e(\alpha_i, s_{i+1}) + \left[Z_e(\alpha_{i-1}, s_{i-1}) - Z_e(\alpha_i, s_{i+1})\right] \frac{\delta\alpha}{\Delta\alpha} \tag{A5}$$

$$Z_e(\alpha', s_i) = Z_e(\alpha_i, s_i) + \left[Z_e(\alpha_{i-1}, s_i) - Z_e(\alpha_i, s_i)\right] \frac{\delta\alpha}{\Delta\alpha} \tag{A6}$$

Then the linearly interpolated value of $Z_e(x,y)_h$ is calculated and is given by

$$Z_e(x,y)_h = Z_e(\alpha', s_i) + \left[Z_e(\alpha', s_{i+1}) - Z_e(\alpha', s_i)\right] \frac{\delta s}{\Delta s} \tag{A7}$$

The quadratic/linear interpolation scheme in the x,y plane (h = constant) is simply a combination of the quadratic and linear interpolation schemes. If the interpolated value of Z_e is less than 0 by using the quadratic interpolation scheme, then the linear interpolation scheme is used.

VITA

Thomas E. Sieland was born in Caro, Michigan, on 23 March 1940, to Edmund E. and Clara E. Sieland. He attended grade school and high school in Caro and graduated from Caro High School in 1958.

He enlisted in the United States Air Force in January 1960. Six years later, he was selected by the Air Force Institute of Technology (AFIT) for undergraduate schooling via the Airman Education and Commissioning Program and attended Florida State University, where he received a Bachelor of Science degree in Meteorology in December 1967. In 1970, he was selected by AFIT to attend graduate school at the University of Michigan, where he received a Master of Science degree in Meteorology in August 1971.

The author entered Texas A&M University in January 1975 to pursue the degree of Doctor of Philosophy under the auspices of AFIT. His permanent mailing address is in care of his parents at Route #1, Box 241, Rose City, Michigan 48654.